NOVEMBER 1978 UMEE 78R4

TORSION IN BUILDINGS SUBJECTED TO EARTHQUAKES

Martin E. Batts
Glen V. Berg
Robert D. Hanson

The University of Michigan Department of Civil Engineering

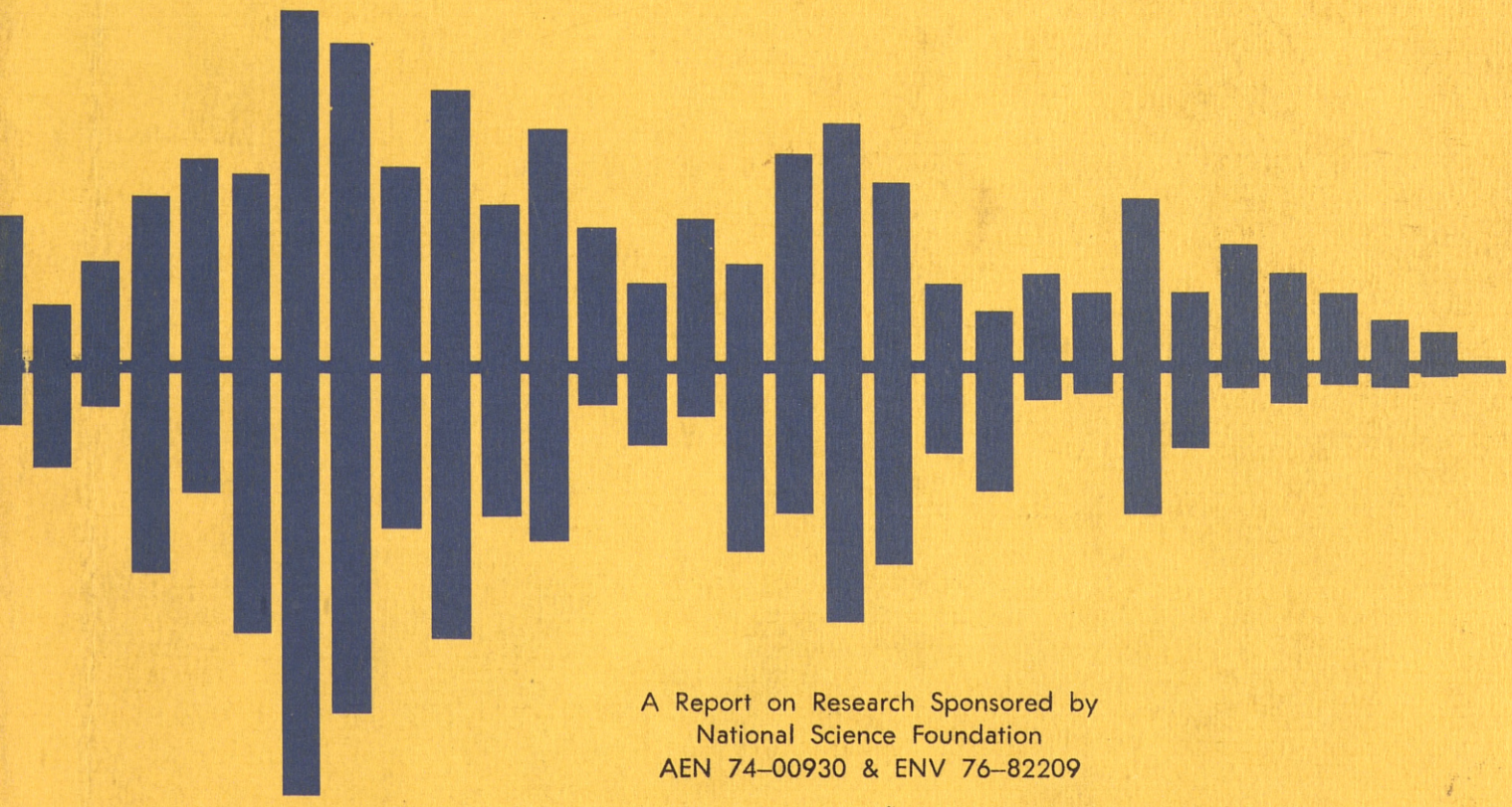

A Report on Research Sponsored by
National Science Foundation
AEN 74–00930 & ENV 76–82209
and
The University of Michigan


UNIVERSITY OF MICHIGAN 1817
Library
ARTES SCIENTIA VERITAS

TORSION IN BUILDINGS SUBJECTED TO EARTHQUAKES

by

Martin E. Batts

Glen V. Berg

Robert D. Hanson

Report on Research Supported by the
National Science Foundation, Grants
AEN &-00930 and ENV 76-82209,
and The University of Michigan

Report UMEE 78R4
Department of Civil Engineering
The University of Michigan
Ann Arbor, Michigan 48109

November 1978

AESTRACT

It is now well known that for buildings with eccentric centers of mass and stiffness, there is a dynamic amplification of torque and a dynamic reduction in building shear. The main concern with building torsion is that the eccentricity induces a rotational motion whose contribution to the displacement at the periphery causes an increased displacement compared to the displacement corresponding to zero eccentricity. Other researchers have reported for a single accelerogram as much as a 40-100% increase in the peripheral response.

In this dissertation, the probabilistic approach is selected for the analysis of linear response. The earthquake ground excitation is discussed and a simple expression relating torsional earthquake power spectra to translational earthquake power spectra is developed. Interaction relations are derived for systems with simultaneous X, ø, and Y ground excitations.

The peripheral response is studied using the probabilistic approach. It is shown that a special case arises where the peripheral response is independent of the eccentricity ratio and frequency ratio.

The state of the art of artificial accelerogram generation is discussed. Various parameters affecting ground rotational motion are discussed.

Nonlinear response characteristics for a four exterior wall model are analyzed and it is concluded that parametric

resonance is not a problem for this model.

Major conclusions from the results of this dissertation include the following: a) the maximum expected increase in peripheral response is on the order of 50%, b) the single most important parameter in building torsion is the torsion-translation frequency ratio, and c) torsional ground excitation must be quite large before it significantly affects the response for systems with well separated frequencies.

ACKNOWLEDGEMENTS

This report was submitted by Dr. Batts to The University of Michigan in partial fulfillment of the requirements for the degree of Doctor of Philosophy (Civil Engineering). Professors Glen V. Berg and Robert D. Hanson provided guidance and assistance throughout this investigation as chairmen of the doctoral committee. The authors would like to thank Professors Frank E. Richart,Jr. and Richard A. Scott (members of the doctoral committee) for reviewing the report and offering helpful suggestions.

This investigation was supported by The University of Michigan and National Science Foundation Grants AEN 74-C0930 and ENV 76-82209. The conclusions arrived at in this paper are solely those of the author and do not necessarily represent the views of any of the sponsors.

TABLE OF CONTENTS

NOTATION

$\{A_{nj}\}$...mode shape

[A]...matrix of eigenvectors

A...constant

B, B_x, B_y...building dimensions

B_i, B_j...fraction critical damping in ith and jth modes

C...period factor

C_s...shear wave speed in rock

{C}...constants

D...complex constant

DHE...dissipated hysteretic energy

DNHE...dissipated nonhysteretic energy

$\{D_j\}$...mode shape

EIE...earthquake input energy

E_{ym}...distance from center of mass to building exterior

E_{ij}...constant

E_x, E_y...eccentricities

F, F_e, F_g...frequencies, cps

F_{y1}, F_{y2}...yield shear force for elements 1 and 2

$G_{Y_m}{}^2(\omega), G_Z{}^2(\omega)$...power spectra

G(t)...function in t

$H_{Y_m}(\omega)$...complex frequency response function

H(t)...Heaviside unit step function

I...use factor

I(t)...intensity function

I_a...Arias intensity

K_x, K_y ... building stiffness in X and Y direction

K_{xl}, K_{yl} ... element stiffness in X and Y direction

K_ϕ ... rotational stiffness

M ... mass

MPF_m ... modal participation factor for mth mode

M_i ... ith moment of power spectrum about origin

N ... number of cycles

P_{mn} ... correlation coefficient

Q ... maximum of q(t)

R ... radius of gyration of building mass

$R_{\ddot{Z}_x}(\tau)$ ... autocorrelation function of $\ddot{Z}_x(t)$

S ... soil factor

$S_v(\omega)$ ... response spectrum

SI ... Housner's spectral intensity

T, T_x ... period

$\bar{T}$ ... torque

U_p ... displacement response of point P

U,V ... ground motion in Cartesian coordinates corresponding to X-direction and Y-direction

$\bar{V}_x, \bar{V}_y$ ... shear force in X and Y direction for coupled system

U_{gx}, U_{gy} .. ground displacements in X and Y direction

U_x, U_y ... response displacements in X and Y direction

W ... weight

X_i, Y_i ... distances from center of mass to stiffness element

$Y_m(t)$ ... mth modal response

$Y_{px}, Y_{p\phi}, Y_{py}$ .. modal responses of point P

Z ... zone factor

$\{Z\}$...$\{Z_{xx}\ Z_{\phi}\ Z_{y}\}$ ground displacement vector

a...constant

c...constant

g...gravity

h(t)...impulse response function

i...$\sqrt{-1}$

s...duration of accelerogram

t'...constant

α, β...constants

γ...constant

δ_e...measure of spread of power spectrum

δ_y...yield displacement

ε...constant

θ...angle

λ...wavelength

ξ...building size to wavelength ratio

σ...variance

τ...transit time and lag time in autocorrelation function

ϕ...ground rotation

ω...frequency

ω_i, ω_j...ith and jth modal frequencies

ω_{di}, ω_{dj}... damped modal frequencies

LIST OF FIGURES

CHAPTER I

INTRODUCTION

According to Herodotus, when Xerxes was planning the second Persian expedition against the Greeks in 480 B.C., a bridge built for the crossing at Hellespont by his Phoenician and Egyptian engineers was destroyed by a storm. The engineers were beheaded and the waters of Hellespont received three hundred lashes(1).

In ancient Mesopotamia, the Code of Hammurabi contained the first building code. Its design philosophy was to prescribe the punishment for a failed building, one of which was the death of the builder(2).

As time passed, society became less barbaric and building became more scientific.

While there is no written historical evidence the Egyptians had knowledge of a theory of structural behavior, their immense and precise civil engineering works suggest they devised empirical rules in their building. The Greeks contribution to structural theory was by Aristotle (384-322 B.C.) and by Archimedes (287-212 B.C.) who formulated the equilibrium principle of statics. The Romans, while profuse builders, designed their structures empirically. The Middle Ages, as is typical of the period, seems devoid of much civil engineering progress. Although a few of the

Renaissance's versatile scientists, Da Vinci and Galileo, discussed structural behavior in their publications, it was not until the 18th century, the Age of Reason, that the basis for the modern theory of mechanics of solids was established by Hooke, the Bernoulli's, Euler, LaGrange, Couloumb, and Navier. The establishment of the theory changed the emphasis of design from empirical observations on strength to a scientific elastic analysis of stresses and strains[3].

Dedicating a bridge, Franklin Delano Roosevelt once remarked that bridge building is the story of civilization. It surely is the story of civil engineering. Nineteenth century bridge failures had a profound effect on the course of the civil engineering profession. In 1876, a Howe truss bridge at Ashtabula, Ohio, collapsed, killing ninety persons. It had been erected by a non-engineer, who also had modified its design. Legislation following the catastrophe required that the design and construction of bridges be directed by professional engineers[4].

While infamous bridge failures in wind in the 1800's brought about studies and design rules for wind bracing, it took the great San Francisco Earthquake of 1906 to spur the profession to studies of earthquake resistant design, resulting in the first American building code for earthquake design rules, namely the Santa Barbara code of 1925[5].

Many studies of earthquake resistant design center on inelastic response. The present design philosophy that

structures be able to withstand a large earthquake while allowing structural damage is based in part on economics and the concept of limit design, introduced by Housner[6]. The principle of limit design is to allow the structure to dissipate energy hysteretically, which results in a ductility demand design requirement.

Ductile moment frame buildings are typically systems of orthogonal plane frames coupled through floor diaphragms. For two-dimensional analysis, the plane frames can be analyzed separately. The hysteretic energy dissipation for a moment frame takes place through plastic hinging of the members when yield moment capacity is exceeded. The simplest model for such plastic hinging is the elasto-plastic model. The elasto-plastic model was used by Berg [7] in the inelastic analyses of plane frames and also by Newmark [8]. The next refinement in the analysis was the use of the bilinear model. This model was employed by Clough [9], Iwan [10], and Giberson [11] to mention a few. Since the moment curvature relation for typical members was not multilinear but curvilinear, the next refinement included the Ramberg-Osgood model [12] utilized by Jennings [13], Goel [14], and Kaldjian [15].

Suggested analytical models for the hysteretic behaviour of shear walls have been used with some success [16 17]. Extensive experimental data also exists on the hysteresis behaviour of reinforced concrete flexural members and the parameters affecting it; however, no generally accepted

modeling technique exists.

Many special purpose computer programs exist for inelastic dynamic plane frame analysis; one widely used general purpose computer program for this purpose is DRAIN2D by Kanaan and Powell [18].

The development of the computer and the increased size of computer core space spurred the development and use of space frame elastic programs. A space frame elastic dynamic analysis program, TABS, developed by Wilson [19] economically utilizes the planar structure of space frames; however, it computes column axial strains that are not compatible in columns common to orthogonal plane frames. In the course of the space program, the National Aeronautics and Space Administration developed a three-dimensional elastic dynamic analysis computer program, NASTRAN[20]. Other public general purpose space frame programs developed are SAP-IV[21] and STRUDL [22].

Three dimensional elastic dynamic computer programs are expensive to use since each joint has six degrees of freedom, requiring a large amount of computer time in matrix manipulation. Simplifying techniques have been employed with some success to show the gross structural response.

Early studies [23] of building torsion have shown that the lateral and torsional motions of the structure are coupled if there exists an eccentricity between the centers of mass and stiffness of the structure. For small eccentricities the usual method of analysis consisted of

computing the static torque, the product of the building shear and the eccentricity. Many studies [24, 25] have shown that the dynamic torque may considerably exceed this product. Most of these studies have shown that a reduction in the horizontal building shear usually occurs along with this dynamic amplification of torque.

Hoerner [26] did a study of modal coupling, meaning a coupling between the two translational and one rotational degrees of freedom such that each mode may contain a component of all three degrees of freedom. Hoerner's study showed that the amount of modal coupling is related to the eccentricity between the center of mass and the center of stiffness divided by the translational-torsional frequency difference. This is confirmed by forced vibration tests [27].

Heidebrecht [28] used modal analysis with the frames and shear walls modeled as prismatic shear and bending beams respectively. With a simplification of the three coupled differential equations of motion, he developed nomographs to determine the higher coupled frequencies.

Berg [29] also used modal analysis in a study of a cantilever shear beam model to show the effect of unsymmetric setbacks. His study showed that torsional oscillations occur and mode shapes are coupled for unsymmetric setbacks.

Tso [30] showed that when a symmetric building with no eccentricity, i.e. uncoupled, is excited in only one

direction, torsional response can arise from the nonlinear coupling between translational and torsional motions, known as parametric resonance.

The final refinement in analysis techniques is the modeling of buildings as inelastic space frames. Okada [31] modeled a one story building as a space frame to show the increased corner damage due to high eccentricity. Padilla-Mora [32] used a four frame shear building as a model to show the effect common column orthogonal strength interaction has on hysteretic dissipated energy.

Shiga [33] developed a special purpose three-dimensional inelastic dynamic response computer program for the analysis of a building damaged by the 1968 Tokachi-Oki earthquake. The results correlated with the damage.

Mondkar et al [34] have developed a general purpose inelastic three-dimensional dynamic finite element computer program, ANSR, which is an extension of DRAIN2D [18]. It is very expensive to utilize.

There have been many attempts to model a building as a beam [35]. For some purposes this technique gives the desired result. For elastic analyses it is difficult, if not impossible, to match both the higher frequencies and mode shapes. For a typical N-story building the beam model's parameters can be adjusted such that the N frequencies will match the actual building's frequencies, but then the mode shapes may not match (and vice versa). For inelastic analyses where higher modes may not be as important, a beam

model cannot simulate the strength interaction of columns common to orthogonal frames. Also, it cannot model the effects of unsymmetrical strength (as opposed to stiffness) in parallel frames. These problems can be avoided by modeling the individual frames as beams, but this creates new problems. For the shear beam model, a change in stiffness at the Ith level changes the stiffness matrix coefficients at the (I-1), (I) and (I+1) rows and columns. For a moment frame, a change in stiffness in a member at the Ith level changes all the coefficients in the lateral stiffness matrix. This problem can also be circumvented by modeling the frame as a bending beam instead of a shear beam; however, the frame's dynamic characteristics are more like a shear beam than a bending beam. Some attempted remedies consist of using Timoshenko beams and series or parallel beams; yet, the modeling of a building as a beam raises more objections than the benefits of economics of the model can justify.

Another modeling technique can be used for 1-story buildings and buildings being analyzed in their fundamental mode only. Kan and Chopra [36] did an exhaustive study of the parameters affecting the torsional response of linear one story buildings. For inelastic behaviour, the single resisting element or generalized coordinate stiffness for multidegree of freedom systems analyzed only in the fundamental mode, can be assigned a hysteresis loop based on theoretical or experimental information depending on the

type of building. For example, in a steel moment frame building a bilinear or Ramberg-Osgood type hysteresis would be appropriate (Fig. 1-1). A symmetrically braced frame type hysteresis, illustrated in Fig. 1-2, exhibits the slip type shape characteristic of bolted frames. A shear wall resisting element differs from moment frame hysteresis in that it is usually of the degrading type. The shear wall type hysteresis is illustrated in Fig. 1-3 and is characterized by the pinched shape near the origin.

A more rigorous method for modeling inelastic building motion is by the member by member approach. Here the matrix structural analysis technique is used with the global stiffness matrix being altered in time as each member changes stiffness in time. There are different types of hysteresis behavior for different resisting element members as described above.

A bifurcation of analysis methods arises in the choice of time domain versus frequency domain analysis. The choice partially rests on the philosophy of the analyst. Time series analysis is generally more expensive and statistically more variant than frequency domain analysis which gives the expected maximum [37] as opposed to a maximum of a member of an ensemble of ergodic processes. For inelastic response, frequency domain analysis cannot be applied without using some approximate technique since the complex frequency response function is time dependent.

At the present time there is no generally accepted method

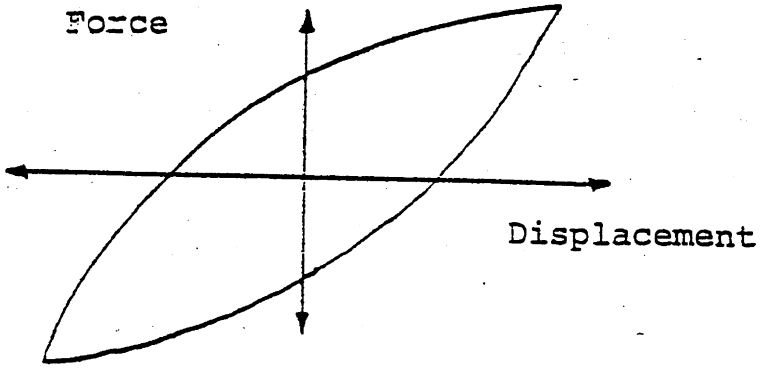

Figure 1-1 Typical Moment Frame Hysteresis

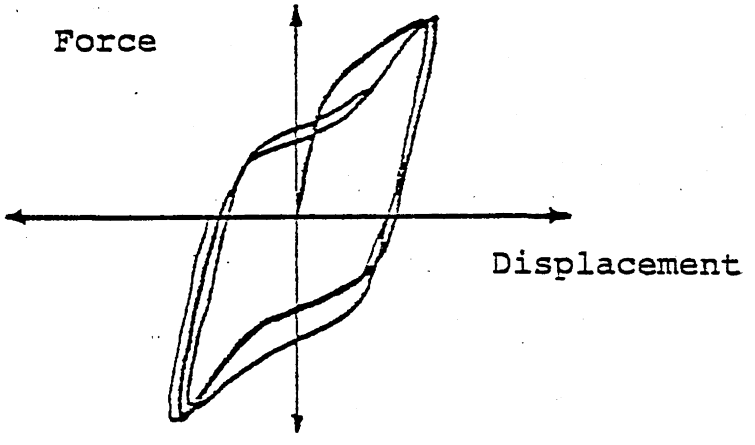

Figure 1-2 Typical Braced Frame Hysteresis

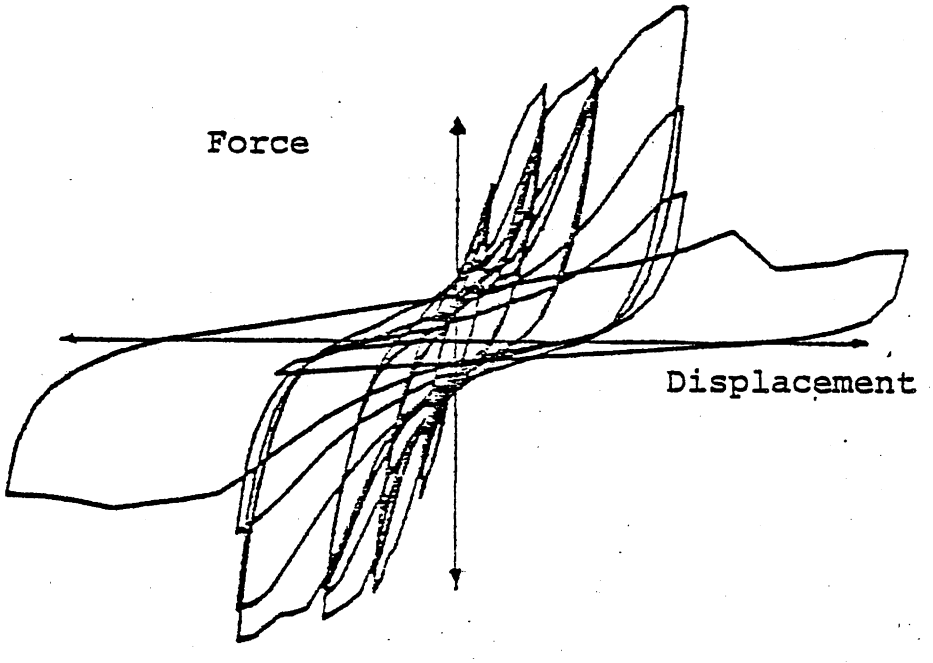

Figure 1-3 Typical Shear Wall Hysteresis

for determining by spectral analysis the statistical parameters of response for a stochastically excited nonlinear hysteretic system. The Fokker-Planck equation approach for nonlinear systems, which involves the solution of a partial differential equation involving the joint probability of displacement, velocity, and time, is not applicable for either nonwhite excitation [38] or hysteretic systems. Equivalent linearization techniques [39], where minimization of the mean squared error is used in finding a statistically equivalent linear stiffness and damping coefficient, is limited to either bilinear systems with nearly equal slopes or systems with small nonlinearities or small ductilities [40].

Probably the most reliable method of studying the response of inelastic hysteretic three-dimensional-structures is by Monte-Carlo methods. Statistical parameters can be determined by analyzing an ensemble of time series analyses of structural response to ergodic excitations. The Monte-Carlo methods will be used in this thesis. Chapter II recounts the state of the art in artificial accelerogram generation, its underlying processes, and the parameters affecting it. Ground rotational motion is also described and discussed. Chapter III describes the elastic torsional response of buildings using as the foundation the excitations described in Chapter II. The torsional response is analyzed in the frequency domain. Chapter IV describes the model used in the

inelastic study and the solution technique used to analyze the response. Chapter V lists the results for the inelastic studies and discusses the nonlinear response characteristics.

CHAPTER II

DESCRIPTION OF EARTHQUAKE EXCITATION

Observations of geologists and current thinking on the origin of the earth make it evident that earthquakes have been occurring for at least hundreds of millions of years.

Early historical and biblical references to earthquakes occur as far back as 1600 B.C. [43]. Historical speculation as to the causes of earthquakes has bases in legend, mythology, science, astrology and religion.

Aristotle believed that earthquakes were caused by subterranean winds produced by an evaporation of moisture imprisoned in the earth's crust. Pliny, a Roman philosopher, later expanded on Aristotle's belief, writing that earthquakes were earth's way of punishing the wickedness of men who mine ores of gold, silver and iron, a theme repeated in variation in different cultures around the world.

Zoomorphic qualities are assigned to earthquakes in the legends of many cultures and countries. In Japan, it was thought there was a giant subterranean spider who caused the earth to shake when he moved. In India the mythical monster was a mole; in Mongolia, a hog; and in North America a tortoise [44]. A BSSA account of the 1811 New Madrid, Missouri earthquake[45] tells of a legend claiming that

earthquake to be caused by a horned comet colliding with the earth.

Scandinavian mythology regarding earthquakes concerned the peccadillos of deities. Indian lore contains seven myths concerning earthquake sources. Fascinating accounts of causes of earthquakes abound in the mythologies of various cultures.

Gods of earthquakes are referred to in various mythologies. A common theme in the beliefs of different cultures regards the earthquake as divine punishment visited upon a wicked people. With time natural explanations of earthquakes were expounded and received to varying degrees. In an article in the esteemed Philosophic Transactions of the Royal Society of London in 1750, a writer in his foreword apologized to "those who are apt to be offended at any attempts to give a natural account of earthquakes." As late as 1930, according to newspaper reports (London Times, July 28, 1930), the Archbishop of Naples referred to the Italian earthquake of July 23, 1930 as God's vengeance visited upon an immoral people.

Historical legends and myths are fascinating to read. The evolution of scientific thought is another interesting and related aspect of earthquakes important to the understanding of two geophysical topics, namely, the mechanism and underlying causes of earthquakes. The currently accepted predominant earthquake mechanism, the Elastic Rebound theory, was proposed in 1908 by Harry

Fielding Reid and Andrew Lawson. They were faced with charges of "mysticism" since they presented the mechanism but not the underlying causes of the earthquakes. The Elastic Rebound Theory postulates a slow accumulation of strain along the fault until rupture occurs. The fault then rebounds to a new equilibrium position radiating shock waves outward.

Much speculation concerns the underlying cause of the slow accumulation of strains necessary to the Elastic Rebound mechanism. A prevalent theory of the 19th century was that earthquakes were caused by contraction of the earth by cooling. Most theories on the origin of the earth assume it has cooled from a molten mass. The cooling of the earth through geologic time has solidified the earth down to the molten core, whose existence is theorized by its inability to transmit seismic shear waves. Yet, the surficial layer of the earth is not changing in temperature and therefore is not changing in volume. The crust thus becomes too large to fit the shrinking layers beneath it, resulting in the folding and faulting of crustal diastrophism. The major criticism of the contraction theory is that the folding of the crust and its associated mountain building process should be more widely distributed over the earth's surface.

The isostatic principle has been called into play by other theories. Experiments have shown that a plumb bob does not deflect towards a mountain as it would if the mountain were merely an added mass on the surface. The theory of

isostasy states that at some depth beneath the surface, all columns of the earth's crust are made up of lighter rocks floating on a layer of heavier rocks requiring that mountains have deep roots consisting of these lighter rocks. Accompanying the process of mountain erosion is the reverse plastic flow of rocks beneath it.

Another popular theory regarding the underlying cause is the convection theory. The convection theory presumes, by various causes, temperature differences in the mantle. As a result, convection currents develop similar to those in the atmosphere. The horizontal current near the surface would drag the crust with it. At points of rising convection currents, crustal stretching occurs, resulting in grabens and normal (tension) fault planes. At points of descending convection currents crustal compression results in mountain building and thrust (compression) fault planes. The general criticism of this theory is that it requires cyclical changes in temperature of the earth, whereas large systems such as the earth tend to thermal equilibrium.

Brief mention should also be made of the magmatic theory. This theory requires thermal changes in the earth's crust, bringing about magmatic differentiation and plastic flow of rock.

The theory of continental drift currently enjoys the most widespread support in the scientific community. The original proponent of the theory was Alfred Wegener [46]. As many a grade schooler has observed, the continents of South

America and Africa fit together like pieces of a puzzle. Currrent thinking on the continental drift theory views the earth's surface as having once consisted of one large supercontinent called the Pangaea. Recent researchers in paleomagnetism have reconstructed the Pangaea by analyzing the change in orientation of land masses by studying the direction of the magnetic field of new rocks (lava) in time [47]. As stated, the continental drift theory is now viewed as the most probable source for the slow accumulation of strain required by the Elastic Rebound Theory.

Whatever the nature of the source of earthquakes, the earthquake succussatory ground motion causes distress in civil engineering structures. To understand the effect on structures it is necessary to know the nature of the ground motions. For elastic structures the usual analysis method is by response spectra. Techniques have been developed to obtain the expected response spectra by the statistics of oscillator response [37]. Other methods have been used to obtain plausible "design spectra" [48]. These methods have their roots in the statistics of stationary stochastic processes, i.e. random vibration theory. Although earthquakes are obviously nonstationary, studies have shown that for linear systems, nonstationarity has little effect on the expected response. However, for inelastic systems, the response is sometimes sensitive to the time variation of the energy of the motion[49]. Thus for inelastic systems, Monte-Carlo methods of analysis are desirable. This in turn

requires families or ensembles of stochastically similar ground motions.

Ensembles of "similar" strong motion accelerograms do not exist. In fact, the occurrence of large earthquakes is modeled statistically as a Poisson process, a model for rare events. Thus the need for data creates a need for mathematical modeling of earthquake ground motion.

For low frequencies and epicentral distances large relative to the source dimension, earthquake sources may be approximated by point sources. The assumed force field must be in equilibrium both before and after the earthquake. One such point source meeting the criteria is the double couple. It consists of two couples of opposite sign 90° out of phase. For a pure shear rebound phenomenon in the low frequency limit, the equivalent point source is a double couple (SO). The scale parameter of the double couple is the seismic moment necessary for the assumed source to be in equilibrium. It can be related to the fault dimension and average fault slip.

The energy released in an earthquake for an elastic rebound phenomenon comes from stored elastic energy. The energy is released in the form of frictional heat from the fault slip and as seismic waves. Various mathematical models exist relating the released energy to the fault area, average displacement, and average stress drop over the fault. The stress drop in turn can be related to the fault displacement and geometry. Estimates of maximum ground

acceleration can be made using the aforementioned parameters. Some disagreement centers on the maximum near source acceleration. For frequencies less than 10 Hz, Brune[50] calculates the maximum acceleration as being in the neighborhood of 2g. The maximum ground acceleration recorded to date is 1.25g for the 1971 Pacoima Dam accelerogram of the San Fernando earthquake [51]. Realistically speaking though, in specifying a maximum ground acceleration, the probability of its occurrence must be taken into account, i.e. similar to many design code philosophies, the maximum acceleration should be related to mean recurrence intervals (return periods). Current proposed codes contain a design maximum ground acceleration of 0.4g.

Another quantity necessary for the stochastic description of ground motion is the predominant frequency, the frequency at the peak of the power spectrum. The predominant frequency near the fault is the subject of current research by seismologists and is not well understood. Among the parameters related to the predominant frequency are the crack propagation velocity, fault geometry, fault size, rock strength, topography, and fault breakout. The site predominant frequency is altered by the local geology. The effect of local geologic structure is similar to passing the motion through a filter with appropriate frequency and damping characteristics. Nonhomogeneity of the transmission medium, multiple reflection and refraction, and sometimes

focusing, cause a widening of the band width in the near field for earthquake ground motion. Because of this and the shape of power spectra of actual recorded ground motions, stochastic modelling of ground motion has become popular.

Different types of artificial earthquake ground motion can be generated according to observed peculiar characteristics. Jennings et al. [52] generated artificial accelerograms to represent four different types of ground motion on firm soil. Newmark and Rosenblueth [41] classify earthquakes into four broader groups: 1) practically a single shock near the epicenter of a shallow earthquake, 2) long, wide band strong ground motion on firm soil similar to the 1940 NS El Centro record, 3) long, narrow band motion on soft soil, and 4) large scale permanent deformations with possible landslides or soil liquefaction.

The first type can be analyzed deterministically, using similar recorded ground motion.

The third kind of ground motion can be obtained by filtering the second type.

The fourth type will not be dealt with here.

The second type is the major concern of this thesis. Actual records of this type are more prevalent than other types. Since it is a wide band process, white noise has been used to represent it. Due to its random appearance, communications theory offers many tools to study its probabilistic nature.

Housner [53], Bycroft [54], and Rosenblueth [55], among

others, modeled ground motion of this type as stationary white noise of limited duration by superposition of randomly arriving short duration pulses with random frequency and amplitude.

The average of Fourier amplitude spectra of existing strong ground motion accelerograms shows that the spectra are not white noise but rather are like a broad band process that damps out with higher frequencies. This suggests filtering white noise with appropriate filter characteristics to match the power spectra. Kanai [56] and Tajimi [57] suggested that the transfer function for total response acceleration be selected with filter properties which match the broad band nature of actual accelerogram spectra. The total acceleration transfer function filter will amplify those frequencies near the filter natural frequency and attenuate the higher frequencies. Singularities occur at zero frequency for velocity and displacement. Jennings, Housner, and Tsai [52] used a high pass filter for response displacement to attenuate these very low frequencies. This eliminates the problem since it causes the power at zero frequency to be zero. The average of many accelerogram power spectra fits closely this filtered white noise spectra.

The next refinement was to simulate the nonstationarity of actual accelerograms. The usual procedure is to use an envelope function to vary the intensity of the process. The nonstationary process uses the product of the stationary

stochastic process and the deterministic envelope function. Several types of envelope functions have been used. Jennings et al.[52] separated it into an initial parabolic phase, a constant strong motion phase, and a decaying tail. The parameters for this intensity function are chosen to match the intensity or variance of actual accelerograms. Goto and Toki[58] used a transcendental intensity function of the type

$$I(t) = a \cdot (t/t') \cdot \exp[(t'-t)/t'] \cdot H(t) \qquad 2.1$$

where a, t', and H(t) are, respectively, a constant, the time of peak I(t), and the Heaviside unit step function. Koopmans et al.[59] used a transcendental intensity function of the shape

$$I(t) = a \cdot [\exp(-\alpha \cdot t) - \exp(-\beta \cdot t)] \qquad 2.2$$

where a, α, and β are constants.

Another step in the refinement of artificial accelerograms is the use of Berg and Housner's[60] baseline correction. This procedure minimizes the mean square velocity in order to remove excessively large ground displacements.

The necessity for including the nonstationarity in the artificial accelerograms is determined by its effect on the response. Amin, Tsao, and Ang[49], Koopmans et al.[59] and Shinozuka and Sato[61], among others have studied this effect. The theoretical information contained in extreme

value theory is very helpful in separating the effects of various parameters of the expected response. Also the relation of the variance with time for nonstationary processes resulting from zero initial conditions is necessary to understanding these effects.

The study of Amin et al.[49] reported the deformation spectra of elastoplastic systems (2% damping) using a stationary excitation and a nonstationary excitation of the Jennings et al. [52] type, both with a total duration of 25 sec. The spectra, reproduced in Figure 2-1, show a decrease in response with increasing ductility. The spectra, reported for initial frequency, also show the response for the stationary and nonstationary excitation to be approximately equal for linear structures. The extreme of a stationary Gaussian process is related to the duration by

$$E(\max|y(t)|) \propto \sqrt{\ln(2 \cdot s \cdot F_e)} \qquad 2.3$$

where E( ) denotes expectation, s is the duration and F_e is the average number of zero crossings/sec. of the process. For s = 25 sec. and F_e = 5 Hz, halving the duration only changes the expected response by approximately 6%. The higher ductilities show a decrease in response larger than 6%, as seen in Figure 2-1. The report concludes that the nonstationarity causes a difference in response for high nonlinearity.

It is possible that the difference lies in the effective durations for the stationary and nonstationary excitations

used. The probability of the latter portion of the nonstationary decaying tail containing the extreme is surely remote, i.e. the effect of the type of nonstationarity can be viewed as resulting in a shorter effective duration.

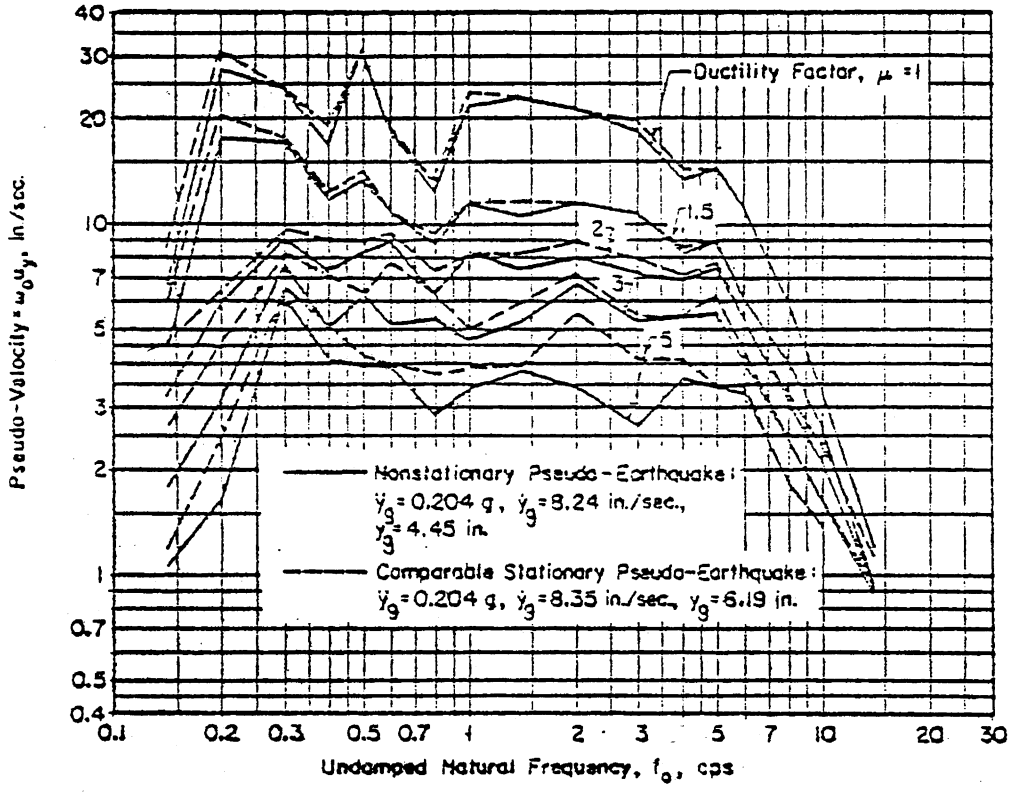

Figure 2-1 Deformation Spectrum for Elastoplastic Systems (B=0.02) [Adapted from Amin et al.[49]]

With increasing ductilities the effective statistical or as sometimes called equivalent linear stiffness decreases. By viewing the elastoplastic response as an equivalent linear system the response nonlinearities tend to reduce the effective natural frequency and increase the effective damping. The possible reduction in natural frequency is presumed the same for the stationary and nonstationary excitation.

The deformation spectrum in Figure 2-1 is shown for ductilities, i.e. maximum displacement nondimensionalized by yield displacement. Penzien and Liu[62], who studied the effect of duration on response, depicted the response of the experimental distribution in the form of Gumbel [63] extreme value Type I charts reproduced in Figure 2-2.

Gumbel Type I extreme value probability distributions vary as

$$P\{Q<X_{max}\} = \exp[-\exp(-Y)]$$

where Q is defined as

$$Q=\max|x(t)|$$

$\bar{Q}$ is the mode of Q and the reduced variate Y is defined as

$$Y=\frac{\sigma_y}{\sigma_q}\cdot[Q-\bar{Q}]$$

and σ_y depends on the number of observed extreme values[64]. Gumbel extreme value charts plot as a straight line with the most probable value at the reduced variate origin. Its slope is proportional to the standard deviation of the extreme values. The slopes in Figure 2-2 increase with increasing nonlinearity implying an increase in the standard deviation of the extreme response, i.e. a larger spread of the values. With an average of a larger number of accelerograms the response spectra anomalies said to be caused by nonstationarity may not be so large since the

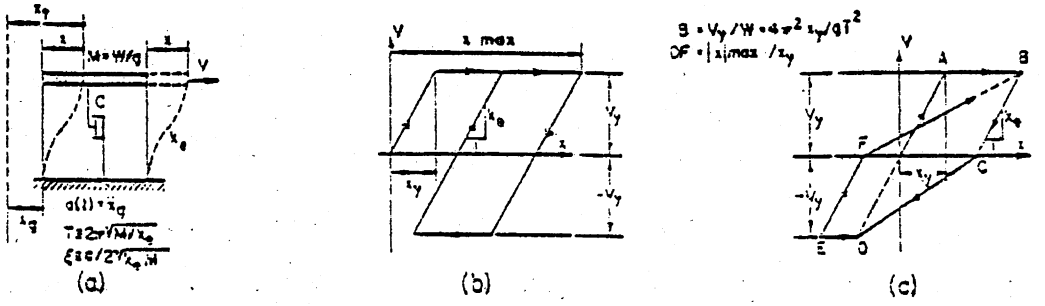

NONLINEAR MODELS OF SINGLE DEGREE OF FREEDOM SYSTEM

TABLE I

CASE NO.	STRUCTURAL TYPE *	PERIOD T-SEC	DAMPING RATIO-ξ	STRENGTH RATIO-β	YIELD DISPL X - IN.	σ_x IN.	$\bar{x}$ IN.	u IN.	I/α
1	E	0.3	0.02	-	-	0.115	0.768	0.722	0.085
2	EP	0.3	0.02	0.10	0.088	1.613	3.214	2.450	1.390
3	SD	0.3	0.02	0.10	0.088	0.711	2.480	2.144	0.613
4	E	0.3	0.10	-	-	0.050	0.354	0.330	0.043
5	EP	0.3	0.10	0.10	0.088	0.910	1.947	1.517	0.784
6	SD	0.3	0.10	0.10	0.088	0.360	1.327	1.157	0.310
7	E	2.7	0.02	-	-	3.07	14.15	12.73	2.59
8	EP	2.7	0.02	0.048	3.42	5.51	16.35	13.75	4.75
9	SD	2.7	0.02	0.048	3.42	5.83	14.32	11.56	5.02
10	E	2.7	0.10	-	-	1.31	8.77	8.24	0.97
11	EP	2.7	0.10	0.048	3.42	4.56	11.57	9.41	3.94
12	SD	2.7	0.10	0.048	3.42	3.25	9.98	8.45	2.80

* E – ELASTIC
EP – ELASTO-PLASTIC
SD – STIFFNESS DEGRADING

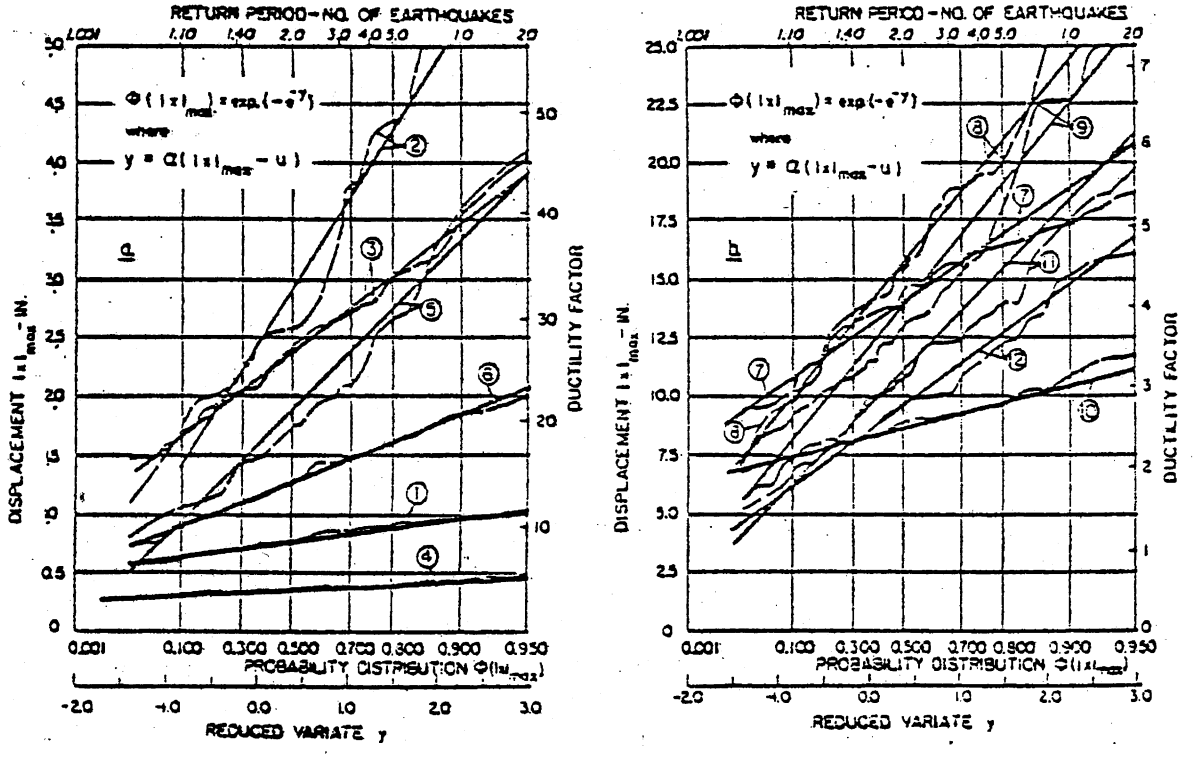

PROBABILITY DISTRIBUTION FOR EXTREME VALUES OF RELATIVE DISPLACEMENT

Figure 2-2 Probability Distribution for Extreme Values of Relative Displacement[Adapted from Penzien and Liu(62)]

spread of the values increases with increasing nonlinearity. The Amin et al. report[49] apparently used an average of eight accelerograms, a rather small statistical sample from which to draw conclusions.

To give an example of the effect of nonstationarity, consider the extreme response from the level crossing approach. Crandall[65] presents an excellent state of the art review. As shown shown in Figure 2-3 the extreme values have a specific probability distribution. The usual method in first passage problems is to determine the mean, mode, or median of the extreme values in terms of its standard deviation, e.g. the most probable extreme is the product of the standard deviation of the response and a peak factor, R. The asymptote of the most probable peak factor for white noise is

$$R = \sqrt{2 \cdot \ln(2.9 \cdot N)} \qquad 2.4$$

where N is the number of cycles the system has undergone, i.e. the natural frequency times the duration. For nonwhite excitation the peak factor is a function of the average number of zero crossings (usually near the natural frequency), the damping, the probability of exceedance, the duration, and a parameter similar to the coefficient of variation of the maxima. An approximate expression for the peak factor R, is[66]

$$R=\sqrt{2\cdot\ln\{2\cdot N\cdot[1-\exp(-\delta\cdot\sqrt{\pi\cdot\ln(2\cdot N)})]\}} \qquad 2.5$$

where δe, a measure of the spread of the power spectrum is

$$\delta e=[1-M_1^2/(M_0\cdot M_2)]^{0.6} \qquad 2.6$$

and M_i, the ith moment of the power spectra about the origin is

$$M_i=\int_{-\infty}^{\infty}\omega^i\cdot G^2(\omega)\cdot d\omega \qquad 2.7$$

The equivalent parameter values derived from the Amin report could decrease the peak factor, R, as much as 13% by halving the duration. Although the different duration would also affect the standard deviation, the difference is negligible for the damping used. The decrease in response thus appears to be caused more by the effective duration than the effect of nonstationarity.

This says nothing, of course, for the effect of nonstationarity of the transcendental type, e.g. Equation 2.1 or Equation 2.2. Here the time rate of change of the intensity and the duration both combine to affect the expected response. An exact solution for the stationary first passage problem does not exist. However, for a sufficient number of cycles the asymptote gives a very good approximation.

Approximate techniques for nonstationary response are just starting to receive attention. For nonstationarity due

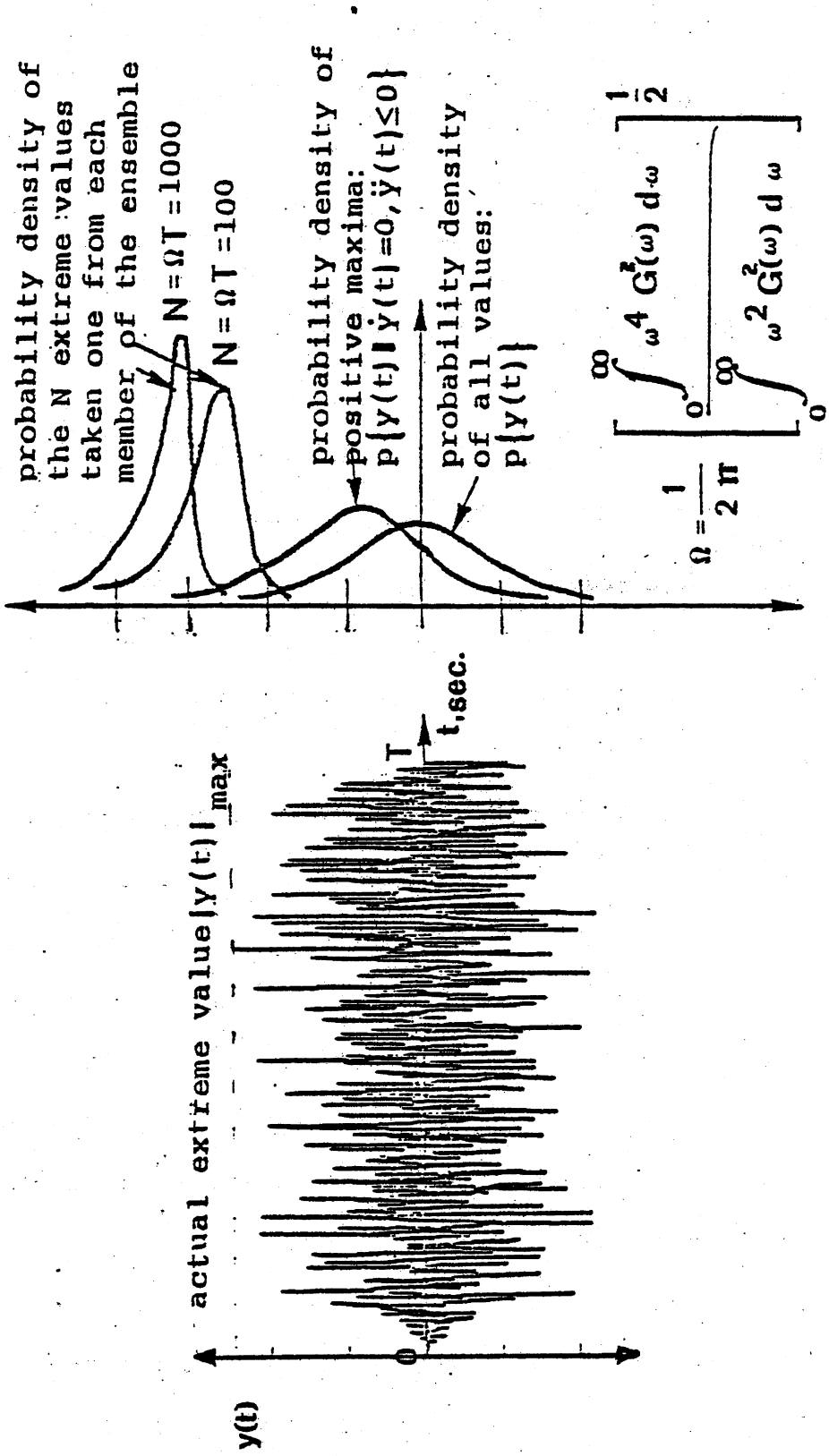

Figure 2-3 Schematic of the statistical distributions for stochastic processes.

to transient response of stationary excitation, one method is to use an equivalent duration. For nonstationary linear response due to nonstationary excitation with a transcendental intensity function, the most logical approach is to consider the extreme a function of the total energy, i.e. proportional to the integral of the intensity function. This follows from stationary response extremes being the product of the standard deviation or power and the peak factor which is proportional to the duration. One approach would be to obtain the marginal probability density function of the maxima by integrating out time dependence of the variance in the Davenport[67] derivation. The statistics of nonstationary peak response are beyond the scope of this report.

Kubo and Penzien[68] studied the accelerograms of the 1971 San Fernando earthquake. Their resulting intensity functions resemble the transcendental intensity function more closely than they resemble the Jennings et al.[52] intensity function. Kubo and Penzien also showed distinct jumps in the phase of the cross correlation between the horizontal ground accelerogram, possibly linked to the arrival of different waves.

Saragoni and Hart[69] presented a method for generating artificial accelerograms incorporating nonstationary power spectra. They used three discrete power spectra for different phases of the duration in order to simulate the decrease in the predominant frequency with time. They used

a transcendental intensity function of the form

$$I(t) = a \cdot t^{\gamma} \cdot \exp(-\varepsilon \cdot t) \qquad 2.8$$

where a, γ, and ε are constants determined by a best fit analysis of existing accelerograms. This concept of evolutionary power spectra is not new. Nevertheless, it immensely complicates the statistics of extreme response making it nearly intractable.

The Saragoni and Hart reports show the intensity function to vary for different earthquakes. Also the phases of the discrete power spectra would change with fault orientation and epicentral distances. A method to simulate this was presented by Rascon and Cornell[70], who produced artificial accelerograms from a physically based model. Their simulation involved a superposition of randomly arriving dilatational and distortional single pulses with a Poisson arrival distribution from a number of elementary foci. The elementary foci generate the single pulses along the fault plane, moving according to the crack propagation velocity. Attenuation was based on spherical spreading and multiple reflection and refraction. The duration and the parameters were based on statistical studies relating these parameters to magnitude, epicentral distances, etc. The resulting simulations closely resemble actual accelerograms.

The preceding descriptions of the various methods to generate artificial accelerograms indicate the increasing

complexity that accompanies more faithful simulation of ground motions. For a particular site of given local geology, many factors are being introduced that influence the accelerograms, such as fault size, orientation, seismic potential, distance from the fault, etc. This emphasizes the nonuniversality of accelerograms and the care with which they should be selected for particular sites. For these reasons, the accelerograms used here will be generated by the computer program PSEQGEN[71]. This program generates ensembles of filtered white noise with an intensity function of the Jennings et al.[55] type to represent strong ground motion on firm soil. The use of these artificial accelerograms should present no drawback through its generality since this dissertation is a study of general building response and not a particular site.

The program PSEQGEN can generate ensembles of stochastically similar artificial accelerograms. Individual members of the ensemble can be used to represent the two orthogonal horizontal ground motions. They will, however, be uncorrelated. Penzien and Watabe[72] have shown that the correlation between the two orthogonal horizontal ground motions will be a minimum in the near field when one is pointed in the direction of the epicenter. They concluded that ground motions generated artificially can be uncorrelated provided the components are directed along principal axes which are perpendicular and parallel to the fault. The fact that the correlation is minimum and

negligible when parallel and perpendicular to the fault is not surprising when you consider the nature of shear and compression waves. Also, Pascon[73] has shown that single degree of freedom response is maximum when the structure is oriented along one of these same principal axes. For these reasons and the argument expounded in Appendix B, this dissertation uses uncorrelated horizontal ground motions.

A complete description of the ground motion involves six components: three translational and three rotational. The two rotational components of rocking whose axes are in the horizontal plane are not included in this analysis. In addition, the vertical translation component will not be included. This leaves the two horizontal translations and the rotation whose axis is vertical. As previously mentioned the horizontal motions will be artificially generated to resemble actual accelerograms and will be statistically uncorrelated. The origin of torsional ground motion is generally thought to be Love waves which are horizontally polarized shear waves near the surface(see Figure 2.4). The torsional motion arises from the quantity $\frac{\partial V}{\partial x}$. The motion V(x) is related to the frequency F, wave speed C_s, and wave length λ, where

$$C_s = F \cdot \lambda \qquad 2.9$$

While the wave speed can be determined, the random nature of the motion is such that there will be a random mixture of frequencies determined by the power spectra. Artificial

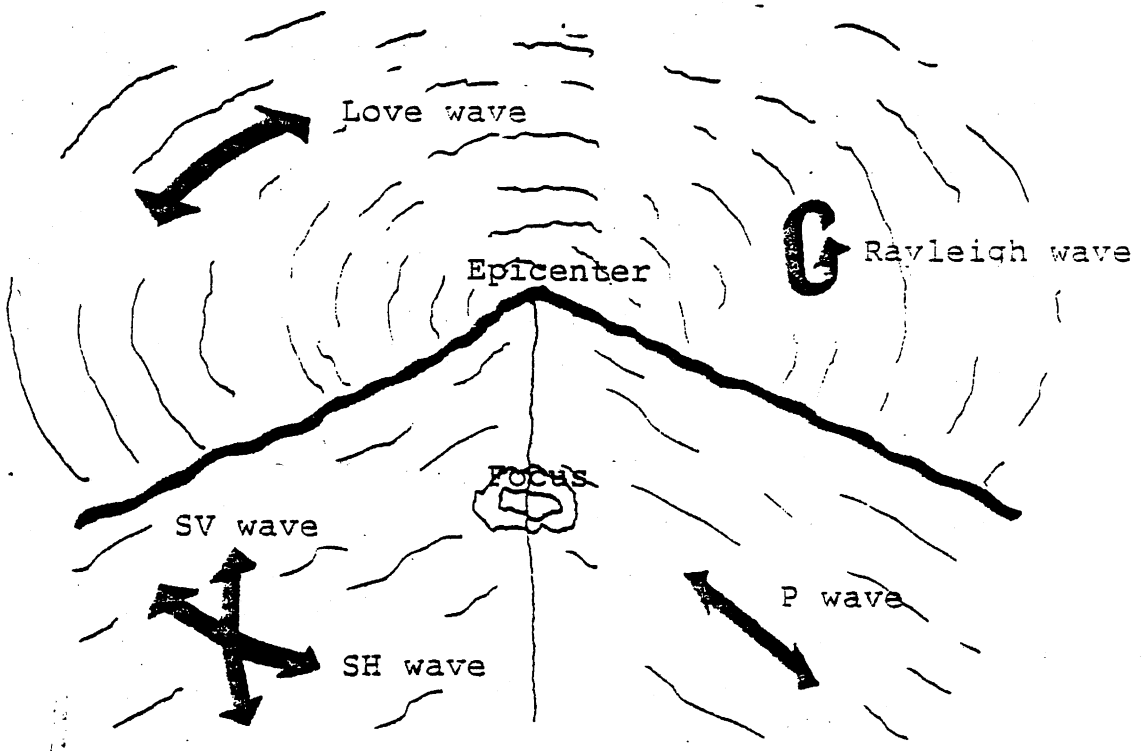

a) Lagrangian description

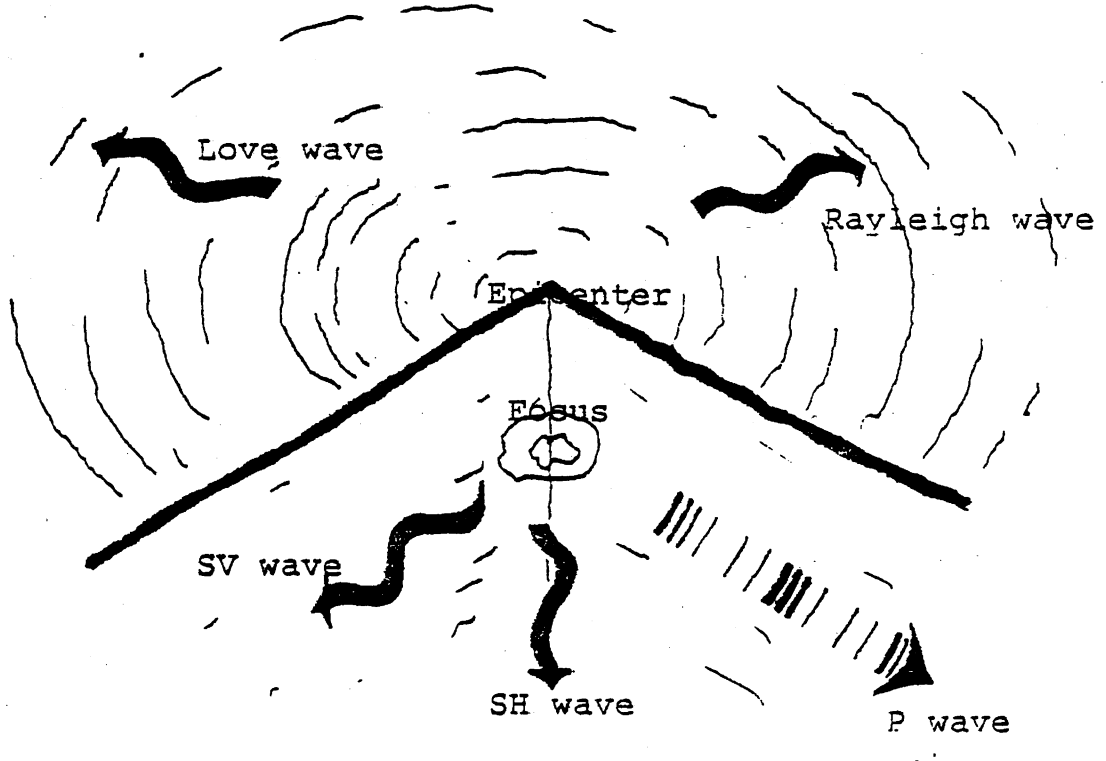

b) Eulerian description

Figure 2-4 Elastic Earthquake Waves

translation accelerograms are based on the average power spectra of many actual earthquake accelerograms. There are yet no reported torsion accelerograms; thus, one cannot determine the correlation between torsion and translation. Neither can the power spectra be determined.

Some means of generating earthquake ground rotation is desired. Starting from the assumption that horizontal surface motion is derived from the nearly vertical refraction of shear waves at the base rock soil interface, Newmark[25] proposed a method to determine the rotation based on the theory of elasticity. That the refraction is nearly vertical arises from a consideration of the respective wave velocities and Snell's Law (Figure 2.5). Thus at the free surface the refracted waves will travel at the wave velocity of the rock not the soil. Newmark calculates the ground rotation ϕ, as

$$\phi = \frac{1}{2}\left[\frac{\partial V}{\partial x} - \frac{\partial U}{\partial y}\right] \qquad 2.10$$

With the ground motions U and V uncorrelated and stochastically similar, the ground motion simplifies to

$$\phi = \frac{\partial V}{\partial x} \qquad 2.11$$

With the further assumption that

$$V = V(t - x/C_s)$$

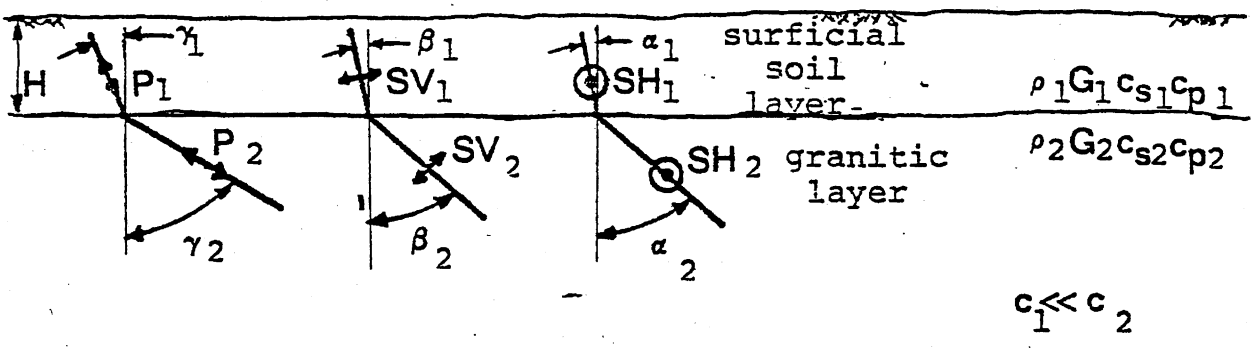

$$\frac{\sin\gamma_1}{c_{P_1}}=\frac{\sin\gamma_2}{c_{P_2}} \quad \frac{\sin\beta_1}{c_{SV_1}}=\frac{\sin\beta_2}{c_{SV_2}} \quad \frac{\sin\alpha_1}{c_{SH_1}}=\frac{\sin\alpha_2}{c_{SH_2}}$$

a) Near Vertical Refraction into Surface Soil Layer

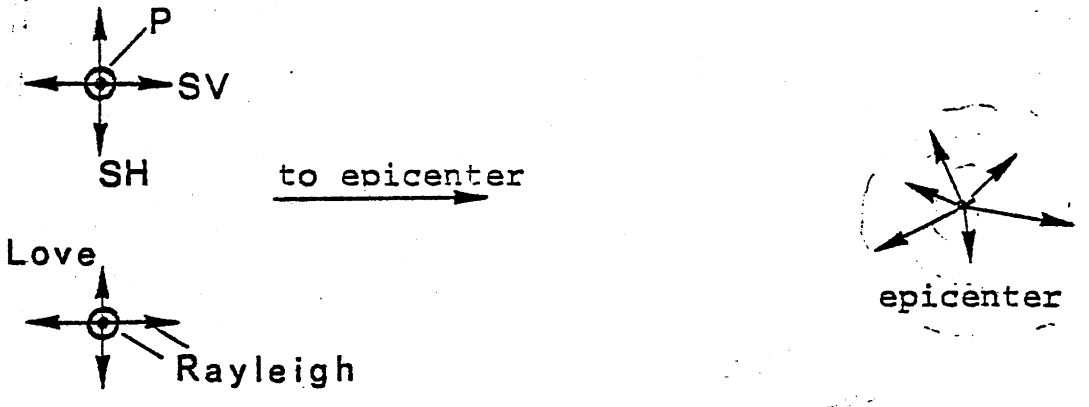

b) Plan view of Simplified ground surface point translation due to different wave types.

Figure 2-5 Surface Wave Motion

$$\phi=\frac{\dot{V}}{C_s} \qquad 2.12$$

Rosenblueth[74] proposed a modification of this to account for the building size. Since Equation 2.12 is valid for a point, the effective or average displacement determined by assuming a rigid building and neglecting back-scattering is

determined by assuming a [illegible]

and neglecting backscattering is

$$\bar{V} = \frac{1}{B} \int_{-B/2}^{B/2} V(t - x/C_s) \cdot dx \qquad 2.13$$

where B is the building width transverse to the motion V. For a sinusoidal translation, Equation 2.13 reduces to

$$\bar{V} = \frac{\sin(\pi \cdot B \cdot \lambda) \cdot \sin(\omega \cdot \tau)}{\pi \cdot B \cdot \lambda} \qquad 2.14$$

where λ is the wavelength. Figure 2.6 depicts the effect of the building length to wavelength ratio has in decreasing the effective translation according to Rosenblueth's assumption. Observations of earthquake damage reinforce this notion that civil engineering works covering larger ground area respond with less intensity.

Nathan and MacKenzie [75] calculated the torsion response spectra by use of Equation 2.12 in a finite difference form expressed in terms of acceleration rather than displacement

$$\ddot{\sigma} = [\ddot{V}(t + \tau) - \ddot{V}(t)] / (C_s \cdot \tau) \qquad 2.15$$

Finite difference techniques are based on small, finite changes where the function is assumed to vary smoothly between the points. The ground acceleration is assumed linear between the digitized values since very high frequencies are deemed unimportant in building response.

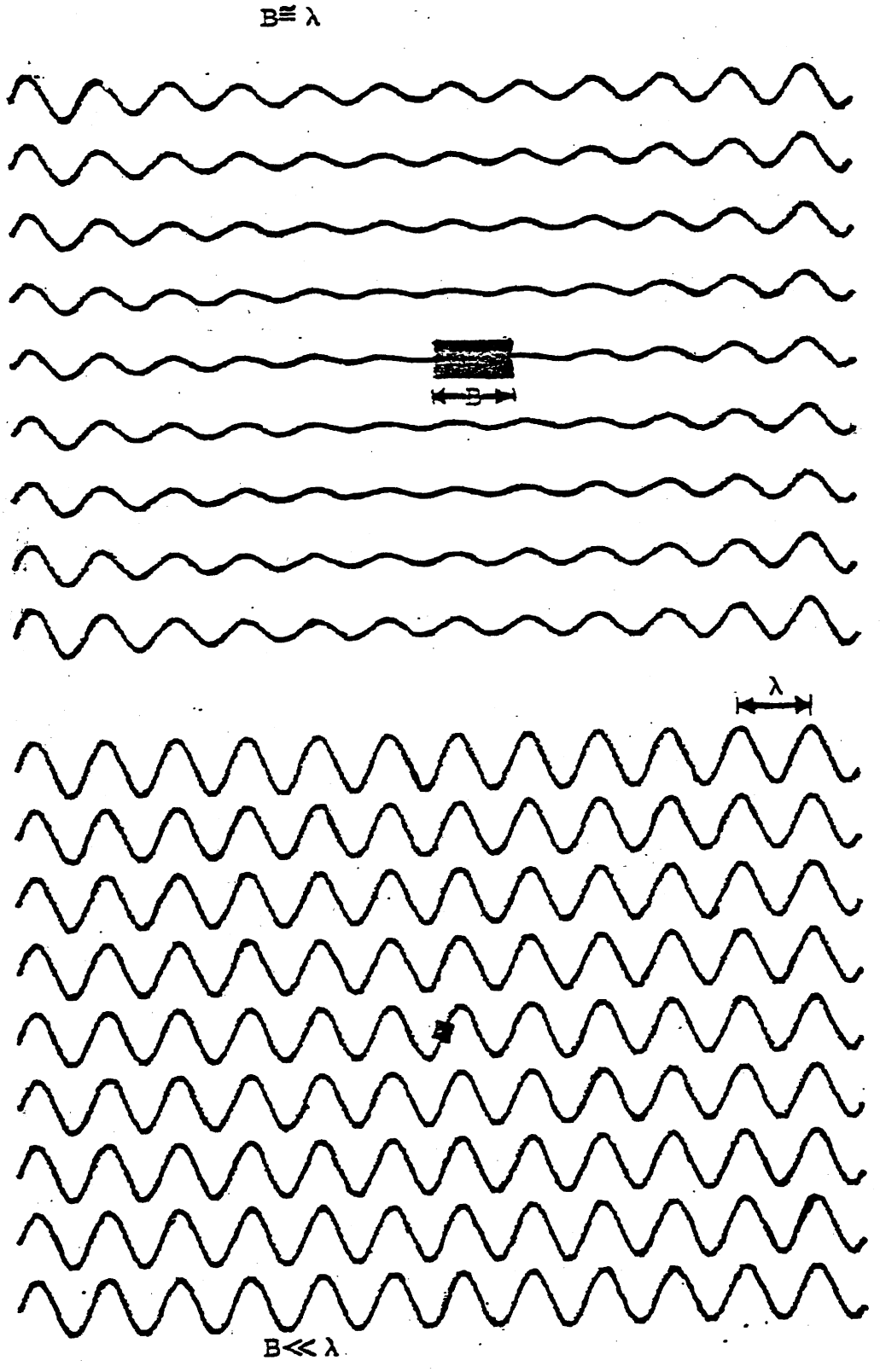

Figure 2-6 Schematic of Effect of Building Width to Wavelength Ratio in Average Translation Neglecting Backscattering

With typical values of the digitizing interval of 0.025 sec, the maximum value allowable for the transit time would be of the order of 0.025 sec. For a wave speed of 300 m/sec and a building width transverse to the motion of 30m the transit time of a shear wave is 0.1 sec, or 4 digitizing intervals. Figure 2-7 illustrates the deficiency of the finite difference approach.

Currently, Newmark et al.[76] are studying the effect of building size or transit time by calculating the response spectra for the input acceleration averaged over the transit time, τ, as

$$\ddot{\bar{V}} = \frac{1}{\tau}\int_{t}^{t+\tau} \ddot{V}(t)\cdot dt = \frac{1}{\tau}[\dot{V}(t+\tau) - \dot{V}(t)] \qquad 2.16a$$

and

$$\dddot{\bar{V}} = \frac{6\cdot[\dot{V}(t+\tau)+\dot{V}(t)]}{C_s\cdot\tau^2} - \frac{12\cdot[V(t+\tau)-V(t)]}{C_s\cdot\tau^3} \qquad 2.16b$$

where $\dddot{\bar{V}}$ is proportional to the third derivative of V, calculated as $\ddot{\Delta V}/\tau$, which in turn is determined by a least squares fit of $\ddot{V}$ over time τ (Figure 2-7). Figure 2-8 shows the effect of this averaging in reducing the extreme values. The excitation used for generating Figure 2-8 was an ensemble of ten stationary filtered white noise accelerograms of 10 sec. duration using the filter

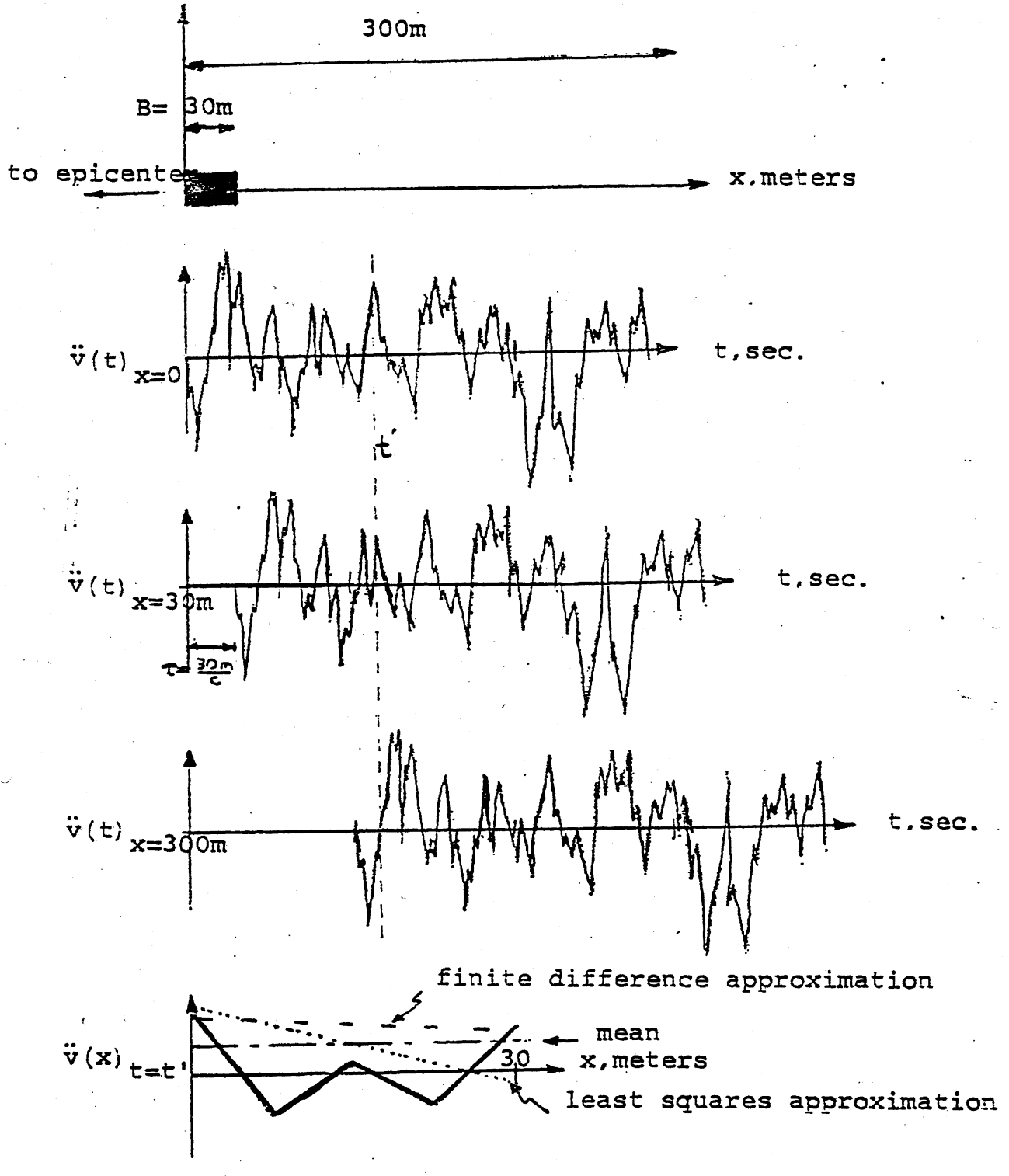

Figure 2-7 Effect of Transit Time on Averaging

characteristics of PSEQGEN [71].

Another method for analyzing the effect this averaging has on building response is frequency domain analysis. The averaged response is the result of convolving the excitation with the averaging filter. As shown in Appendix A, the resulting power spectrum is reduced by the factor multiplying $\sin(\omega t)$ in Equation 2.14. The resulting reduction of the power spectra reduces the excitation variance, which in turn reduces the expected peak value. The response power spectrum is the product of the input power spectrum, averaging filter, and the complex frequency response function. It is readily apparent that the variance and thus the peak response should decrease more for higher frequencies. This expected trend is verified in Figure 2-8.

The transit time reduction increases with increasing building size. Also, it is dependent on the assumed wave speed which is dependent on the assumed wave type. For small buildings this reduction will be slight. Another source for the reduction of idealized input excitation is the soil-structure interaction. Luco[77] found the effect of embedment of the foundation to be quite significant. The excitation used in Luco's study was obliquely incident SH waves. The input twist for a hemispherical foundation was determined to be half that of a circular disk foundation. This reduction was attributed to the effect of scattering and the increased foundation stiffness. The results are presented in a nondimensionalized form via a frequency ratio

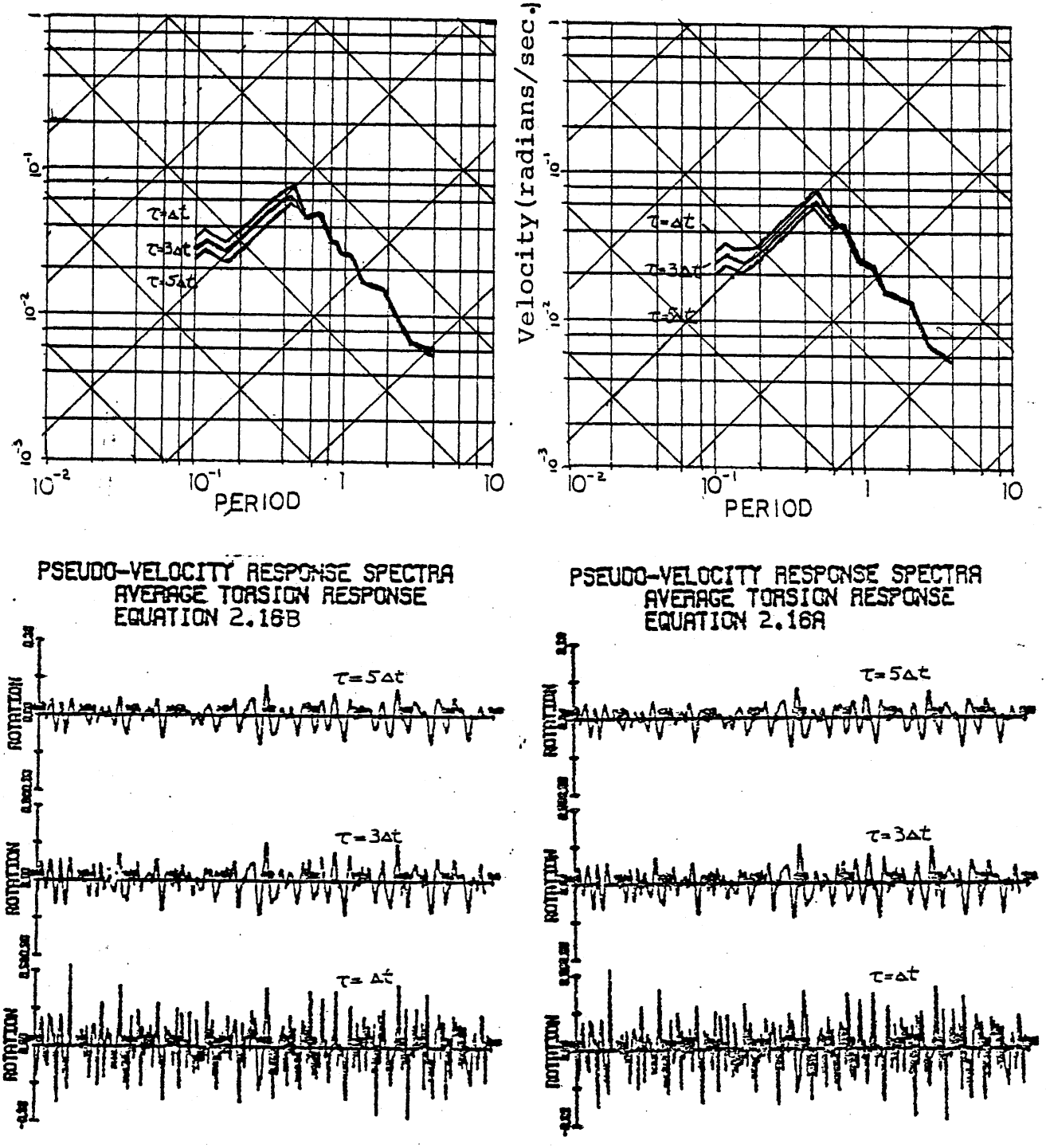

Figure 2-8 Effect of Transit Time τ, on Response

parameter commonly used in foundation dynamics which is proportional to the foundation size to wavelength ratio.

Yet another reduction in the expected maximum ground torsion is discussed by Newmark and Rosenblueth. Their proposed reduction is due to the statistical relation between extreme values in the orthogonal direction.

As evident, the Newmark approach to ground torsion can be viewed as an upper limit. The values determined are reduced by building to wavelength ratios, soil-structure interaction, scattering, etc. Since the Uniform Building Code does not include ground rotation, Newmark's values for ground rotation will be used in this thesis to determine its effect.

The need for actual free-field rotation and translation records is apparent. It is especially necessary to determine the correlation between ground rotation and translation and its relative effect.

CHAPTER III

ELASTIC RESPONSE

Buildings with coincident centers of mass and stiffness are called uncoupled systems in this thesis. For the dynamic analysis of uncoupled systems, responses along the principal directions are analyzed independently. When an eccentricity between the centers of mass and stiffness exists, the responses along the principal axes are coupled. Analyzing the responses along the principal axes independently may give good results if these three frequencies are well separated and the eccentricities are not too large. Full scale tests[27] have confirmed the strong coupling that occurs with close natural frequencies even if the eccentricities are small.

The usual design procedure to account for an eccentric mass is to add a force due to the torque, calculated as the product of story shear and eccentricity. Many studies[24, 36] have shown that the dynamic story shear decreases when there is an eccentricity and that the dynamic torque exceeds the product of shear and eccentricity. For tall buildings consisting of moment resisting planar frames, although lateral-torsional coupling decreases the total story shear, the story torque increases the shear in the peripheral

lateral force resisting elements. Thus the statement that story shear decreases, must not be taken to imply that lateral-torsional coupling is beneficial.

The torsional response of large civil engineering works such as bridges and pipelines is a result of eccentricities as well as the horizontal ground motion not being in phase over the length of the structure. This type of structure is not considered in this study. There is of course torsional ground motion; however, the effect of ground rotation as studied in this chapter is based on Newmark's [24] treatment of the subject, which is described in Chapter II.

The objective of this chapter is to formulate a method to study the elastic response of torsionally coupled buildings by modal analysis based on statistical concepts similar to that developed by Rosenblueth[24], but extended to three-dimensional systems. This method will be used primarily to show the effect of ground rotation and the absence of correlation between the horizontal ground translations.

Structural Systems

Most tall buildings are either shear wall type, moment frame type, or a combination of the two. Shear wall buildings are commonly multiply connected vertical plates like that illustrated in Figure 3-1a). For this type of building, shear flow must be considered. A moment frame type building is illustrated in Figure 3-1b). Both will be

assumed to have rigid floor diaphragms.

The origin of the principal axes of these structural systems is the center of stiffness (sometimes called center of rigidity, resistance, twist or torsion, or shear center). The principal axes are orthogonal and are defined such that a force in the direction of one of the principal axes causes a displacement only in that direction.

The principal axes in a moment frame system consisting of planar frames that are not orthogonal are determined by statics[24].

Once the principal axes have been determined the lateral stiffness in the principal directions can be determined as

$$K_x = \sum_i K_{xi}$$

$$K_y = \sum_i K_{yi}$$

while the torsional stiffness, defined about the center of mass and neglecting individual element torsional stiffnesses, is

$$K_\phi = \sum_i K_{xi} \cdot Y_i^2 + \sum_i K_{yi} \cdot Y_i^2$$

The eccentricities are

$$E_x = \sum_i X_i \cdot K_{yi} / K_y$$

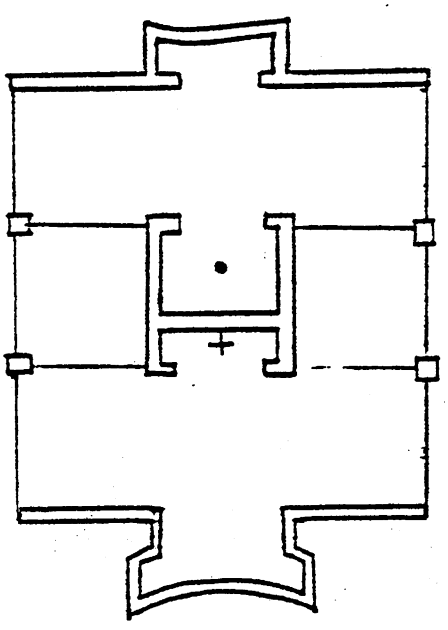

a) Shear Wall Type

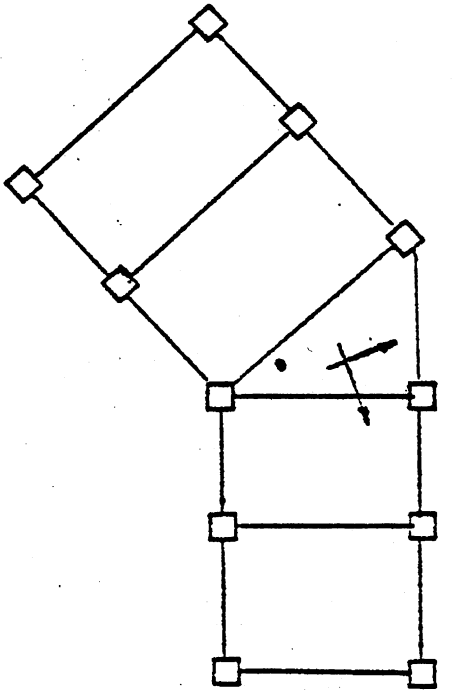

b) Moment Frame Type

Figure 3-1 Structural Systems

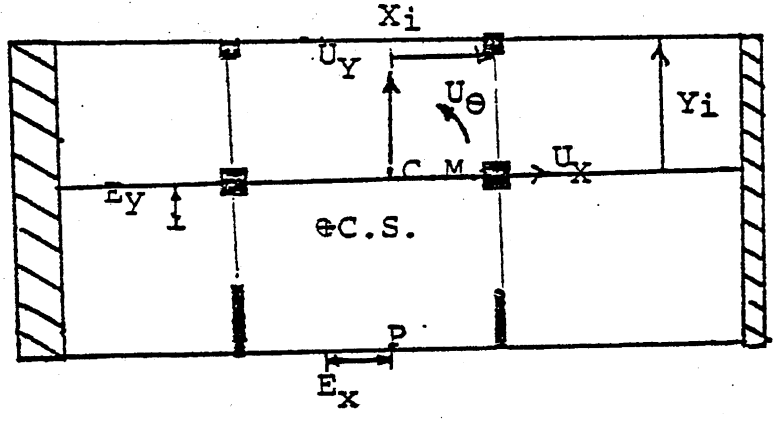

Figure 3-2 Example Building Layout

$$E_y = \sum_i Y_i \cdot K_{xi} / K_x$$

for X_i and Y_i as shown in Figure 3-2.

Analysis of an N-story structure generally requires 3N degrees of freedom. Shiga[42] and Hoerner[26] have developed a procedure to simplify this to N three degree of freedom systems. The mode shape is

$$\{A_{nj}\} = \begin{Bmatrix} C_{xn} \cdot \{D_j\} \\ C_{\phi n} \cdot \{D_j\} \\ C_{yn} \cdot \{D_j\} \end{Bmatrix}$$

for structures where the story masses are colinear, the story stiffnesses are colinear, and the ratio of the lateral stiffnesses is the same for all stories. $\{C\}_n$ is the nth mode of the 3DOF system and $\{D_j\}$ is the jth mode of the NDOF system, which is the same for x, ø, and y.

Generally, it is assumed that the first three mode shapes of a multistory structure are two primarily translation modes and the primarily torsion mode. The torsion frequency is nearly always less than twice the fundamental. The second mode in the fundamental direction is usually greater than 3 times the fundamental; so, the translation stiffnesses would have to be an order of magnitude different before the assumption would not be true. A multistory structure can be analyzed approximately as a three degree of freedom system by using the first three

modes as described above.

Equations of Motion

The equations of motion for the single story three degree of freedom system shown in Figure 3-2 are

$$\begin{bmatrix} \ddot{U}_x \\ R\cdot\ddot{U}_\phi \\ \ddot{U}_y \end{bmatrix} + \begin{bmatrix} \omega_x^2 & -\omega_x^2\cdot E_y/R & 0 \\ -\omega_x^2\cdot E_y/R & \omega_\phi^2 & \omega_y^2\cdot E_x/R \\ 0 & \omega_y^2\cdot E_x/R & \omega_y^2 \end{bmatrix} \begin{bmatrix} U_x \\ R\cdot U_\phi \\ U_y \end{bmatrix} = -\begin{bmatrix} \ddot{U}_{gx} \\ R\cdot\ddot{U}_{g\phi} \\ \ddot{U}_{gy} \end{bmatrix} \qquad 3.1$$

where M is the mass, R is the radius of gyration, and

$$\omega_x=(K_x/M)^{0.5} \quad \omega_y=(K_y/M)^{0.5} \quad \omega_\phi=(K_\phi/I_p)^{0.5} \quad I_p=M\cdot R^2 .$$

The characteristic equation for this system is

$$\omega^6-[\omega_x^2+\omega_y^2+\omega_\phi^2]\cdot\omega^4 +[\omega_x^2\cdot\omega_y^2+\omega_y^2\cdot(\omega_\phi^2-\omega_y^2\cdot E_x^2/R^2)+\omega_x^2\cdot(\omega_\phi^2-\omega_x^2\cdot E_y^2/R^2)]\cdot\omega^2 -[\omega_x^2\cdot\omega_y^2\cdot(\omega_\phi^2-\omega_y^2\cdot E_x^2/R^2-\omega_x^2\cdot E_y^2/R^2)]=0 \qquad 3.2$$

or

$$F^3+P\cdot F^2+Q\cdot F+R=0$$

where $F=\omega^2$.

Let $C=(3-P^2)/3$, and $D=(2\cdot P^3-9\cdot P\cdot Q+27\cdot R)/27$

and $A=[-D/2+(D^2/4+C^3/27)^{0.5}]^{1/3}$, $B=[-D/2-(D^2/4+C^3/27)^{0.5}]^{1/3}$

then the coupled frequencies can be directly computed as

$$\omega_1^2 = -(A+B)/2 - (A-B)\cdot(-3)^{0.5}/2 - P/3$$

$$\omega_2^2 = -(A+B)/2 + (A-B)\cdot(-3)^{0.5}/2 - P/3 \qquad 3.3$$

$$\omega_3^2 = A+B-P/3$$

The solution can be unstable for some extreme combinations of eccentricities and uncoupled frequencies.

For $E_x, E_y \neq 0$ and $\omega_y \neq \omega_x$ the unnormalized mode shapes are

$$[A] = \begin{bmatrix} 1 & -\omega_x^2 \cdot E_y / R & -\omega_x^2 \cdot E_y \cdot (\omega_3^2 - \omega_y^2) \\ & (\omega_2^2 - \omega_x^2) & \omega_y^2 \cdot E_x \cdot (\omega_3^2 - \omega_x^2) \\ -(\omega_1^2 - \omega_x^2) & 1 & (\omega_3^2 - \omega_y^2) \\ \omega_x^2 \cdot E_y / R & & \omega_y^2 \cdot E_x / R \\ -\omega_x^2 \cdot E_y \cdot (\omega_1^2 - \omega_x^2) & \omega_y^2 \cdot E_x / R & 1 \\ \omega_y^2 \cdot E_x \cdot (\omega_1^2 - \omega_y^2) & (\omega_2^2 - \omega_y^2) & \end{bmatrix}$$

or, if $E_y \neq 0$ and $E_x = 0$

$$[A]=\begin{bmatrix} 1 & \dfrac{-\omega_x^2 \cdot E_y/R}{(\omega_2^2-\omega_x^2)} & 0 \\ \dfrac{-(\omega_1^2-\omega_x^2)}{\omega_x^2 \cdot E_y/R} & 1 & 0 \\ 0 & 0 & 1 \end{bmatrix}$$

and if $E_x=E_y=0$

$$[A]=\begin{bmatrix} 1 & 0 & 0 \\ 0 & 1 & 0 \\ 0 & 0 & 1 \end{bmatrix}$$

which is the mode shape of the uncoupled system.

Once the uncoupled frequencies and mode shapes have been determined, the maxima can be estimated by modal combination. The usual method is the root sum square(RSS)

$$Q=\left(\sum_i Q_i^2\right)^{0.5} \qquad 3.4$$

which is based on the assumption of near independence of modal responses. The modal responses are nearly independent if the frequencies are well separated. In an analysis of a planar structure, the ratio of frequencies are approximately 1:3:5:...;however, in three-dimensional systems the

frequencies can be very close together.

In systems where the frequencies are close together the usual procedure in modal combination is to use a method proposed by Rosenblueth[24] in which the distribution of the response q(t) is assumed to be Gaussian with zero mean. The necessary further assumption, consistent with extreme value theory, is that the maximum response $Q=\max|q(t)|$ is proportional to the standard deviation, i.e.

$$E(Q)^2 \propto \langle q^2(t) \rangle \quad . \qquad 3.5$$

where $E(\ )$ denotes expectation and $\langle\ \rangle$ denotes time average.

The response can be expressed in terms of its impulse response function, h, as

$$q(t)=\int_{-\infty}^{t} h(t-t') \cdot z(t')\,dt'$$

or in discretized form

$$q(t)=\int_{-\infty}^{t} h(t-t') \cdot z(t') \cdot dt' = h_1 z_1 + h_2 z_2 + \ldots + h_n z_n \qquad 3.6$$

where z(t) is white noise of intensity G_o.

With the further assumption that each term in Equation 3.6 is independent, the variance of q becomes

$$\langle q^2(t) \rangle = \Sigma(h^2 \cdot z^2) \qquad 3.7$$

and by the Cauchy-Schwarz inequality, $\Sigma(h^2 \cdot z^2) \leq \Sigma h^2 \cdot \Sigma z^2$,

$$\langle q^2(t)\rangle \leq \Sigma h^2 = c\int_{-\infty}^{t} h^2(t-t')\cdot dt' = c\int_{0}^{\infty} h^2(t)\cdot dt \qquad 3.8$$

for Gaussian excitation. The inequality in Equation 3.8 becomes a proportionality by virtue of Parseval's relation,

$$\int_{-\infty}^{\infty} h^2(t)\,dt = [\int_{-\infty}^{\infty} |H(\omega)|^2 d\omega]/(2\cdot\pi) = \langle q^2(t)\rangle/(G_o^2\cdot 2\cdot\pi) \qquad 3.9$$

where $H(\omega)$, the complex frequency response function, is the Fourier transform of the transfer function $h(t)$, and G_o^2 is the intensity of the white noise excitation.

For a MDOF system, by expressing the response $q(t)$ as the sum of its modal values

$$q(t) = \sum_i q_i(t)$$

and inserting this in terms of its modal transfer function into Equation 3.8 Rosenblueth obtains

$$Q^2 = \sum_i Q_i^2 + \sum_{i\neq j}\sum \frac{Q_i\cdot Q_j}{1+E_{ij}^2} \qquad 3.10$$

$$E_{ij}^2 = \frac{\omega_{di}-\omega_{dj}}{B_i\cdot\omega_i + B_j\cdot\omega_j}$$

where B_i is the ith mode's fraction of critical damping and ω_{di} the ith mode's damped natural frequency. The quantity $1/(1+E_{ij}^2)$ can be interpreted as the correlation coefficient.

To understand the limitations of Equation 3.10 due to its underlying assumptions, it is necessary to understand its derivation and the effect of the assumptions. For this reason a modal combination expression will be derived based on Rosenblueth's approach, i.e. maximum square response proportional to the variance; but the mathematical approach will be in the frequency domain rather than the time domain.

The expected peak response is likewise presumed proportional to the standard deviation, the root of the variance. The mean square value in turn will be described by the complex frequency response function, i.e.

$$\langle Y_m(t) \cdot Y_n(t) \rangle = \int_{-\infty}^{\infty} G_{Y_m Y_n}{}^2(\omega) \cdot d\omega \qquad 3.11$$

where

$$G_{Y_m Y_n}{}^2(\omega) = H_{Y_m}(\omega) \cdot \overline{H_{Y_n}}(\omega) \cdot G_{Z_m Z_n}{}^2(\omega) \qquad 3.12$$

and $G_{Z_m Z_n}{}^2(\omega)$ is the cospectrum of the mth and nth DOF's excitation.

Usually the input excitation is assumed to be white noise to simplify the mathematics. Initially, this same assumption will be made in the following derivation. Thus Equation 3.11 becomes

$$\langle Y_m(t) \cdot Y_n(t) \rangle = \int_{-\infty}^{\infty} H_{Y_m}(\omega) \cdot \overline{H_{Y_n}}(\omega) \cdot G_o{}^2 \cdot d\omega \quad . \qquad 3.13$$

$H_{Y_m}(\omega)$ is by definition

$$H_{Y_m}(\omega) = 1/\{[\omega_m{}^2 + i \cdot 2 \cdot B_m \cdot \omega_m \cdot \omega - \omega^2] \cdot M_m{}'\} \qquad 3.14$$

where M_m' is the modal mass and ω_m and B_m are the mth natural frequency and fraction of critical damping, respectively.

The response is expressed in terms of its modal responses, and thus the variance of the response is expressed in terms of the modal variances and covariances. The equations of motion for a MDOF system with classical modes are

$$[M]\{\ddot{X}\}+[C]\{\dot{X}\}+[K]\{X\}=-[M]\{\ddot{Z}\} \quad .$$

In uncoupled form where $[A]$ is the matrix of eigenvectors and $\{Y\}=[A]\{X\}$,

$$\{\ddot{Y}\}+[2\cdot B\cdot \omega]\{\dot{Y}\}+[\omega^2]\{Y\}=-[M']^{-1}[A]^T[M]\{\ddot{Z}\}\equiv-[M']^{-1}[A]^T\{P\} \qquad 3.15$$

where $[M']=[A]^T[M][A]$.

A response quantity of interest $q(t)$ can be expressed as

$$q(t)=\sum_n C_{rn}\cdot Y_n(t)=\{C_r\}^T\cdot\{Y(t)\} \qquad 3.16$$

and by definition,

$$G_q^2(\omega)=\sum_m\sum_n C_{rm}\cdot C_{rn}\cdot G_{Y_mY_n}^2(\omega) \qquad 3.17$$

Combining Equations 3.12, 3.15, and 3.17 gives

$$G_q^2(\omega) = \{C\}^T [H_Y(\omega)]^H [A]^T [G_p^2(\omega)] [A] [H_Y(\omega)] \{C\} \qquad 3.18$$

For a two-dimensional system,i.e. planar frames, each degree of freedom is subjected to the same excitation and each element of the matrix $[G_Z^2(\omega)]$ is the same. Introducing this into Equation 3.18, rearranging terms and integrating gives

$$\langle q^2(t) \rangle = \sum_m \sum_n (C_m \cdot MPF_m) \cdot (C_n \cdot MPF_n) \cdot \langle Y_m(t) \cdot Y_n(t) \rangle \qquad 3.19$$

where MPF_m is the modal participation factor for mode m, defined as

$$MPF_m = \left(\sum_n M_n \cdot A_{mn} \right) / \left(\sum_n M_n \cdot A_{mn}^2 \right) \quad . \qquad 3.20$$

and $\{Y(t)\}$ is the solution to Equation 3.15 where the right hand side is just $\{\ddot{Z}\}$.

Equation 3.19 can be rewritten as

$$\langle q^2(t) \rangle = \sum_{mn} \sum (C_m \cdot MPF_m) (C_n \cdot MPF_n) \langle Y_m^2(t) \rangle^{.05} \cdot \langle Y_n^2(t) \rangle^{.05} \cdot P_{mn} \qquad 3.21$$

where P_{mn} is the correlation coefficient of $Y_m(t)$ and $Y_n(t)$. Since the RMS value is assumed proportional to the peak value,Q, Equation 3.21 can be rewritten as

$$Q^2 = \sum_{mn} \sum Q_m \cdot Q_n \cdot P_{mn} \qquad 3.22$$

where Q_m, the peak response of the mth mode, is

$$Q_m = C_m \cdot MPF_m \cdot S_v(\omega_m) \qquad 3.23$$

and

$$P_{mn} = \beta \cdot (\omega_m \cdot B_m + \omega_n \cdot B_n) \cdot (\omega_m^3 \cdot B_m \cdot \omega_n^3 \cdot B_n)^{0.5} / |D|^2 \qquad 3.24$$

$$D = [(\omega_{dm}^2 - \omega_{dn}^2) - (\omega_m \cdot B_m + \omega_n \cdot B_n)^2] + i \cdot [2 \cdot \omega_{dm} \cdot (\omega_m \cdot B_m + \omega_n \cdot B_n)]$$

(see Appendix C for derivation). For small damping Equation 3.24 gives values of the correlation very close to those inherent in Equation 3.10.

Equation 3.22 has two limiting assumptions, namely white noise excitation and identical excitation for each degree of freedom. As explained in Appendix D, the effect of the white noise assumption is not considered significant for cases of practical interest. The effect of the second assumption is not so evident. It is clear though, that the second assumption is not valid for a three-dimensional system. For the two-dimensional system each element of the matrix of $[G_Z^2(\omega)]$ is the same but for the three dimensional system it is

$$[G_Z^2(\omega)] = \begin{bmatrix} G_{Z_x}^2(\omega) & G_{Z_x Z_\phi}^2(\omega) & G_{Z_x Z_y}^2(\omega) \\ G_{Z_\phi Z_x}^2(\omega) & G_{Z_\phi}^2(\omega) & G_{Z_\phi Z_y}^2(\omega) \\ G_{Z_y Z_x}^2(\omega) & G_{Z_y Z_\phi}^2(\omega) & G_{Z_y}^2(\omega) \end{bmatrix} . \qquad 3.25$$

where $\{Z\} = \{U_{gx} \quad R \cdot U_{g\phi} \quad U_{gy}\}^T$

Chapter II describes the current state of the art in ground motion description.

Equation 3.25 can be greatly simplified by incorporating the approximations described in Chapter II, namely Newmarkian ground rotation and uncorrelated ground translations. For ground rotation defined as

$$\ddot{Z}_{\phi} = \frac{R}{2}\left[\frac{d\ddot{Z}_y}{dx} - \frac{d\ddot{Z}_x}{dy}\right]$$

the excitation, following Newmark's procedure is

$$\ddot{Z}_{\phi} = [\ddot{Z}_y - \ddot{Z}_x]\cdot R/(2\cdot C_s) \qquad 3.26$$

where C_s is the shear wave speed in the underlying rock. Since we are assuming uncorrelated ground translations we can set $G_{\ddot{Z}_x\ddot{Z}_y}{}^2(\omega)=0$. The autocovariance function for the ground rotational excitation is

$$R_{\ddot{Z}_{\phi}}(\tau) = E[\ddot{Z}_{r\phi}(t)\cdot\ddot{Z}_{r\phi}(t+\tau)]$$

Inserting Equation 3.26 gives

$$R_{\ddot{Z}_{\phi}}(\tau) = [R_{\ddot{Z}_y}(\tau) - 2\cdot R_{\ddot{Z}_y\ddot{Z}_x}(\tau) + R_{\ddot{Z}_x}(\tau)]\cdot(R/(2\cdot C_s))^2$$

For uncorrelated but equal spectral density ground translations, this reduces to

$$R_{\ddot{Z}_{\phi}}(\tau) = 2\cdot R_{\ddot{Z}_y}(\tau)\cdot(R/(2\cdot C_s))^2$$

Thus,

$$G_{\ddot{Z}_{r\phi}}{}^2(\omega) = (R^2/2\cdot C_s{}^2)\cdot G_{\ddot{Z}_y}{}^2(\omega)$$

$$= (R^2/2 \cdot C_s^2) \cdot \omega_g^2 \cdot G_{\ddot{Z}_y}^2(\omega)$$

and

$$\int_{-\infty}^{\infty} G_{\ddot{Z}_{r\phi}}^2(\omega) \cdot d\omega = (R^2/2 \cdot C_s^2) \frac{\int_{-\infty}^{\infty} \omega^2 \cdot G_{\ddot{Z}_y}^2(\omega) \cdot d\omega \cdot \int_{-\infty}^{\infty} G_{\ddot{Z}_y}^2(\omega) \cdot d\omega}{\int_{-\infty}^{\infty} G_{\ddot{Z}_y}^2(\omega) \cdot d\omega}$$

$$= (R^2/2 \cdot C_s^2) \cdot \omega_g^2 \cdot \int_{-\infty}^{\infty} G_{\ddot{Z}_y}^2(\omega) \cdot d\omega$$

where ω_g is the predominant frequency.

The crosscovariance function for rotation and translation is

$$R_{\ddot{Z}_\phi \ddot{Z}_x}(\tau) = E[\ddot{Z}_{r\phi}(t) \cdot \ddot{Z}_x(t+\tau)]$$

$$= \{E[\ddot{Z}_y(t) \cdot \ddot{Z}_x(t+\tau)] - E[\ddot{Z}_x(t) \cdot \ddot{Z}_x(t+\tau)]\} (R/2 \cdot C_s)$$

$$= 0 - E[\ddot{Z}_x(t) \cdot \ddot{Z}_x(t+\tau)] \cdot (R/2 \cdot C_s)$$

$$= - \frac{R}{2 \cdot C_s} \frac{dR_{\ddot{Z}_x}}{d\tau}$$

where

$$R_{\ddot{Z}_x}(\tau) = \int_{-\infty}^{\infty} G_{\ddot{Z}_x}^2(\omega) \cdot \exp(-i \cdot \omega \cdot \tau) \cdot d\omega$$

Differentiating this gives

$$R_{\ddot{Z}_\phi \ddot{Z}_x}(\tau) = (R/2 \cdot C_s) \cdot \int_{-\infty}^{\infty} i \cdot \omega \cdot G_{\ddot{Z}_x}^2(\omega) \cdot \exp(-i \cdot \omega \cdot \tau) \cdot d\omega$$

$$= \int_{-\infty}^{\infty} G_{\ddot{Z}_{r\phi} \ddot{Z}_x}^2(\omega) \cdot \exp(-i \cdot \omega \cdot \tau) \cdot d\omega$$

Thus,

$$G_{\ddot{Z}_{r\phi}\ddot{Z}_x^2}(\omega) = (R/2 \cdot C_s) \cdot i \cdot \omega \cdot G_{\ddot{Z}_x^2}(\omega)$$

where $G_{\ddot{Z}_x^2}(\omega)$ is real, symmetric and

$$\langle \ddot{Z}_{r\phi} \cdot \ddot{Z}_x \rangle = \int_{\infty}^{\infty} G_{\ddot{Z}_{r\phi}\ddot{Z}_x^2}(\omega) \cdot d\omega = (R/2 \cdot C_s) \int_{\infty}^{\infty} i \cdot \omega \cdot G_{\ddot{Z}_x^2}(\omega) \cdot d\omega = 0$$

For $\xi \equiv R \cdot \omega_g / (2 \cdot C_s)$, Equation 3.25 reduces to

$$[G_{\ddot{Z}^2}(\omega)] = \begin{bmatrix} 1 & 0 & 0 \\ 0 & 2\xi^2 & 0 \\ 0 & 0 & 1 \end{bmatrix} \cdot G_{\ddot{Z}_x^2}(\omega) \qquad 3.27$$

For $C_s = F_g \cdot \lambda$, λ being the seismic wavelength in the underlying rock and F_g the corresponding frequency, ξ becomes $\pi \cdot R/\lambda$. Combining Equation 3.27 and 3.18 and integrating gives Equation 3.21 where $MPF_m \cdot MPF_n$ is now

$$MPF_m \cdot MPF_n = A_{1m} \cdot A_{1m} + A_{3m} \cdot A_{3m} + 2 \cdot \cdot A_{2m} \cdot A_{2n} \qquad 3.28$$

The RMS value determined by using Equation 3.23 should be less than that calculated using Equation 3.20 because the latter assumes all degrees of freedom have the same excitation and are thus identical.

As an example, consider the shear wall building analyzed by Heidebrecht [28], which is shown in Figure 3-3 with the corresponding frequencies and mode shapes. The fundamental mode is predominantly y motion, the second mode predominantly x motion and the third mode mostly rotation. The values of C_i for the y displacement of point B, $A_{3i} + 17m/R \cdot A_{2i}$ are

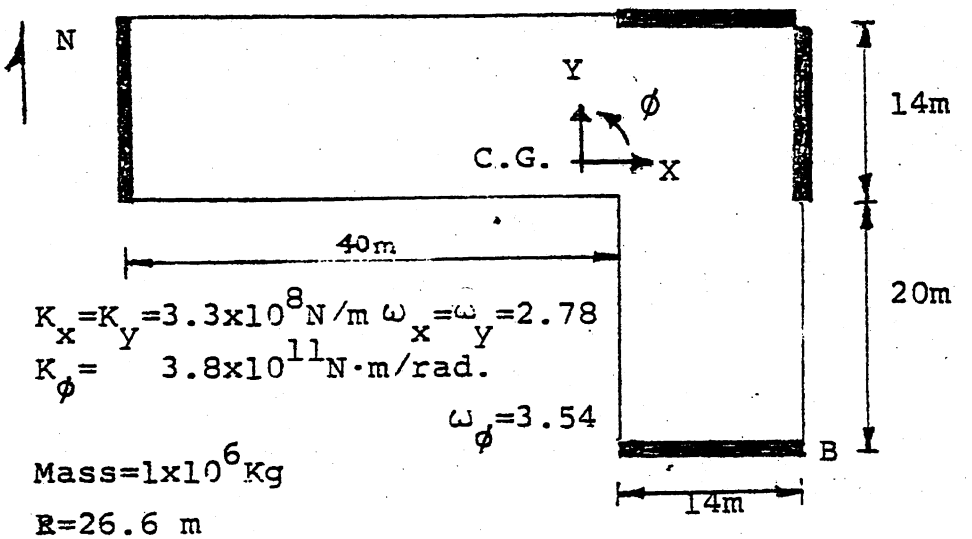

$K_x = K_y = 3.3 \times 10^8$ N/m $\omega_x = \omega_y = 2.78$

$K_\phi = 3.8 \times 10^{11}$ N·m/rad. $\omega_\phi = 3.54$

Mass $= 1 \times 10^6$ Kg

R = 26.6 m

$E_x = -10$m

$E_Y = -5$m

Mode 1

$f_1 = 2.46$cps

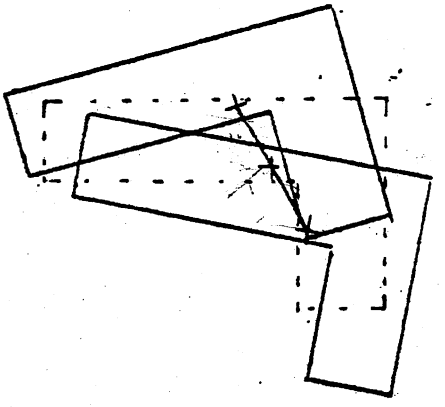

$$A_1 = \begin{Bmatrix} A_{1x} \\ A_{1\phi} \\ A_{1y} \end{Bmatrix} = \begin{Bmatrix} -.4 \\ .45 \\ .80 \end{Bmatrix}$$

Mode 2

$f_2 = 2.78$ cps

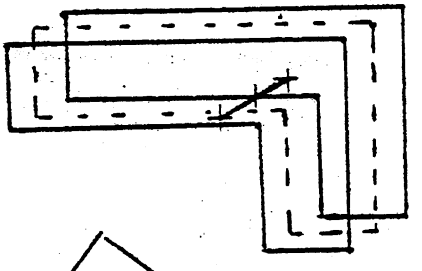

$$A_2 = \begin{Bmatrix} .89 \\ .0 \\ .45 \end{Bmatrix}$$

Mode 3

$f_3 = 3.76$cps

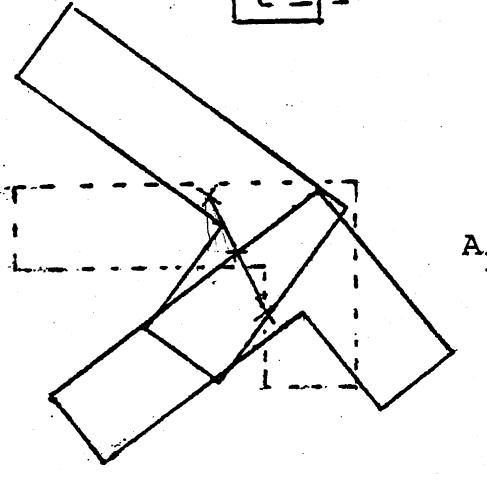

$$A_3 = \begin{Bmatrix} .20 \\ .89 \\ -.40 \end{Bmatrix}$$

Figure 3-3 Example Building and Coupled Modes
[Adapted from Heidebrecht[28]]

$$\{C\} = \{.45 \quad .17 \quad 1.09\}^T \quad .$$

The matrix of correlation coefficients P_{mn}, the same for Equations 3.10 and 3.24 are

$$[P_{mn}] = \begin{bmatrix} 1.0 & .09 & .00 \\ .09 & 1.0 & .07 \\ .00 & .07 & 1.0 \end{bmatrix}$$

which assumes a percentage of critical damping of 5% in each mode.

The modal participation factors as calculated by Equation 3.28 for a wavelength of 1000m, are

$$[MPF_{mn}] = \begin{bmatrix} 0.80 & -0.39 & 0.00 \\ -0.39 & 0.02 & -0.00 \\ 0.00 & -0.00 & 1.00 \end{bmatrix} \quad .$$

The matrix of the mean square modal values as determined by Equations 3.22, 3.24 and 3.28 are

$$\begin{bmatrix} 2.73 & -0.02 & 0.00 \\ -0.02 & 0.02 & 0.00 \\ 0.00 & 0.00 & 12.27 \end{bmatrix}$$

for the response spectrum shown in Figure 3-4.

The RMS displacement of point B is thus 3.87

centimeters. By means of comparison, if Equation 3.20 were used instead of Equation 3.28 the RMS displacement would be 4.88 centimeters, and if the absolute sum of the modal values were used it would be 5.51 centimeters.

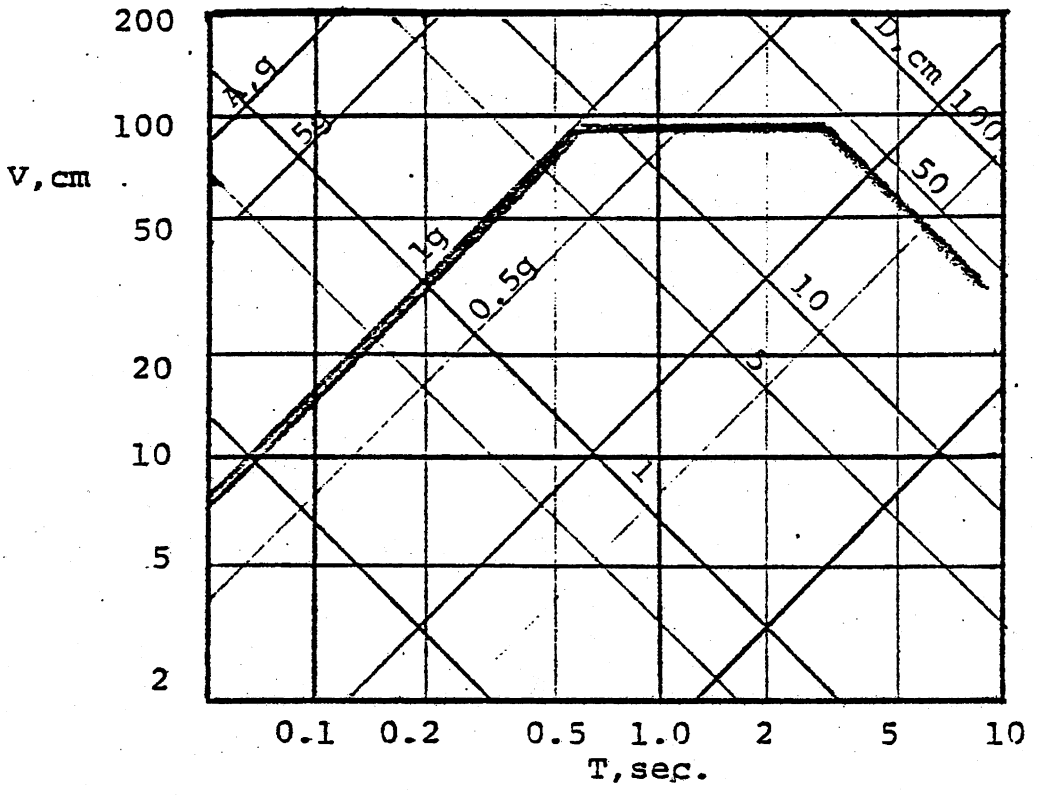

Figure 3-4 Example Design Response Spectrum

The difference between the values for Equation 3.28 and 3.20 lies in the correlation of the excitations. The former assumes only the spectra to be the same while the latter assumes the spectra and the excitations themselves to be identical.

Another way of showing this effect is by a graph of the interaction equations. Rosenblueth and Elorduy [24] and Kan and Chopra [36] presented the effect of torsional coupling as graphs of the dynamic forces, nondimensionalized by the

uncoupled force in the direction of the excitation, versus a nondimensional frequency ratio for a flat acceleration spectrum. The torque is presented as the ratio of dynamic to static eccentricity.

For a ground excitation consisting of only X translations, Kan and Chopra[36] also derived the interaction surface of the normalized forces as

$$\bar{V}_x^2+\bar{V}_y^2+\bar{T}^2 = 1$$

where the bar denotes the value normalized by the uncoupled force in the direction of the excitation, i.e. for $E_x=E_y=0$.

Figure 3-5 shows the interaction between the forces for a ground excitation consisting of only Y translation with a flat acceleration spectrum. The forces are not normalized here.

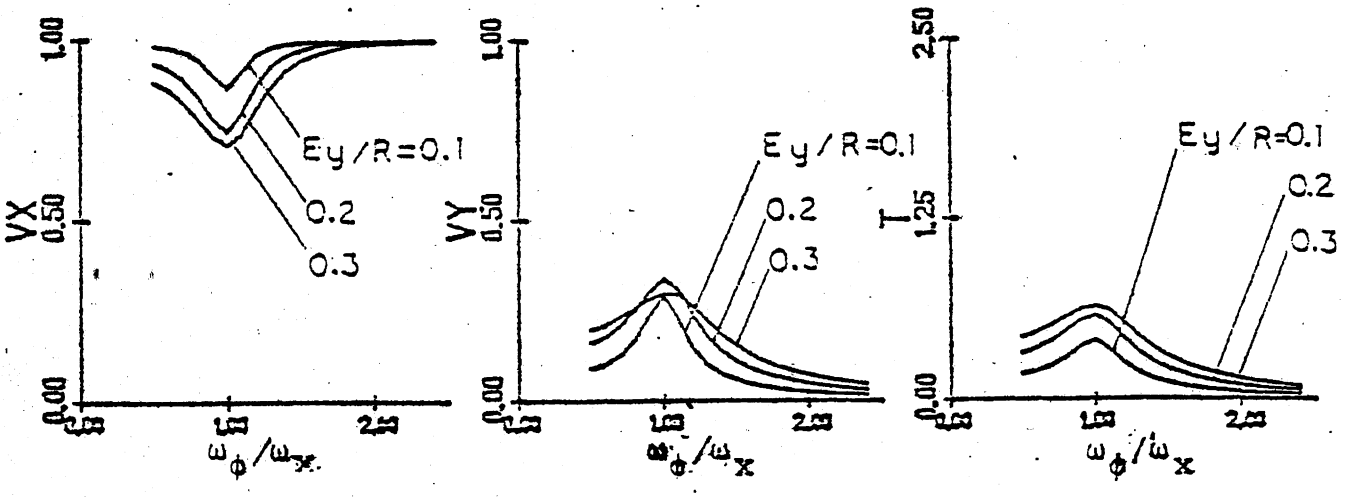

Figure 3-5 Force Interaction for X Ground Excitation Only and Flat Acceleration Spectrum ($E_x/R=0, \omega_y/\omega_x=1$)

The effect of the coupling is to decrease the shear in

the X direction while causing a shear in the Y direction and a torque.

For a ground excitation consisting of rotation only, a similar interaction for a flat acceleration spectrum is shown in Figure 3-6 for different values of the radius of gyration to wavelength ratio. Here the effect of the coupling is to decrease the torque while inducing building shears. The decrease in the torque for different eccentricity ratios shown in Figure 3-6 is much less than the decrease in the shear in the direction of excitation as shown in Figure 3 5.

Interaction relations can also be derived for systems with simultaneous X, ø, and Y excitations. For uncorrelated ground translations, and ground rotation excitation defined by Equation 3.26, all the excitations are uncorrelated as shown by Equation 3.27. For uncorrelated excitations the variance of the sum of the modal responses is the sum of the response modal variances and the interaction surface is

$$\bar{V}_x^2+\bar{V}_y^2+\bar{T}^2 = 2(1+\xi^2) \qquad 3.29$$

Figure 3-7 shows the interaction between the forces for excitations described by Equation 3.27 and with flat acceleration spectra.

The increases in the shear for higher levels of the radius of gyration to wavelength ratio are not great. Although Figure 3-6 shows an increase in the shears due to the ground rotation, the decrease in shear shown in

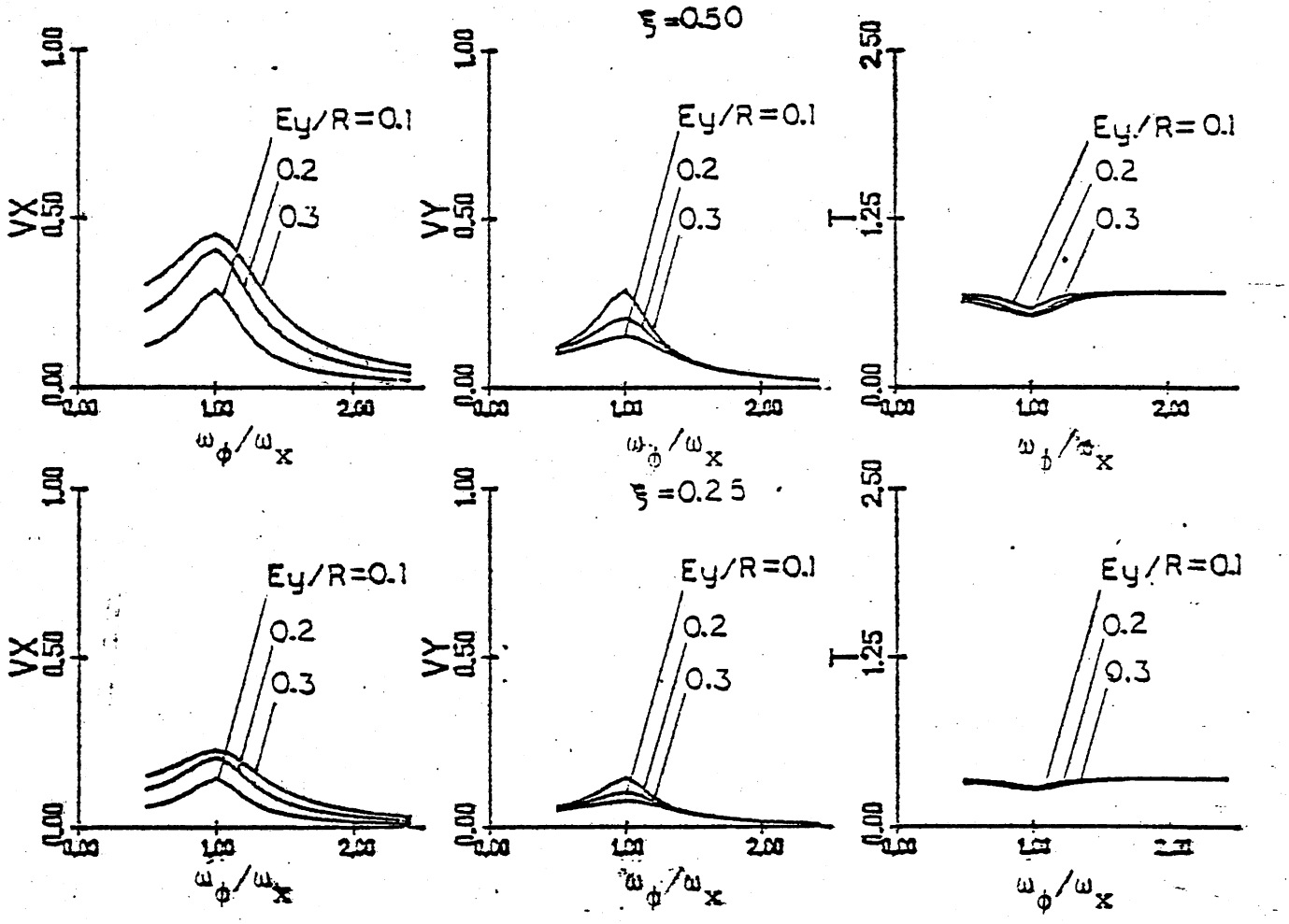

Figure 3-6 Force Interaction for o Ground Excitation Only and Flat Acceleration Spectrum ($E_x/R=0, \omega_y/\omega_x=1$)

Figure 3-5 for the ground translation excitation more than offsets this as shown in Figure 3-7. Also, it must be remembered that the shortest wavelength of interest is of the order of 600-1000 meters since the reasoning behind the ground rotation excitation assumes the wavelength to be that associated with the underlying rock and the shortest natural periods of interest are 0.2 sec. or longer. Thus for typical building sizes the ratio ξ will be of the order 0.0-0.1. As

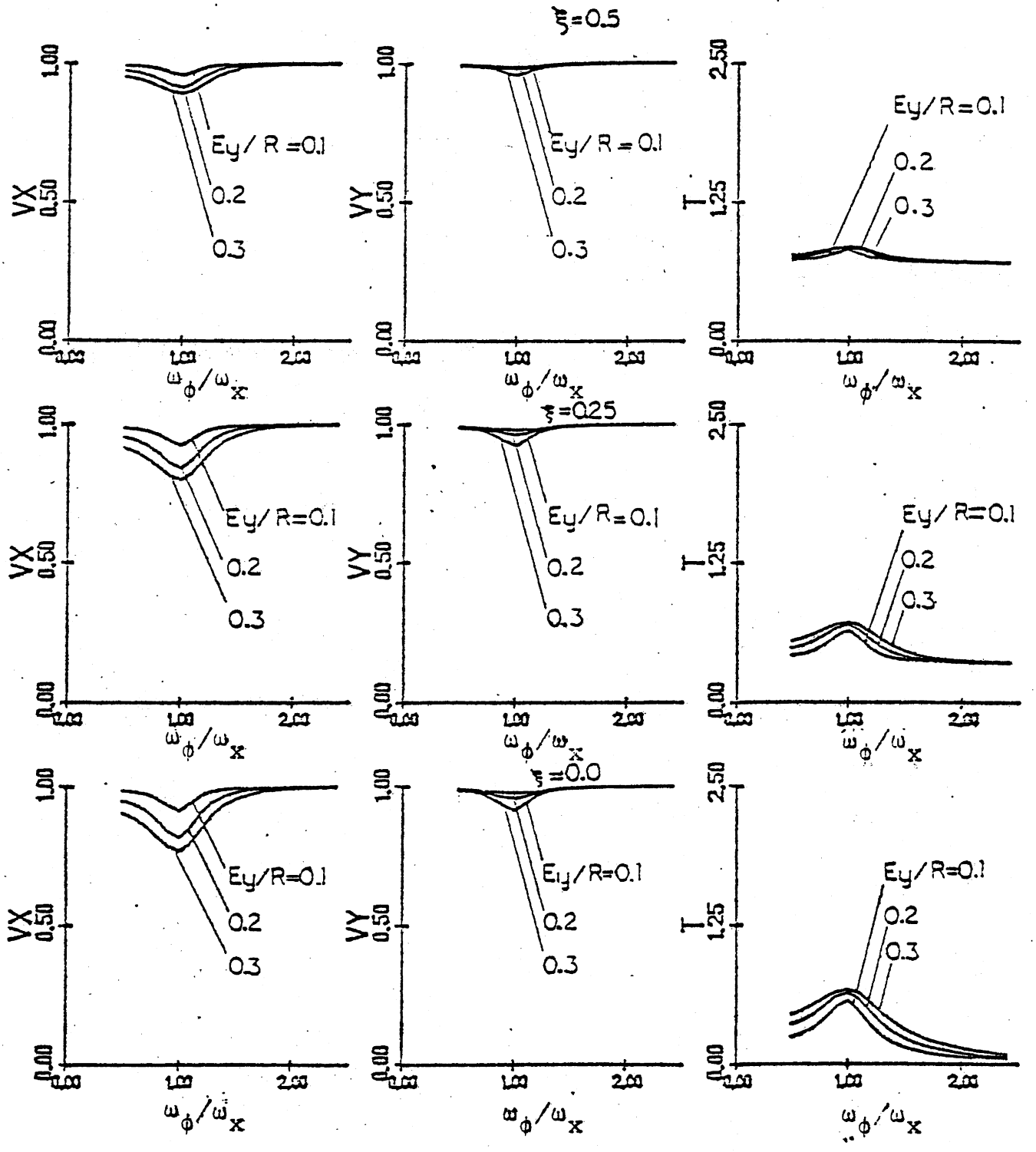

Figure 3-7 Force Interaction For Uncorrelated Ground Excitations With Flat Acceleration Spectra ($E_x/R=0, \omega_y/\omega_x=1$)

seen in Figure 3-7, even for the worst case of $\omega_x=\omega_\phi=\omega_y$, for $\xi=0.1$, only the torque is appreciably affected by the coupling.

It is now well established that the story shear decreases with increasing eccentricity. It can also be said that the story displacements ,i.e., the displacement at the center of mass, decrease with increasing eccentricity. The shear and displacement at the periphery of the building, however, is generally thought to increase with eccentricity. The reason it is thought to increase is that the eccentricity induces a rotational motion whose displacement at the periphery more than offsets the decrease in the average or story displacement that occurs with increasing eccentricity.

The method presented in this chapter can also be used to examine the peripheral response and the parameters affecting it. For the system shown in Figure 3-2, the displacement at the center of mass(C.M.) is less than what it would be if the centers of mass and stiffness were coincident. The origin of the coordinate system is the center of mass. The displacement of the point marked P is determined by the relation

$$U_p = U_x + (E_{ym}/R)\bullet(U_\phi)$$

or in matrix form

$$U_p = \{1 \quad E_{ym}/R \quad 0\}\bullet\{U\} = \{C\}^T\{U\} \qquad 3.30$$

With this relation, the power spectral density of U_p is determined to be

$$G_{U_p}{}^2(\omega) = \{C\}^T[\,G_U{}^2(\omega)\,]\{C\}$$
$$= \{C\}^T[\,H(\omega)\,]^H[\,A\,]^T[\,G_Z{}^2(\omega)\,][\,A\,][\,H(\omega)\,]\{C\}$$

where the spectral density of the ground motion $[\,G_Z{}^2(\omega)\,]$ is determined by Equation 3.27.

The variance of U_p then is

$$\langle U_p{}^2\rangle = \int_{-\infty}^{\infty} G_{U_p}{}^2(\omega)\cdot d\omega$$

$$= \int_{-\infty}^{\infty} G_Z{}^2(\omega)\cdot\{C\}^T[\,H(\omega)\,]^H[\,A\,]^T \begin{bmatrix} 1 & 0 & 0 \\ 0 & 2\cdot\xi^2 & 0 \\ 0 & 0 & 1 \end{bmatrix} [\,A\,][\,H(\omega)\,]\{C\}\cdot d\omega$$

which upon expanding, becomes

$$\langle U_p{}^2\rangle = \int_{-\infty}^{\infty} G_Z{}^2(\omega)\cdot\{H_1{}^2(\omega)\cdot(A_{xx}{}^2 + 2\cdot\xi^2\cdot A_{\phi x}{}^2 + A_{yx}{}^2)$$
$$+2\cdot E_{ym}/R\cdot H_1(\omega)\cdot H_2(\omega)\cdot(A_{x\phi}\cdot A_{xx} + 2\cdot\xi^2\cdot A_{\phi x}\cdot A_{\phi\phi} + A_{yx}\cdot A_{y\phi})$$
$$+ (E_{ym}/R)^2\cdot H_2{}^2(\omega)\cdot(A_{x\phi}{}^2 + 2\cdot\xi^2\cdot A_{\phi\phi}{}^2 + A_{y\phi}{}^2)\}\cdot d\omega$$

and after integrating, becomes

$$\langle U_p{}^2\rangle = \langle Y_{px}{}^2\rangle\cdot(A_{xx}{}^2 + 2\cdot\xi^2\cdot A_{\phi x}{}^2 + 2\cdot E_{ym}/R\cdot A_{yx}{}^2)$$
$$+ (E_{ym}/R)^2\cdot\langle Y_{p\phi}{}^2\rangle\cdot(A_{x\phi}{}^2 + 2\cdot\xi^2\cdot A_{\phi\phi}{}^2 + 2\cdot E_{ym}/R\cdot A_{y\phi}{}^2)$$
$$+2\cdot E_{ym}/R\cdot\langle Y_{px}\cdot Y_{p\phi}\rangle\cdot(A_{xx}\cdot A_{x\phi} + 2\cdot\xi^2\cdot A_{\phi x}\cdot A_{\phi\phi} + 2\cdot E_{ym}/R\cdot A_{yx}\cdot A_{y\phi}) \qquad 3.31$$

The variance of the input ground translations are assumed the same. The variance of the ground rotation is determined by the quantity ξ. The area of interest in building torsion concerns systems where the frequencies are close together. For such systems the modal quantities $\langle Y_{px}{}^2\rangle$, $\langle Y_{p\phi}{}^2\rangle$, and $\langle Y_{py}{}^2\rangle$ can be assumed approximately equal

$$\langle Y_{px}{}^2\rangle = \langle Y_{p\phi}{}^2\rangle = \langle Y_{py}{}^2\rangle \doteq \sigma^2$$

where σ is a constant.

A special case of interest arises when $\xi = \sqrt{2}/2$.

Equation 3.31 then can be reduced to

$$\langle U_p^2 \rangle = \sigma^2 \cdot \{(A_{xx}^2 + A_{\phi x}^2 + A_{yx}^2) + (E_{ym}/R)^2 \cdot (A_{x\phi}^2 + A_{\phi\phi}^2 + A_{y\phi}^2) + P_{x\phi} \cdot 2 \cdot E_{ym}/R \cdot (A_{xx} \cdot A_{x\phi} + A_{\phi x} \cdot A_{\phi\phi} + A_{yx} \cdot A_{y\phi})\}$$

$$= \sigma^2 \cdot (1 + (E_{ym}/R)^2 + 0) \qquad 3.32$$

It should be noted that Equation 3.32 is independent of the eccentricity, i.e., the maximum response at the periphery does not increase with eccentricity, regardless of its value. A value of $\xi = \sqrt{2}/2$ is higher than typical though.

In order to examine the effects of the different parameters, Figure 3-8 was plotted using different frequency ratios, eccentricity ratios, distances from the center of mass (E_{ym}/R), and different values of ξ. The first column of graphs represents the response for $E_{ym}/R=0.0$, i.e. at the center of mass. It shows the familiar reduction with increasing eccentricity. The second column represents $E_{ym}/R=0.6$, and the third 1.22 (which would represent the periphery of a square building).

The bottom row of graphs in Figure 3-8 represents $\xi=0.0$, i.e. no ground rotation. It shows a significant increase for $E_{ym}/R=1.22$. The middle row represents $\xi=0.25$ and the top row $\xi = \sqrt{2}/2$.

The maximum increase for $\xi=0.0$ and $E_{ym}/R=1.22$ (the exterior of a square building) is about 55% when $\omega_\phi/\omega_x=1$. This is about the same when $\xi = \sqrt{2}/2$ and $E_{ym}/R=1.22$. This represents a static eccentricity of about 33% of the building width.

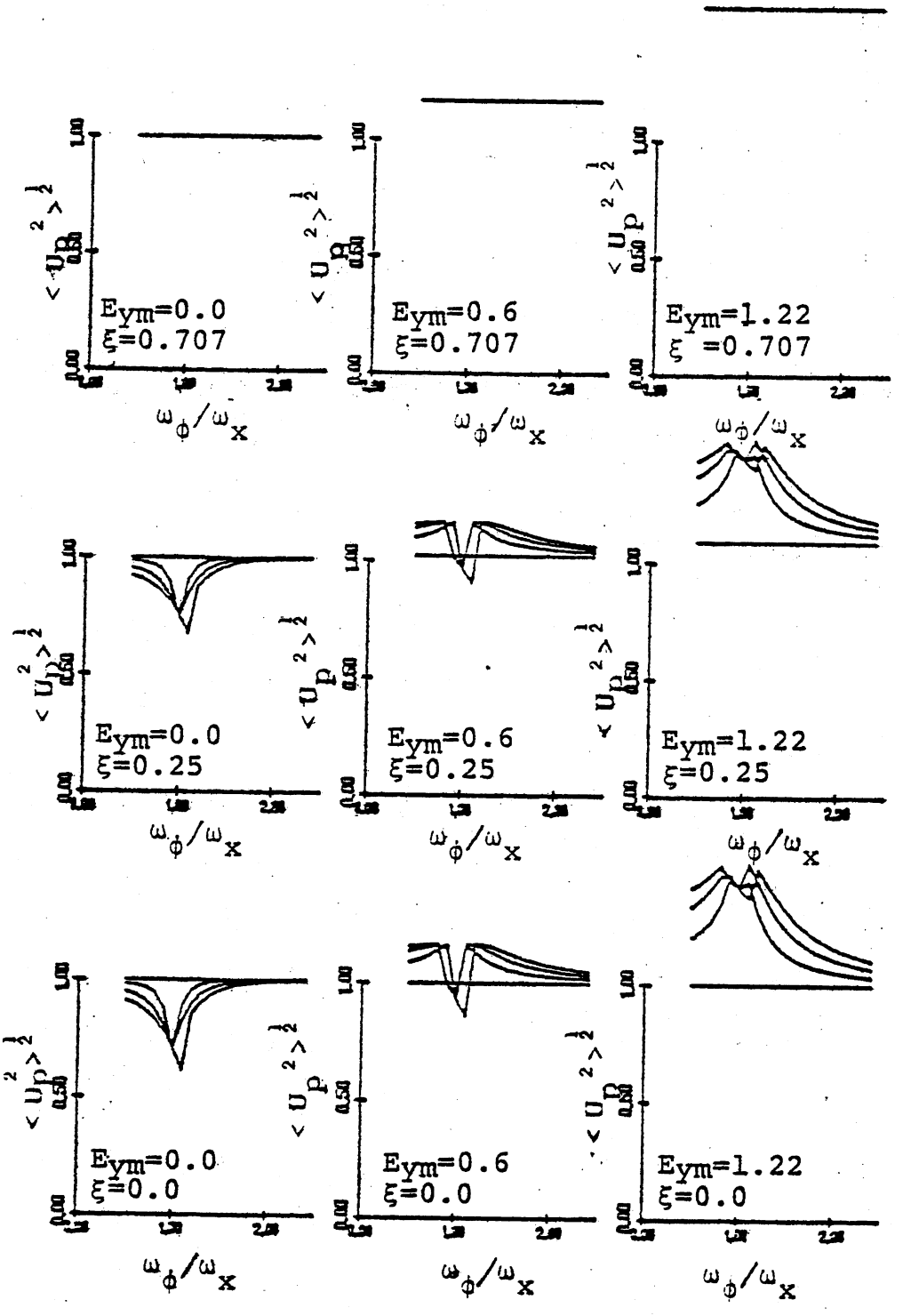

Figure 3-8 Effect of Ground Rotation

What this means is that the expected maximum peripheral response is essentially independent of the level of ground rotation for systems where the torsional and lateral frequencies are the same.

This is not true, however, for systems where the torsional and lateral frequencies are not close together. In this case the level of ground rotation directly affects the level of response as seen in Figure 3-8. The response in this case can be approximated by the root sum square of the torsional and lateral responses.

The single most important variable in determining the peripheral response is the torsional lateral frequency ratio since in most cases ξ should be less than 0.1.

The method presented should give reasonable estimates of the elastic torsional response of three-dimensional building systems. The relative effect of the different parameters on the expected maximum response is based on a probabilistic description of the ground motion. The power spectral density matrix of the ground motions is taken to be a diagonal matrix. The expected maximum peripheral response is determined as the standard deviation of the response which is based on the diagonal power spectral density matrix of ground motions.

CHAPTER IV

NONLINEAR RESPONSE MODEL

As previously stated, the nonlinear model must be kept simple for reasons of economy. Since earthquake peak response coefficients of variation vary from 0.1 to 0.3, several samples must be averaged to interpret the results meaningfully. Also, nonlinear systems, especially three-dimensional nonlinear systems are complex and expensive to simulate.

The characteristics of nonlinear torsional response are needed though, since buildings respond inelastically to some earthquakes. It is desired to know the effect of ground rotation in a nonlinear system. Also, nonlinearities in an unsymmetric building tend to increase the eccentricity. The effect on ductility requirements of peripheral lateral load elements is also needed.

In order to analyze accurately and efficiently the effect hysteretic energy dissipation has on the parameters eccentricity ratio, frequency ratio, and strength ratio, a simple single story model is used. The single story building that will be studied is shown in Figure 4-1. The load resisting elements exhibit a single degree of freedom

hysteresis where the force is a function of only one displacement as opposed to, say, a beam-column where the forces are a function of several displacements. This simplifies the nonlinear torsional response computations by enabling the use of simple hysteresis types.

Many different simple hysteresis types are available depending on what is being modelled. The elastoplastic model was developed to model the elastic-plastic behaviour of steel. The bilinear model is similar to the elasto-plastic model but allows strain-hardening.

For moment-resisting members the gradual yielding inward of the cross section requires smoothing of the sharp yielding in the bilinear model. This together with the Bauschinger effect brought about the use of the Ramberg-Osgood hysteresis model which is a curvilinear model very similar to the bilinear model.

Another single degree of freedom hysteresis model is the origin oriented shear model. In this model the unloading is always directed through the origin giving a pinched hysteresis loop. This model is used where nonlinear deformations and failure characteristics are governed primarily by shear.

The stiffness degrading model is used for members whose stiffness degrades upon reloading, where the degree of degradation depends on the current ductility. The stiffness degrading and origin-oriented shear models are usually used to model reinforced concrete members.

The building model used to study the nonlinear behaviour of buildings subject to torsional motion is shown in Figure 4-1. It consists of a rigid diaphragm roof and four independent exterior lateral load resisting elements, e.g., steel moment frames or braced frames.

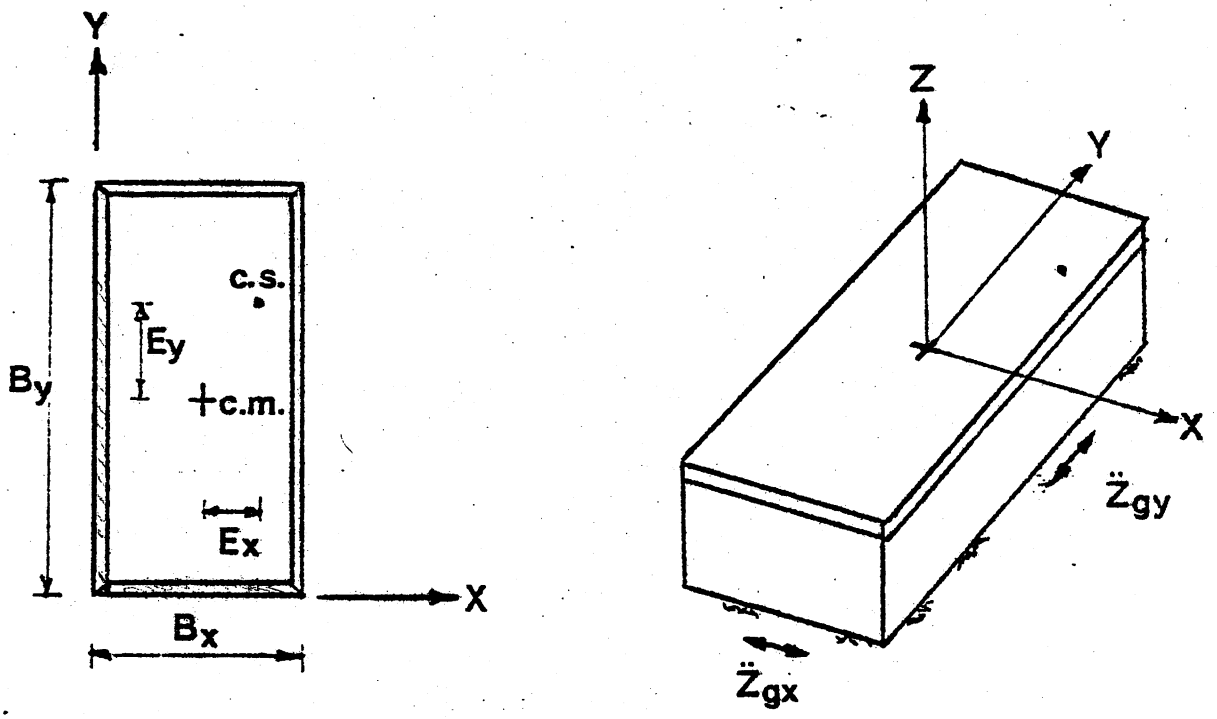

Figure 4-1 Building Model

This model can represent many different single story buildings in use. Some of the buildings on nuclear reactor sites are single story four frame buildings. Industrial buildings are commonly one story and for better utilization of space, often have only exterior frames. Warehouses are often similar to such industrial buildings.

Small commercial buildings are commonly one story.

Also, such buildings often have very high eccentricities. One side of these buildings is typically all glass, leaving only 3 exterior frames. This can result in the center of stiffness located at the exterior which gives rise to the very high eccentricity.

Sports arenas, auditoriums, and meeting halls are other examples of single story exterior framed buildings.

Multistory, multibay structures obviously don't fit the criteria for this model; however, with some crude approximations this model can give the multistory, multibay gross response. For example, if the response can be presumed to consist primarily of the fundamental mode then this approximation should give reasonable results.

Some multistory structures are not suitable for modelling as a single story structure even for gross results. Buildings with eccentric penthouses are one example. Buildings with sudden changes in stiffness or changes in the eccentricity are another example.

Multibay structures require another approximation in order to be modelled as a single bay structure. The frames on each side of the center of stiffness are lumped together each as one frame keeping the total stiffness constant so the frequency isn't changed. For the building shown in Figure 4-2, the stiffness of the equivalent frames in the Y-direction would be as follows

$$K_{yt1} = K_{y1} + K_{y2}$$

$$K_{yt2} = K_{y3} + K_{y4}$$

In order to keep unchanged the rotational stiffness due to these frames, the distances X_{t1}, X_{t2} would be determined from

$$K_{y1} \cdot X_1^2 + K_{y2} \cdot X_2^2 = K_{yt1} \cdot X_{t1}^2$$

$$K_{y3} \cdot X_3^2 + K_{y4} \cdot X_4^2 = K_{yt2} \cdot X_{t2}^2$$

where X_{t1} would be between X_1 and X_2.

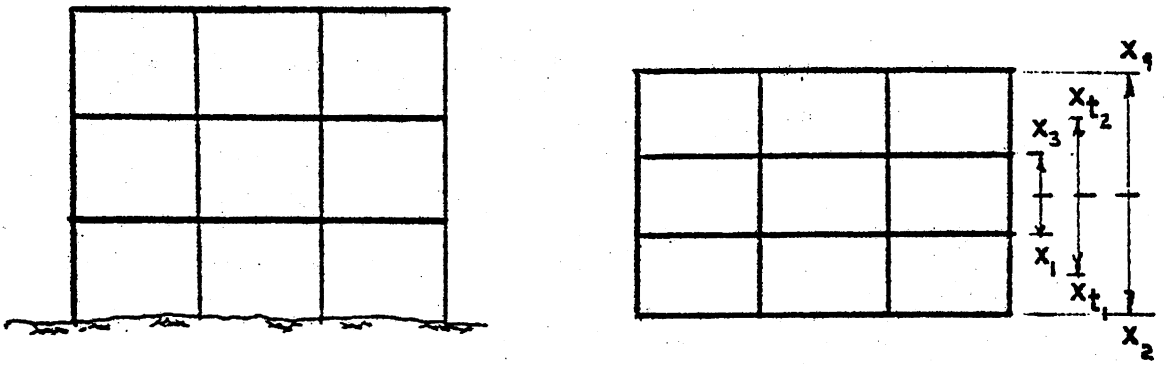

Figure 4-2 Multibay Building

For a linear multibay system this method of modelling would give the same results; however, a problem arises in nonlinear response. If the yield levels of frames 1 and 2 were F_{y1} and F_{y2}, then the obvious choice for the equivalent frame's yield level would be $F_{y1}+F_{y2}$. For a system with no eccentricity and no torsional excitations, the response of the actual multibay structure and the four frame equivalent model would not be the same unless the yield levels of frames 1 and 2 were identical. For bilinear hysteresis with

different yield levels for the frames labelled one and two, the equivalent frame would have to exhibit a trilinear hysteresis to match the response of the actual structure. Also, when a torsional response exists, the rotational displacement which would cause one of the frames in the multibay structure to yield, would not necessarily be the same yield rotational displacement as that of the equivalent model. The maximum moment for each system will be approximately the same though. So modelling nonlinear multibay structures as single bay structures does require some approximations. It should model the gross response adequately, though.

EQUATIONS OF MOTION

For the four frame structure being analyzed, the rigid diaphragm reduces the system to three degrees of freedom; two lateral displacements and a rotation about a vertical axis.

The dynamic equations of motion for the three degree of freedom nonlinear system shown in Figure 4-1 are

$$[M]\{\ddot{U}\}+[C]\{\dot{U}\}+\{F(U)\} = -[M]\{\ddot{U}_g\} \qquad 4.1$$

where

$$\{F(U_i)\}=\{F(U_{i-1})\}+[K_{i-1}]\{U_i-U_{i-1}\}$$

and $[K_i]$ is the tangent stiffness at time t_i.

The displacement vector $\{U\}$ is the same as in Equation 3.1, i.e.

$$\{U\}=\{U_x \quad R\cdot U_\phi \quad U_y\}^T$$

The mass matrix then becomes

$$[M]=\begin{bmatrix} m & 0 & 0 \\ 0 & m+E & 0 \\ 0 & 0 & m \end{bmatrix}$$

The hysteresis model chosen for this study is the bilinear model. The numerical integration method used is fourth order Runge-Kutta.

Fourth order Runge-Kutta numerical integration of a second order differential equation, e.g. Equation 3.1, is conditionally stable for $T_n/\Delta t>2.43$, where T_n is the period of the system. The linear acceleration method, sometimes referred to as Newmark's β method[41], is conditionally stable for $T_n/\Delta t>1.81$. In a limited test of single degree of freedom linear responses to sine waves, the fourth order Runge-Kutta method was more accurate than the linear acceleration method in terms of peak response and earthquake input energy, which is defined simply as the energy input to the structure. The linear acceleration method is more efficient for the same $T_n/\Delta t$ ratio though. The reason the Runge-Kutta method is used is its accuracy and ease in programming changes in the time step Δt.

For a bilinear hysteresis model the amount by which the force can overshoot the yield envelope can be considerable; especially for low values of $T_n/\Delta t$. The usual procedure taken when the force overshoots the yield envelope is to redo this step's calculations with a much smaller time increment, say one-fifth the original; then, when the force is beyond the yield envelope, presumably by a small amount,

the time increment is reset to the original value and the computations resume.

A special algorithm is used here to compute the time step necessary to reach the yield force precisely. The fourth order Runge-Kutta method is used to solve Equation 4.1. The initial time step increment Δt is chosen on the basis of stability and accuracy. When the force for one of the elements overshoots the yield envelope, this time step's calculations are redone with a new time step increment.

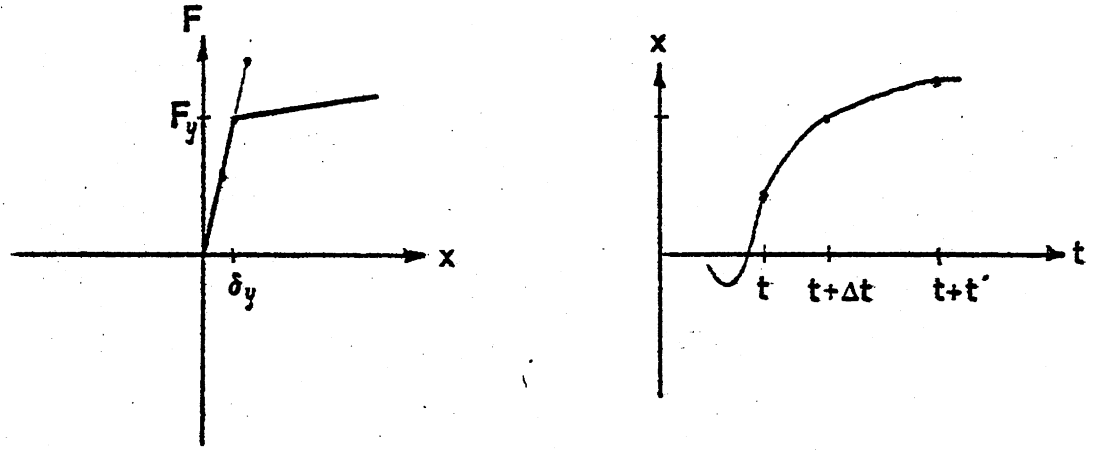

Figure 4-3 Bilinear Yield Envelope

When the force overshoots the yield envelope, as shown in Figure 4-3, the displacement necessary for the force to equal the yield force is known. If the displacement is assumed to be a third order function of time, i.e. linear acceleration, then the time increment corresponding to that displacement can be computed. That displacement then is

$$\Delta X = (Fy - F(t))/K = \Delta t \cdot \dot{X}(t) + \Delta t^2 \cdot [2 \cdot \ddot{X}(t) + \ddot{X}(t+\Delta t)]/6 \qquad 4.2$$

where

$$\ddot{X}(t+\Delta t) = \ddot{X}(t) + [\ddot{X}(t+t') - \ddot{X}(t)] \cdot \Delta t/t' \qquad 4.3$$

A cubic equation in Δt is obtained by combining Equations 4.1 and 4.2.

$$G(\Delta t) = \Delta t^3 \cdot [\ddot{X}(t+t') - \ddot{X}(t)]/(6 \cdot t') + \Delta t^2 \cdot \ddot{X}(t)/2 + \Delta t \cdot \dot{X}(t) - \Delta X = 0.$$

Δt can be solved for directly or by Newton iteration

$$\Delta t_{i+1} = \Delta t_i - G(\Delta t_i)/G'(\Delta t_i)$$

In practise, only a few iterations are required to achieve the necessary accuracy. This time step increment is then used in the fourth order Runge Kutta integration scheme for this step only. The computed element force is then compared to the yield value and if it is within 1%, the solution proceeds with the initial time step increment. For the simulations used in this study the accuracy has always been within 1%. The computer program using this algortihm is listed in Appendix E.

This solution technique for bilinear systems can be efficiently used for structures with few yielding elements. For a structure with many yielding elements, the constant changing of the time step would make this technique expensive, computationally.

CHAPTER V

NONLINEAR RESPONSE RESULTS

The importance of the various torsional parameters, eccentricity ratio, torsional ground motion, and strength ratio for the model as described in Chapter IV are studied, especially the peripheral response as it pertains to the ductility demand.

Since the model is a nonlinear hysteretic system, Monte Carlo methods are used. An ensemble of artificial nonstationary accelerograms is generated as described in Chapter II using the computer program PSEQGEN [71] which uses filtered white noise with an intensity function of the Jenning's et al[52] type. The intensity function I(t) is shown in Figure 5-1d). The accelerograms are the product of the stationary filtered white noise and the intensity function I(t). The power spectral density shown in Figure 5-1c) is the product of the filter's two frequency response functions shown in Figure 5-1a) and b). The accelerograms generated are intended to simulate strong ground motion on firm soil in the vicinity of the epicenter[55]. The generated accelerograms are shown in Figures 5-2 through 5-6.

Other parameters that characterize the accelerograms include the maximum acceleration which averages 0.4g for the five accelerograms with a standard deviation of 0.01g. The duration is 60 seconds with a duration of 31 seconds for the strong ground motion (stationary) portion. The Arias intensity[78] which is defined as

$$I_a = \pi/(2 \cdot g) \cdot \int_0^t \ddot{z}_g^2(t) \cdot dt$$

is 32.2 ft/sec. The rms acceleration is 0.1g.

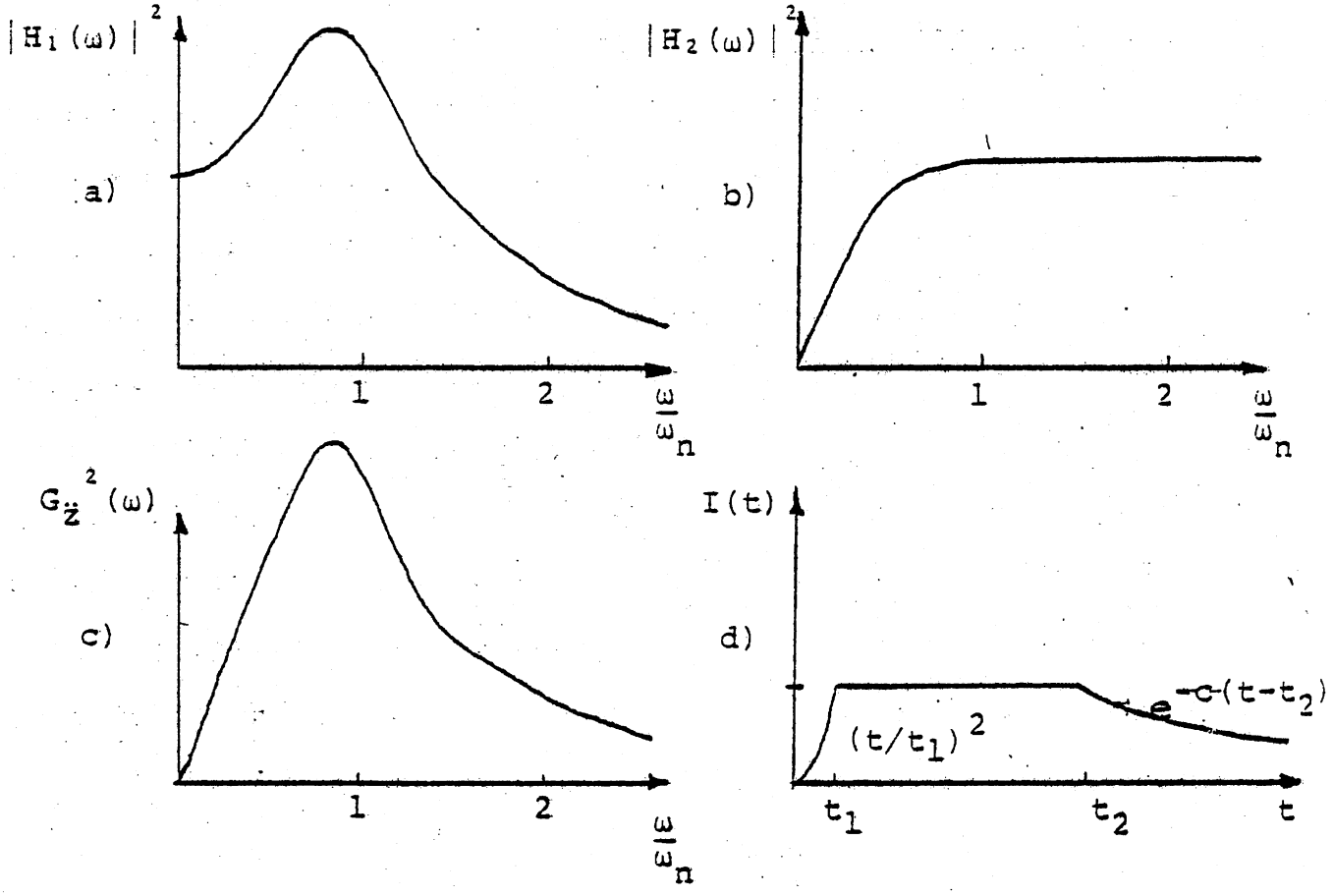

Figure 5-1 Artificial Accelerogram Data

Housner's spectrum intensity SI, is defined as

$$SI = \int_{0.1}^{2.5} V \cdot dT$$

where V is the pseudovelocity response in ft/sec, often for 20% damping, and T is the natural period. For the five generated accelerograms the average spectrum intensity SI is 3.9 ft for 20% damping. Ground rotation was included and computed according to Equation 2.15. The shear wave speed used was a conservative 1000 ft/sec. This corresponds to a value of 0.15 for the parameter ξ as described in Chapter III for the wavelength corresponding to the predominant frequency of excitation.

Model parameters

The normalized eccentricity ratio, E/R, is defined as the eccentricity between the center of mass and stiffness divided by the mass radius of gyration. The values 0.0, 0.1, 0.2, 0.3, and an unusually high value of 1.0 were used for this ratio. The structure's dimension ratio B_y/B_x, was 2.0. The stiffness was assumed proportional to the dimensions of the structure i.e., $K_y/K_x=2.0$, so the frequency ratio ω / ω_x was $\sqrt{2}$. The torsional-lateral frequency ratio ω_ϕ/ω_x is determined by the geometry of the structure. For a uniform mass distribution the mass radius of gyration is

$$R= \sqrt{(B_x^2+B_y^2)/12}$$

and the torsional frequency is

$$\omega_\phi= \sqrt{3\cdot(K_x\cdot B_y^2 + K_y\cdot B_x^2)/[M\cdot(B_x^2+B_y^2)]}$$

For $B_y=B_x$ and $K_y=K_x$, $\omega_\phi/\omega_x=\sqrt{3}=1.73$. For $B_y/B_x=K_y/K_x=2$, $\omega_\phi/\omega_x=1.90$.

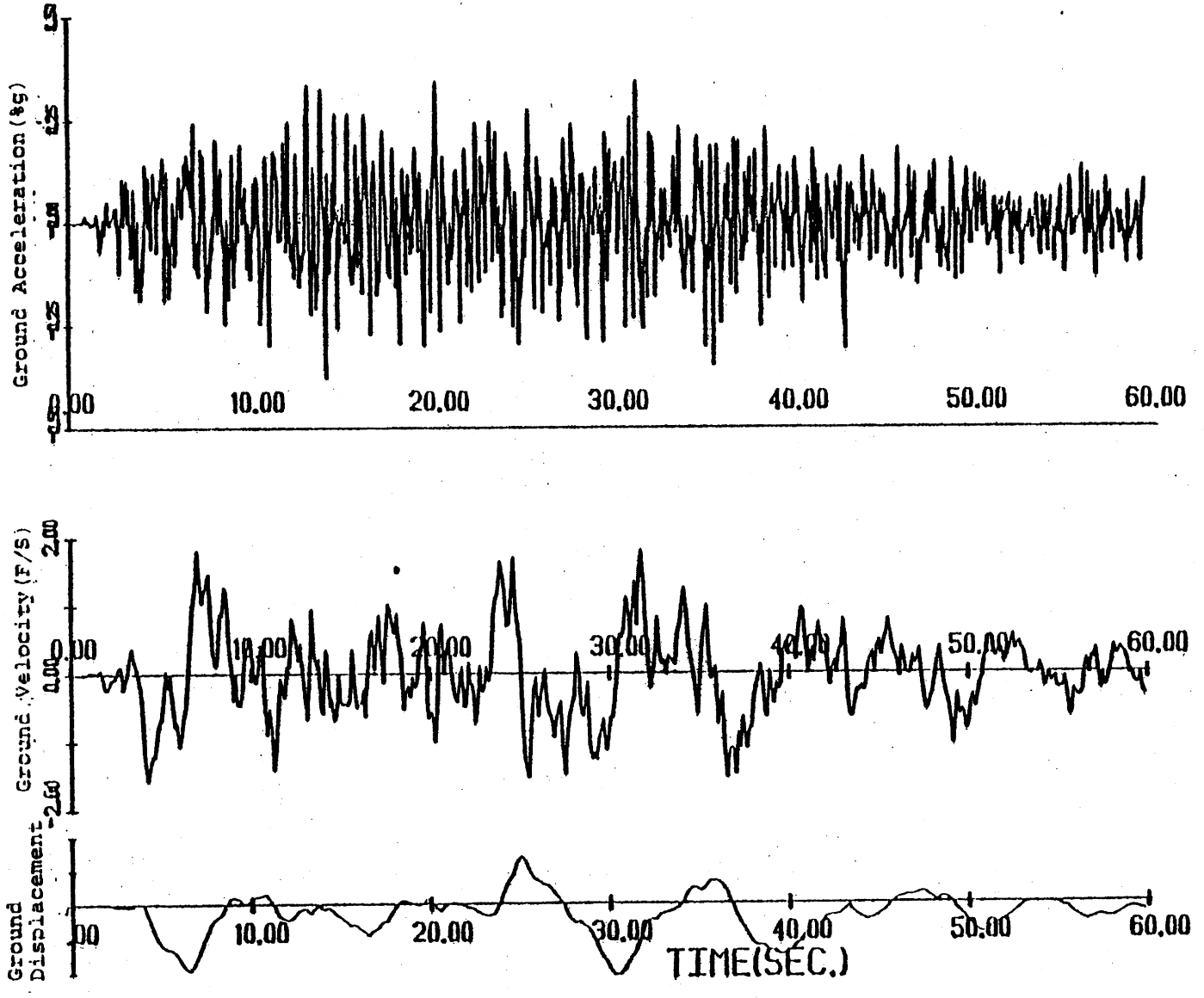

Figure 5-2 Accelerogram 1

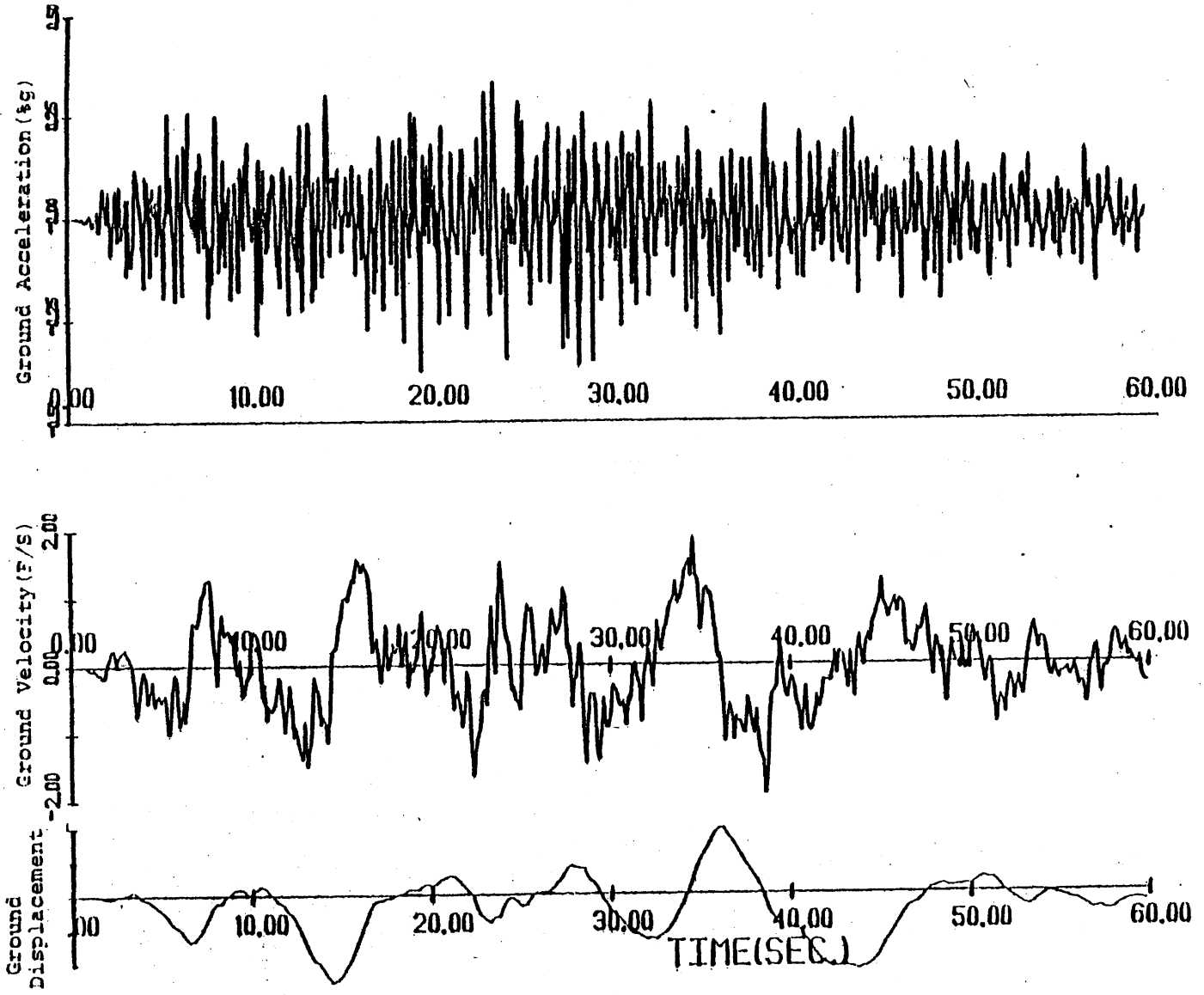

Figure 5-3 Accelerogram 2

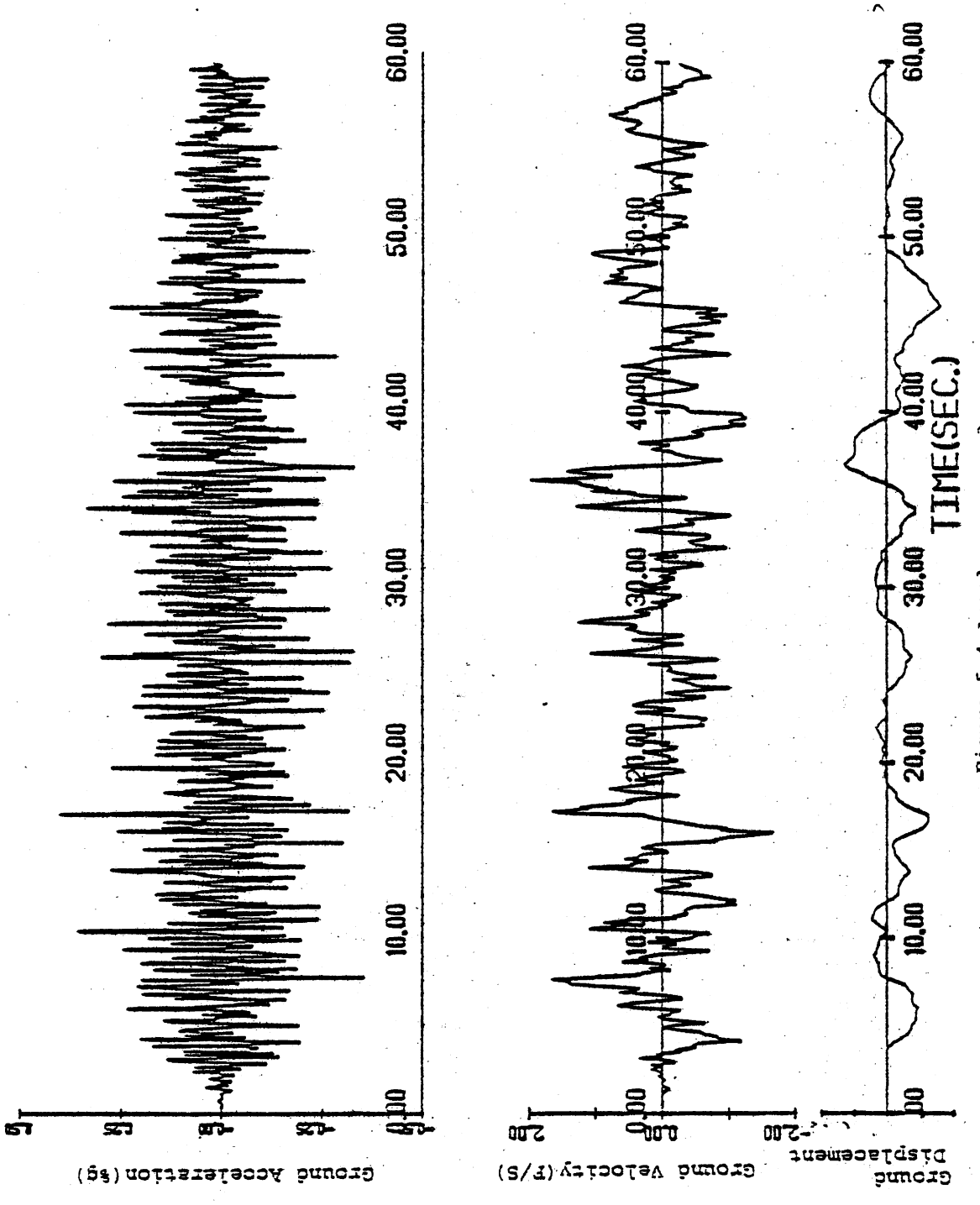

Figure 5-4 Accelerogram 3

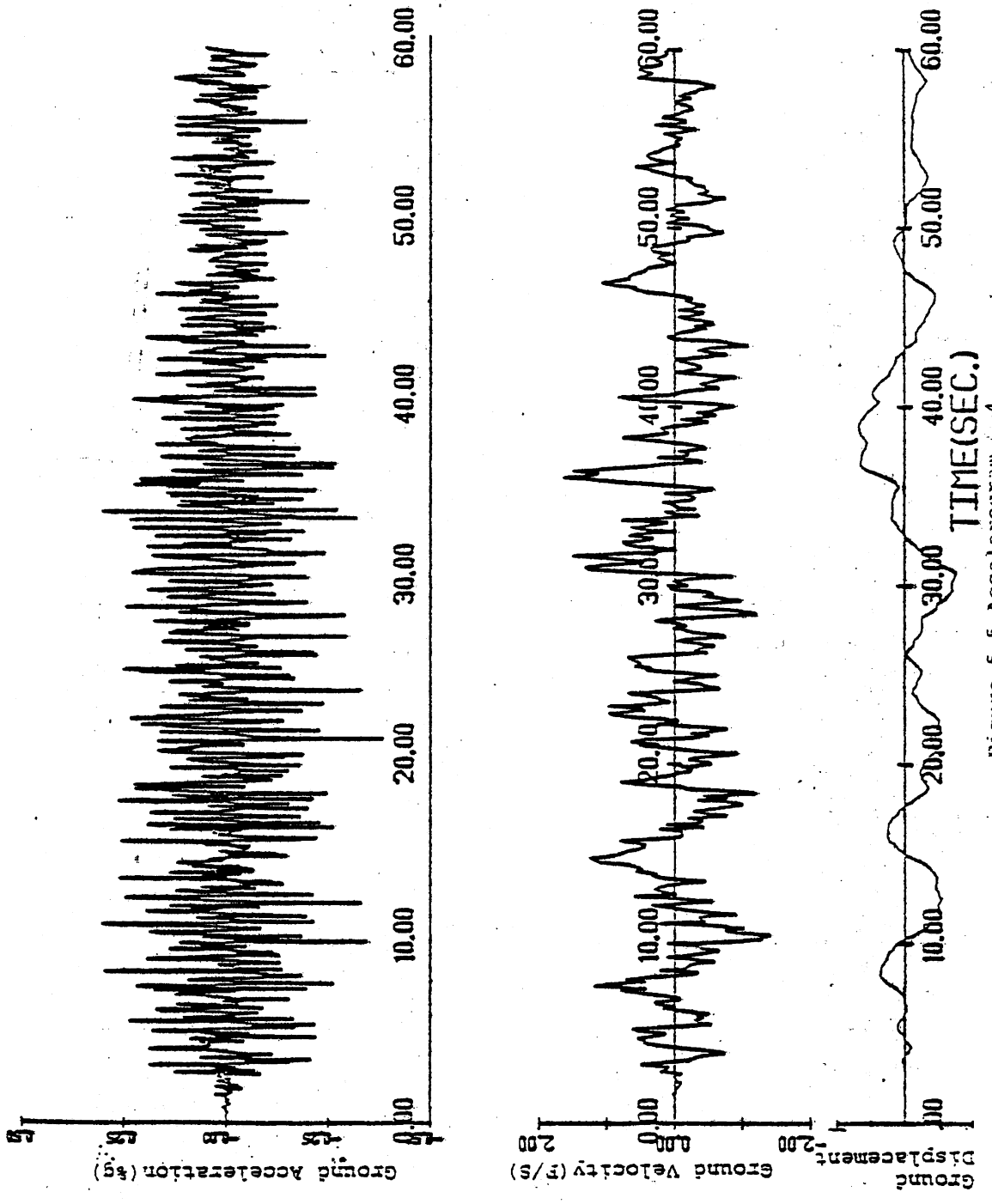

Figure 5-5 Accelerogram # 4

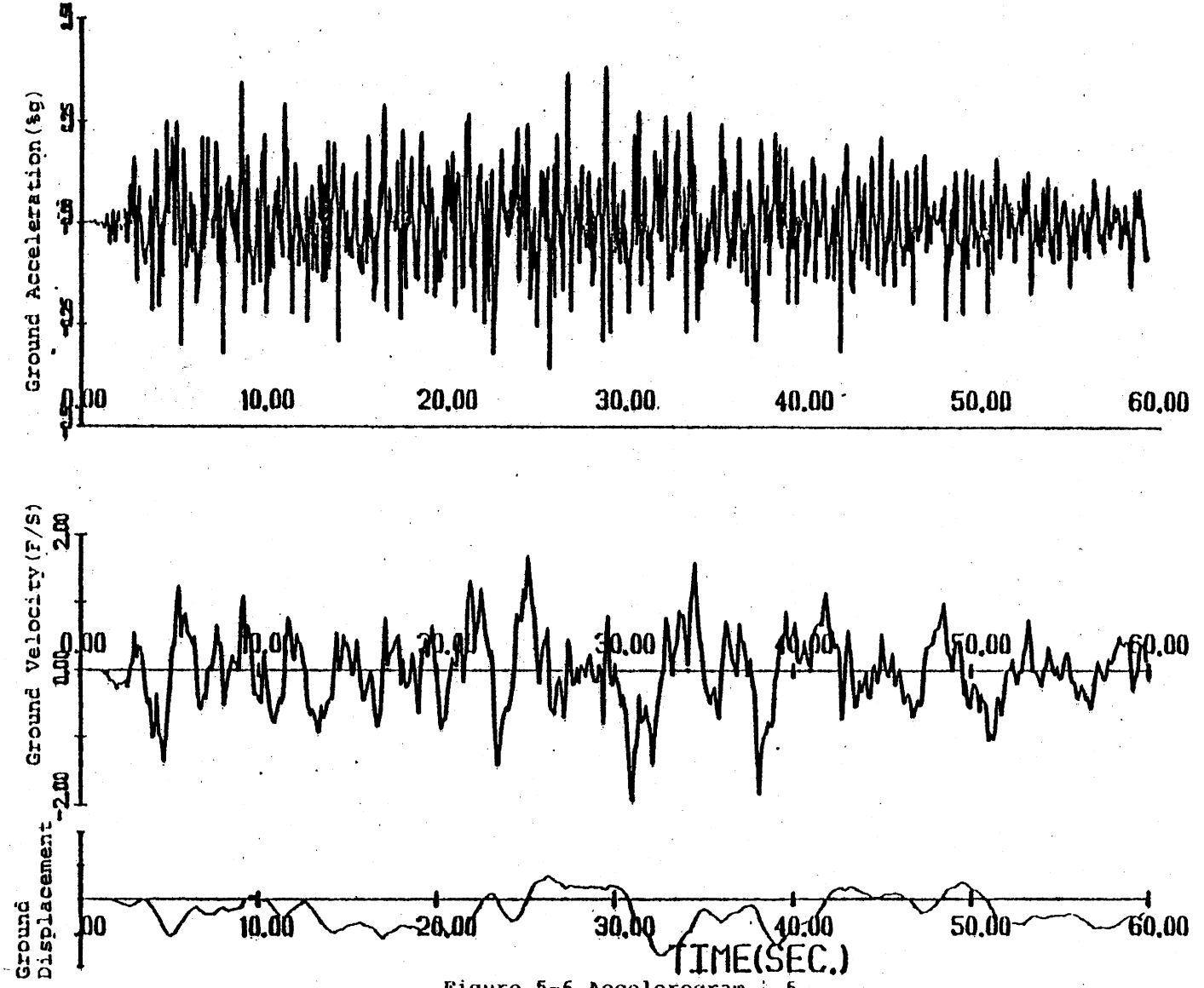

Figure 5-6 Accelerogram 5

The mass of the model, assumed uniformly distributed, was 0.5 kips•sec²/inch. Other important parameters of the nonlinear response are the natural frequencies and a strength parameter. The natural periods used were 0.2,0.6,1.0, and 1.4 seconds.

The other parameter determining nonlinear response relates to the yield level. This strength parameter can be expressed in many different ways. The current UBC(79) code specifies the base shear V, as

$$V=Z \cdot I \cdot K \cdot C \cdot S \cdot W$$

where Z,I,K,C,S, and W are a zone factor, an importance factor, a framing system factor, a natural period factor, a site-structure resonance factor, and the building weight(or mass times gravity). A natural choice for the strength parameter then is the yield shear F_y, divided by the weight, M•g.

The values for $F_y/(M \cdot g)$ used were 1/8,1/4, and 1/2.

Results

The excitation for the first analysis consisted of accelerogram 1 for the X-direction, accelerogram 2 for the Y-direction, and using Equation 2.15 to determine the rotational acceleration. The excitation for the second analysis consisted of accelerogram 2 for the X-direction, accelerogram 3 for the Y-direction, and again using Equation 2.15 to determine the rotational acceleration. The excitation for the third, fourth, and fifth analyses are similarly determined. All results presented are the average

of the results of the five dynamic analyses.

The maximum displacements and ductilities at the center of mass for different values of the eccentricity ratio and a strength ratio of 1/2 are shown in Figure 5-7 as functions of the period in the X-direction. The displacements in the X-direction don't vary much with eccentricity. The displacements in the Y-direction appear to increase with eccentricity, but only slightly.

The maximum peripheral displacements and ductilities for different values of the eccentricity ratio and a strength ratio of 1/2 are shown in Figure 5-8. The displacements in both directions increase with eccentricity for the most part.

The maximum displacements of the center of mass and their corresponding ductilities for different values of the eccentricity ratio and a strength ratio of 1/4 are shown in Figure 5-9 as a function of the period in the X-direction. The displacements in the X-direction and Y-direction don't vary much with eccentricity.

The maximum peripheral displacements and ductilities for different values of the eccentricity ratio and a strength ratio of 1/4 are shown in Figure 5-10. The displacements in both directions increase with eccentricity for the most part.

The maximum displacements and ductilities at the center of mass for different values of the eccentricity ratio and a strength ratio of 1/8 versus the period in the X-direction

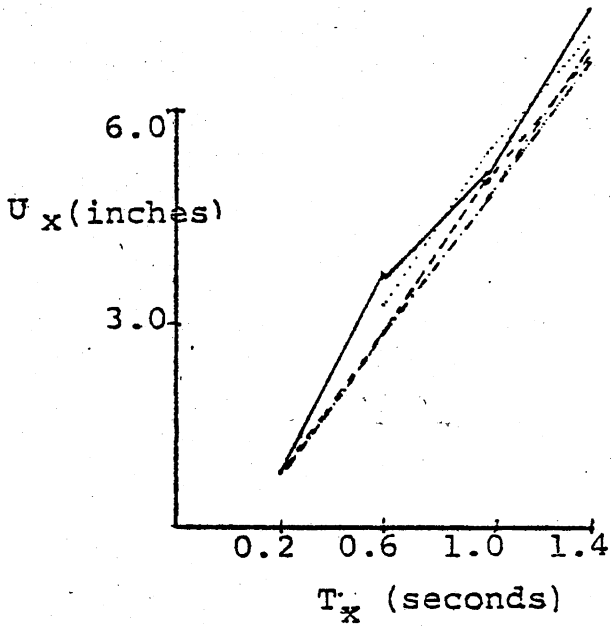

a) Maximum Displacement of Center of Mass in X Direction

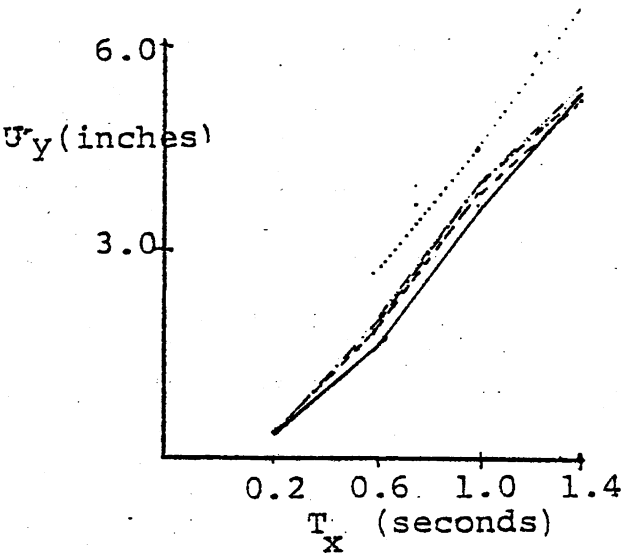

b) Maximum Displacement of Center of Mass in Y Direction

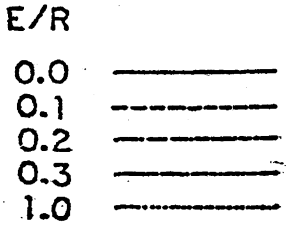

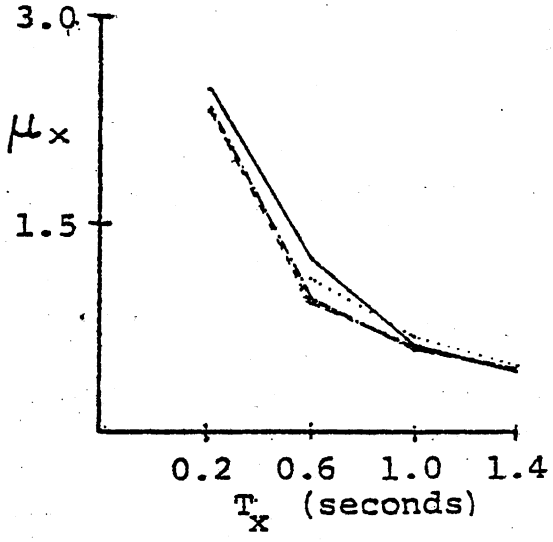

c) Ductility of Center of Mass in X Direction

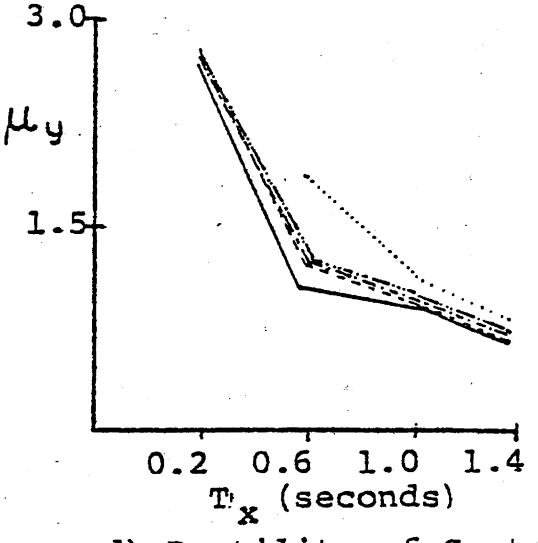

d) Ductility of Center of Mass in Y Direction

Figure 5-7 Displacements and Ductilities of Center of Mass

$(F_y/(M*g)=1/2)$

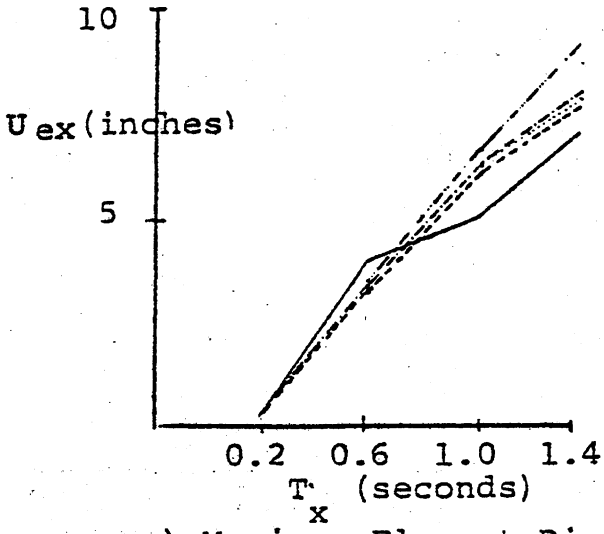

a) Maximum Element Displacement in X-Direction

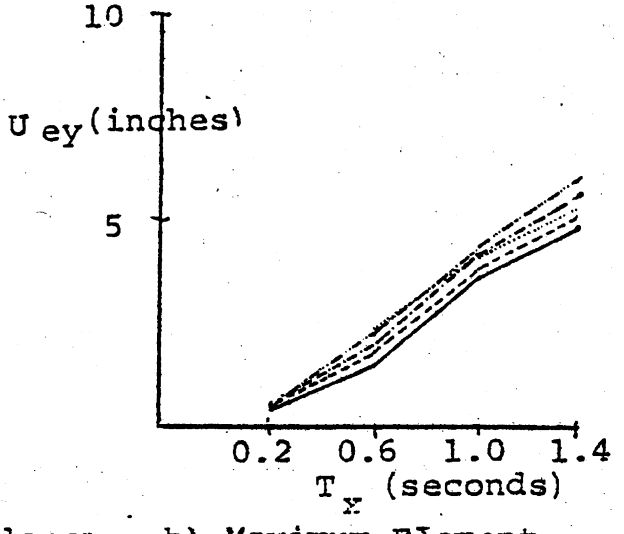

b) Maximum Element Displacement in Y-Direction

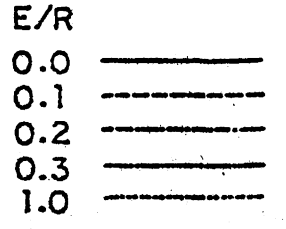

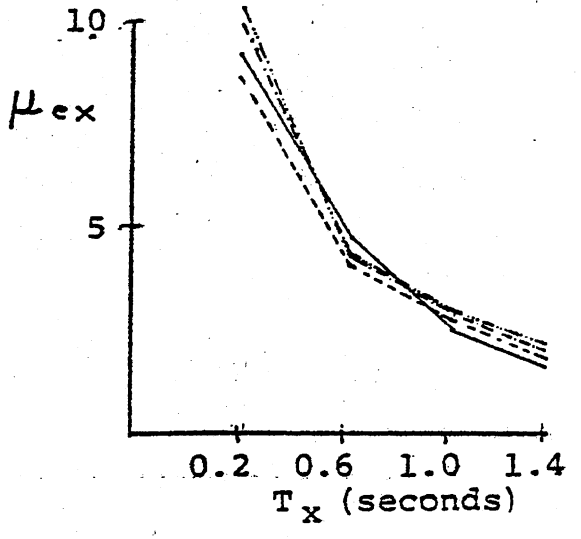

c) Element Ductility in X Direction

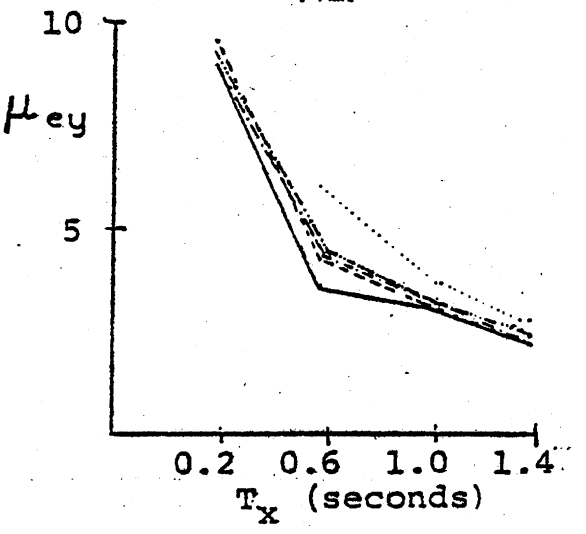

d) Element Ductility in Y Direction

Figure 5-8 Peripheral Displacements and Ductilities ($F_y/(M \cdot g) = 1/2$)

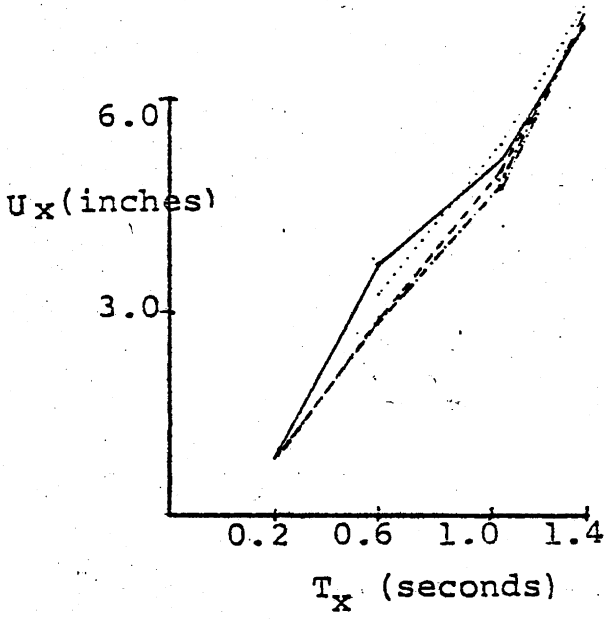

a) Maximum Displacement of Center of Mass in X Direction

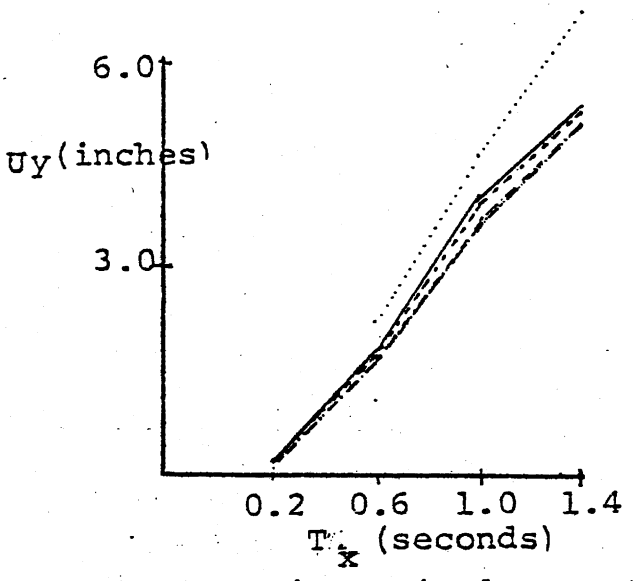

b) Maximum Displacement of Center of Mass in Y Direction

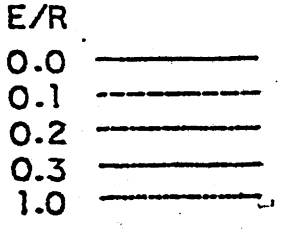

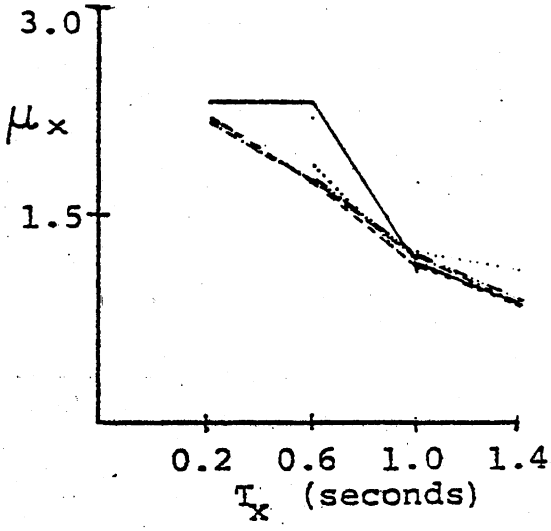

c) Ductility of Center of Mass in X Direction

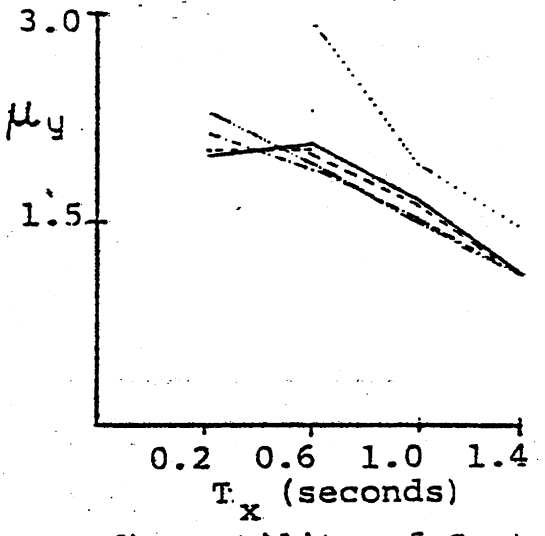

d) Ductility of Center of Mass in Y Direction

Figure 5-9 Displacements and Ductilities of Center of Mass

$(F_y/(M \cdot g) = 1/4)$

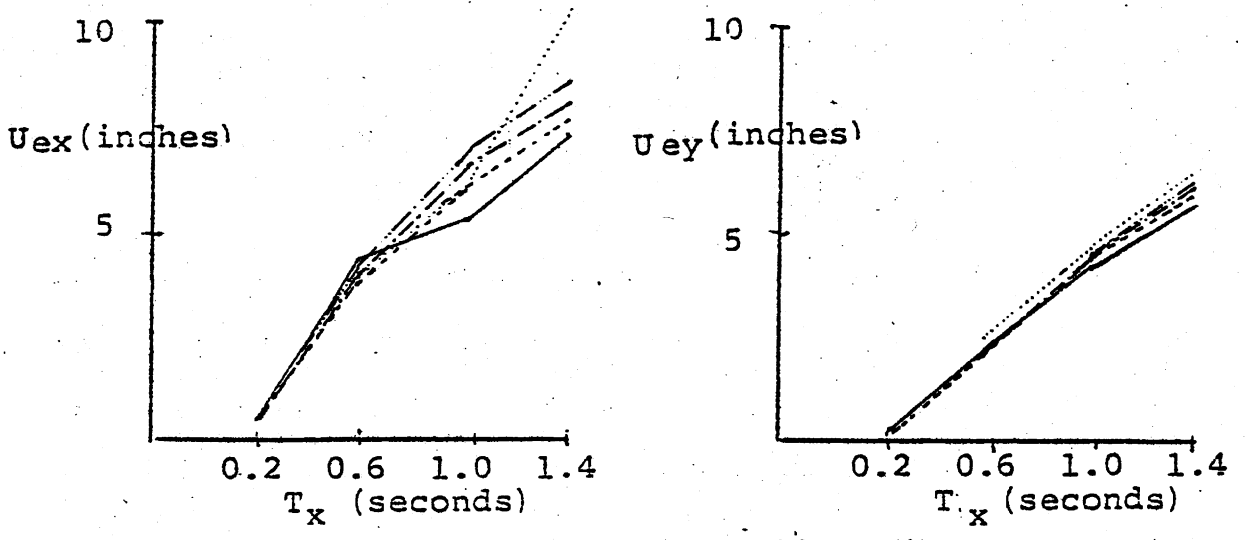

a) Maximum Element Displacement in X-Direction

b) Maximum Element Displacement in Y-Direction

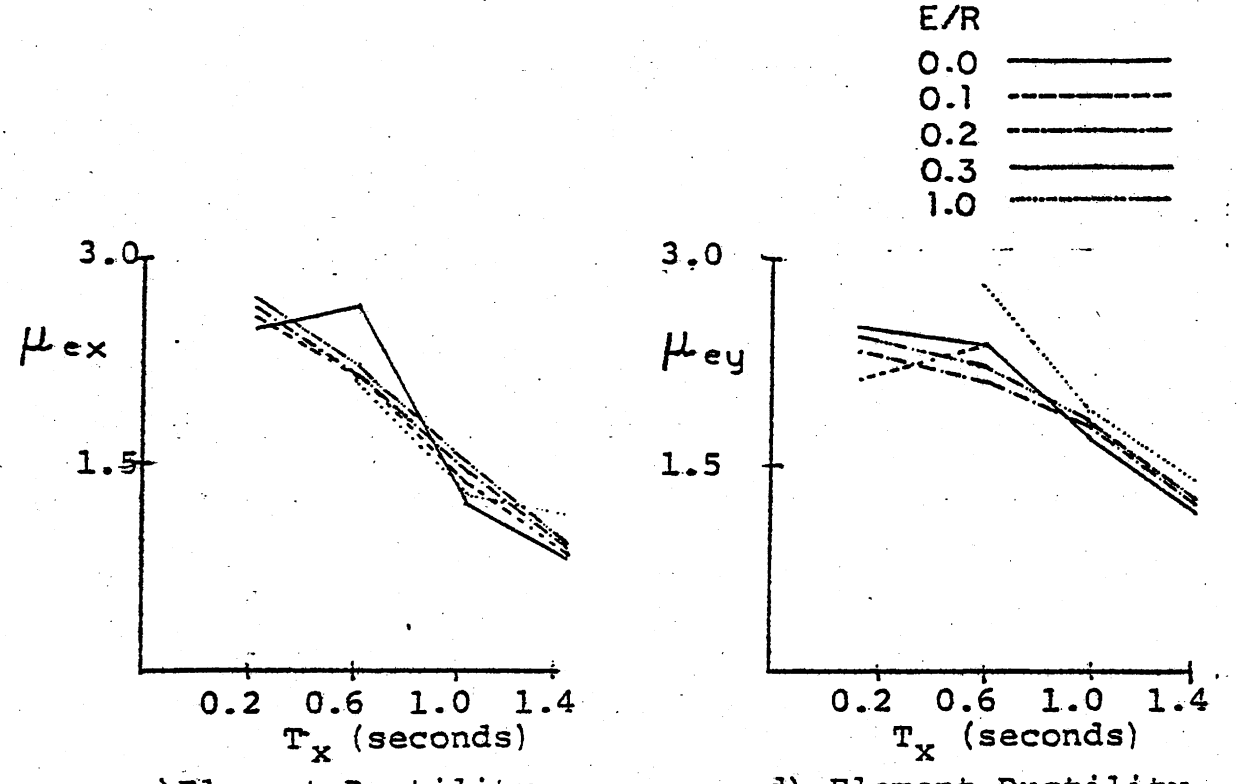

c) Element Ductility in X Direction

d) Element Ductility in Y Direction

Figure 5-10 Peripheral Displacements and Ductilities ($F_y/(M*g)=1/4$)

are shown in Figure 5-11. The displacements in the X-direction don't show a discernible trend. The displacements in the Y-direction appear to increase with eccentricity, but only slightly.

The maximum peripheral displacements and ductilities for different values of the eccentricity ratio and a strength ratio of 1/8 are shown in Figure 5-12. The displacements in both directions increase with eccentricity for the most part. The values for a period of 0.2 seconds were left out because the ductilities were in the hundreds, which for all practical purposes are not meaningful.

Earthquake Energy Partition

The partition of energy in the model was also computed. The earthquake input energy (EIE) is defined as the total acceleration integrated over the ground displacement

$$EIE = \int_0^t M \cdot (\ddot{U} + \ddot{U}_g) \cdot dU_g$$

The dissipated hysteretic energy (DHE) is the stiffness related force integrated over relative displacement less the recoverable strain energy

$$DHE = \int_0^t F(U) \cdot dU - F^2(t)/(2 \cdot K)$$

The dissipated nonhysteretic energy (DNHE) is the damping force integrated over relative displacement plus the recoverable strain energy and kinetic energy. The strain and kinetic energy are included since they are eventually dissipated through damping. The fraction of critical viscous damping in all cases was 5%. (See Appendix F for

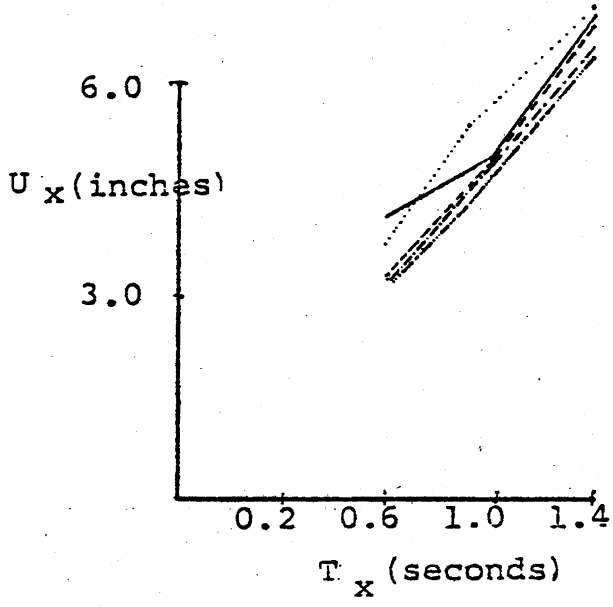

a) Maximum Displacement of Center of Mass in X Direction

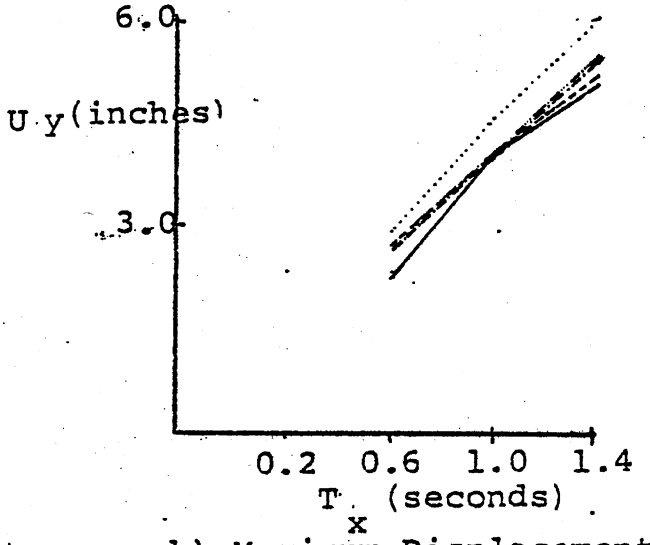

b) Maximum Displacement of Center of Mass in Y Direction

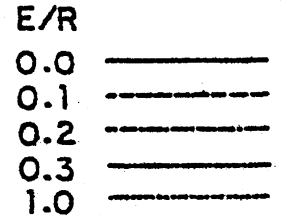

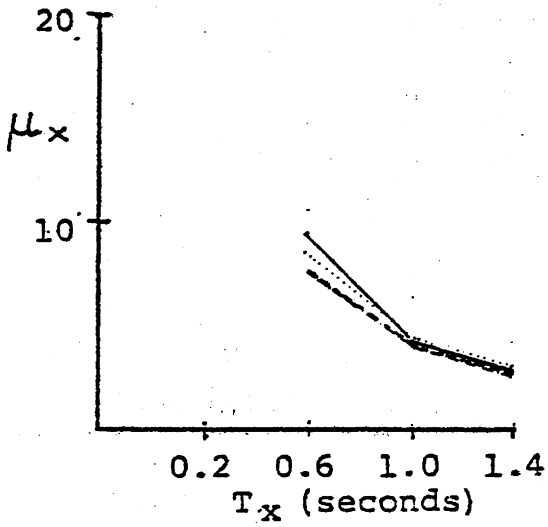

c) Ductility of Center of Mass in X Direction

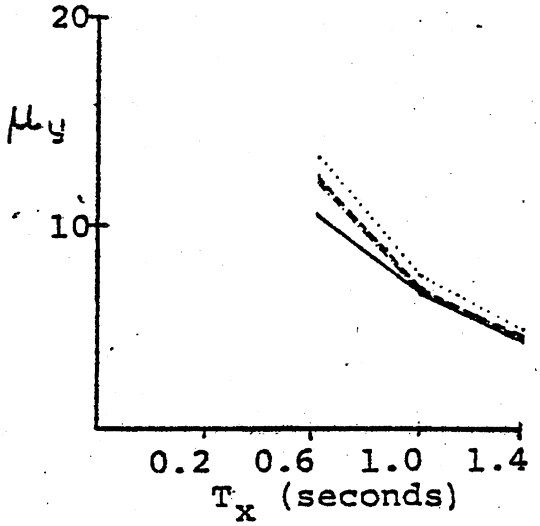

d) Ductility of Center of Mass in Y Direction

Figure 5-11 Displacements and Ductilities of Center of Mass

$(F_y/(M \cdot g) = 1/8)$

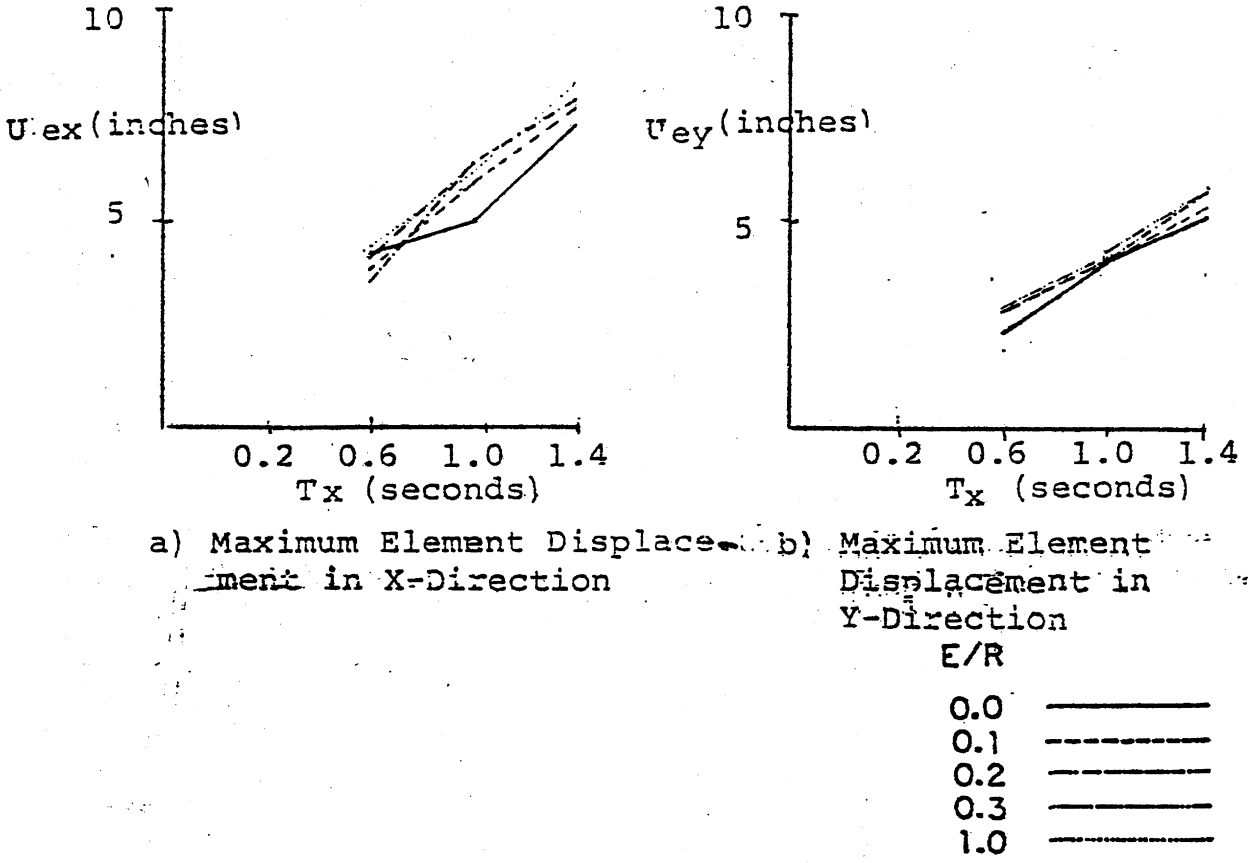

a) Maximum Element Displacement in X-Direction

b) Maximum Element Displacement in Y-Direction

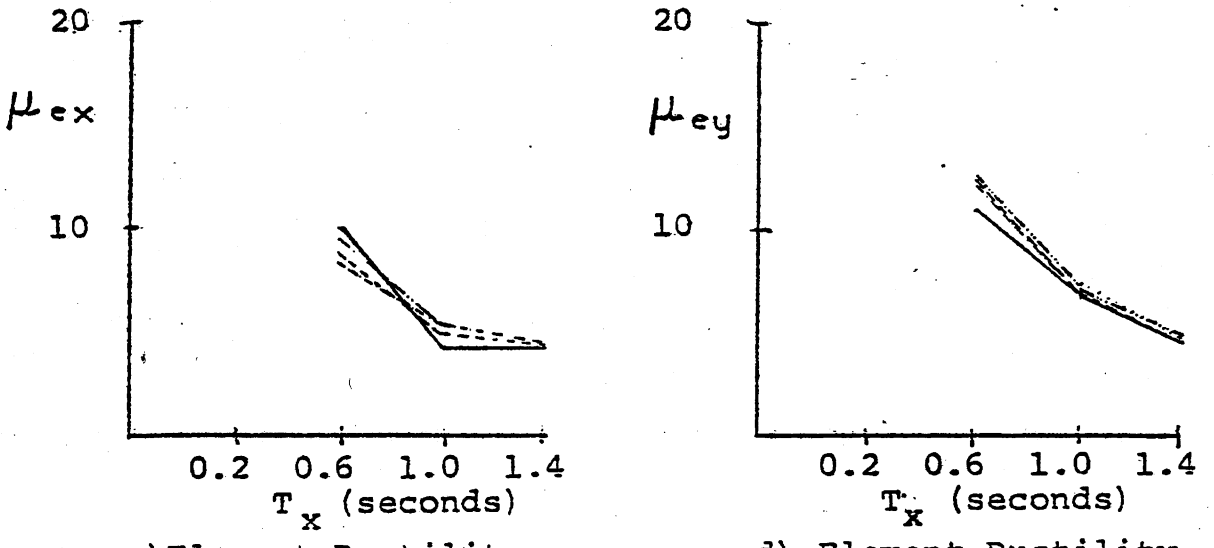

c) Element Ductility in X Direction

d) Element Ductility in Y Direction

Figure 5-12 Peripheral Displacements and Ductilities ($F_y/(M \cdot g) = 1/8$)

The earthquake input energy, dissipated damping energy, and dissipated hysteretic energy for different values of the eccentricity ratio and a strength ratio of 1/2 versus the period in the X-direction are shown in Figure 5-13. The values for a strength ratio of 1/4 and 1/8 are shown in Figures 5-14 and 5-15.

Several things are noteworthy in these figures. First, there doesn't seem to be any definite relation between the values and eccentricity, i.e. they don't uniformly increase or decrease with eccentricity. Second, as would be expected, the dissipated hysteretic energy increases for lower values of $F_y/(M \cdot g)$. Third, the earthquake input energy decreases for lower values of $F_y/(M \cdot g)$. The reason for this is not clear. Finally, there is a definite peak in the value of earthquake input energy versus period. This can be explained. If the dissipated hysteretic energy were viewed as an equivalent viscous damping dissipated energy, then the total value of the damping parameter C would be the sum of the viscous damping and the equivalent hysteretic damping. The earthquake input energy would be approximately

$$EIE = \int_0^T C \cdot \dot{U}^2 \cdot dt \doteq C \cdot \langle \dot{U}^2 \rangle \cdot t$$

The mean square velocity can be represented in terms of the input power spectral density and the velocity response function which in this case are unimodal functions, functions with one peak.

$$\langle \dot{U}^2 \rangle = \int_{-\infty}^{\infty} |H_{\dot{U}}(\omega)|^2 \cdot G_{\ddot{U}_g}{}^2(\omega) \cdot d\omega$$

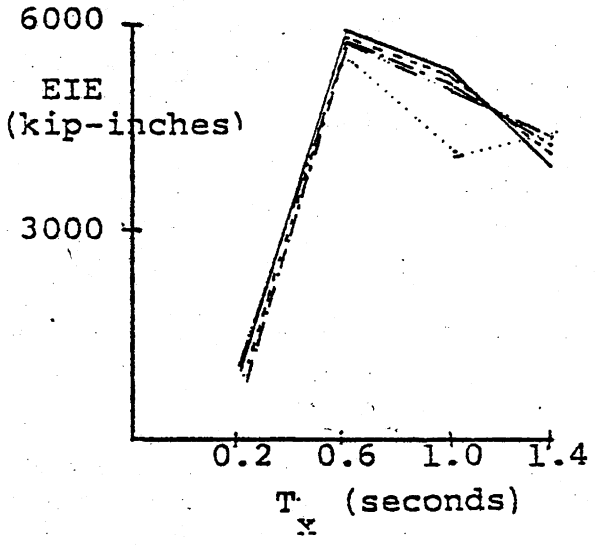

a) Earthquake Input Energy(EIE)

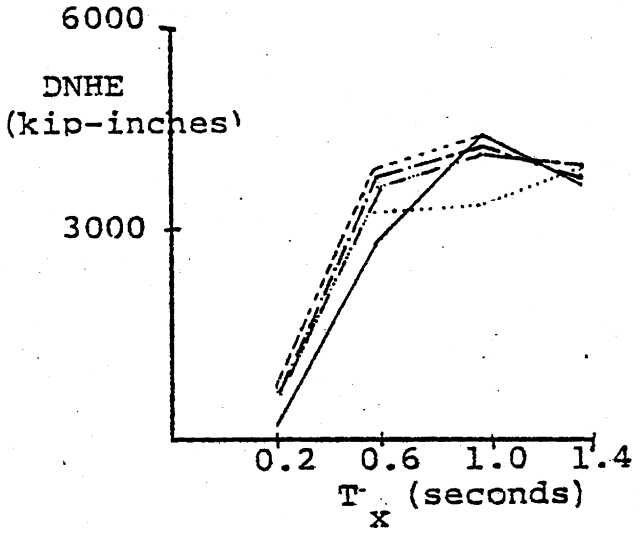

b) Dissipated Nonhysteretic Energy

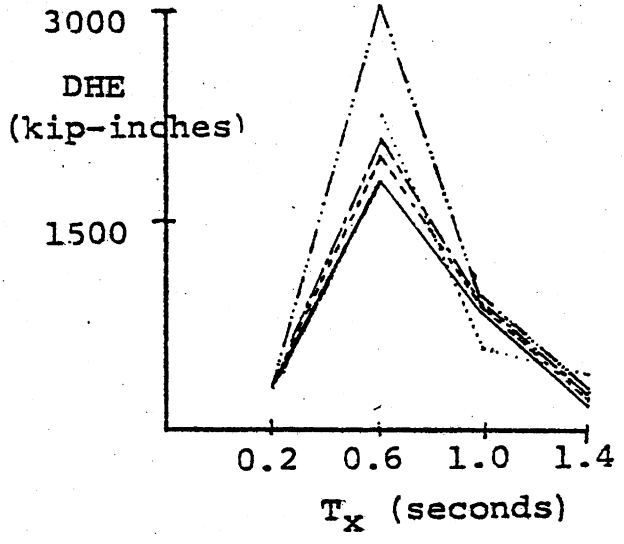

c) Dissipated Hysteretic Energy(DHE)

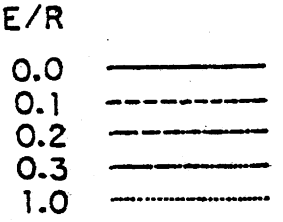

Figure 5-13 Energy Partition($F_y/(M*g)=1/2$)

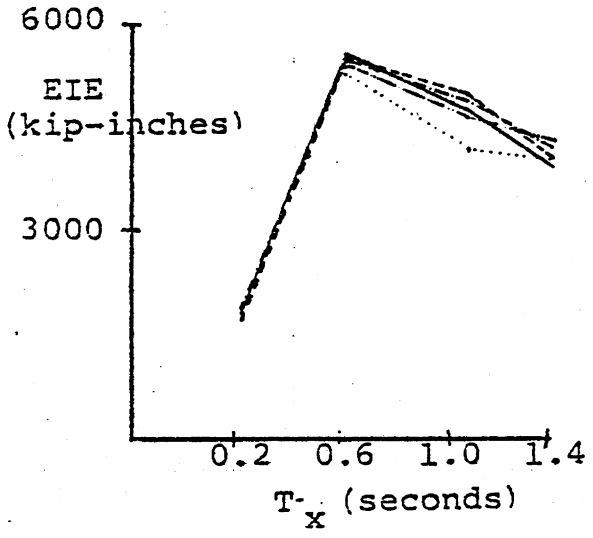

a) Earthquake Input Energy(EIE)

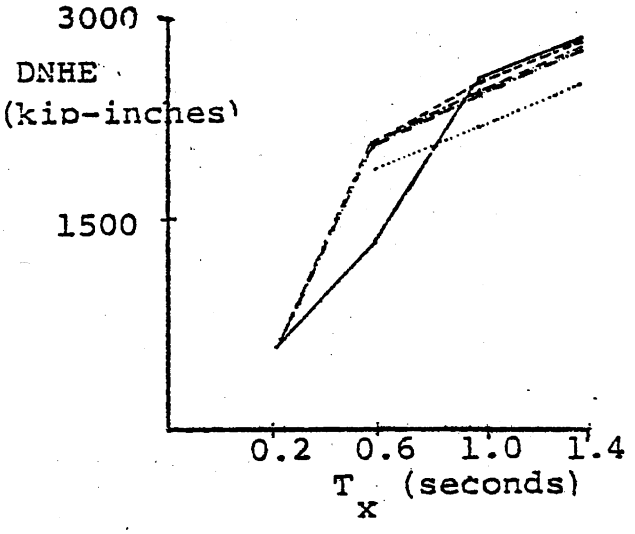

b)Dissipated Nonhysteretic Energy

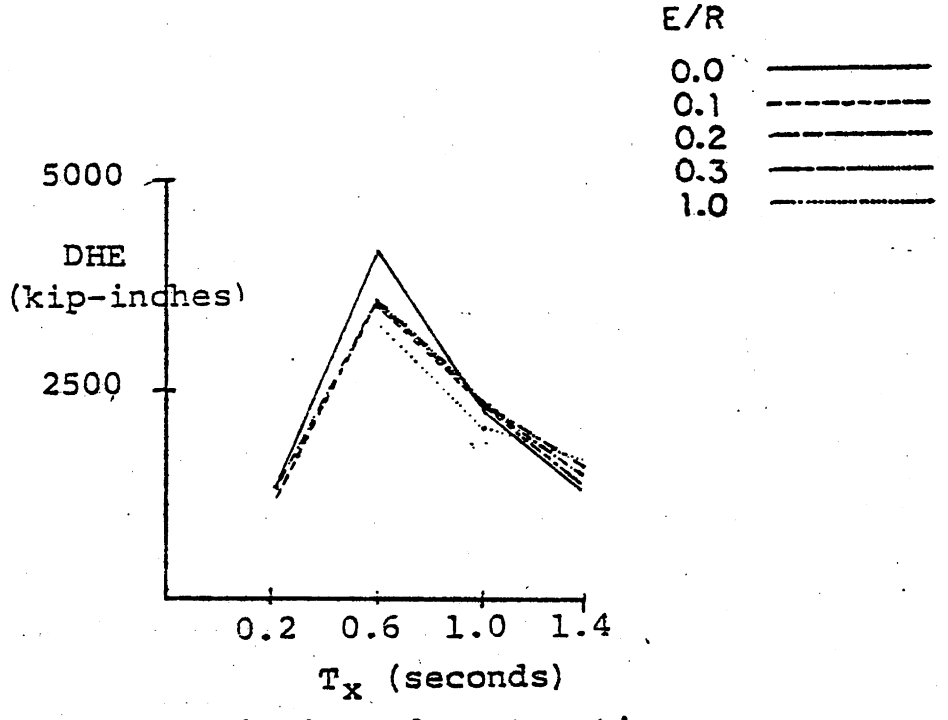

c) Dissipated Hysteretic Energy(DHE)

Figure 5-14 Energy Partition ($F_y/(M \cdot g) = 1/4$)

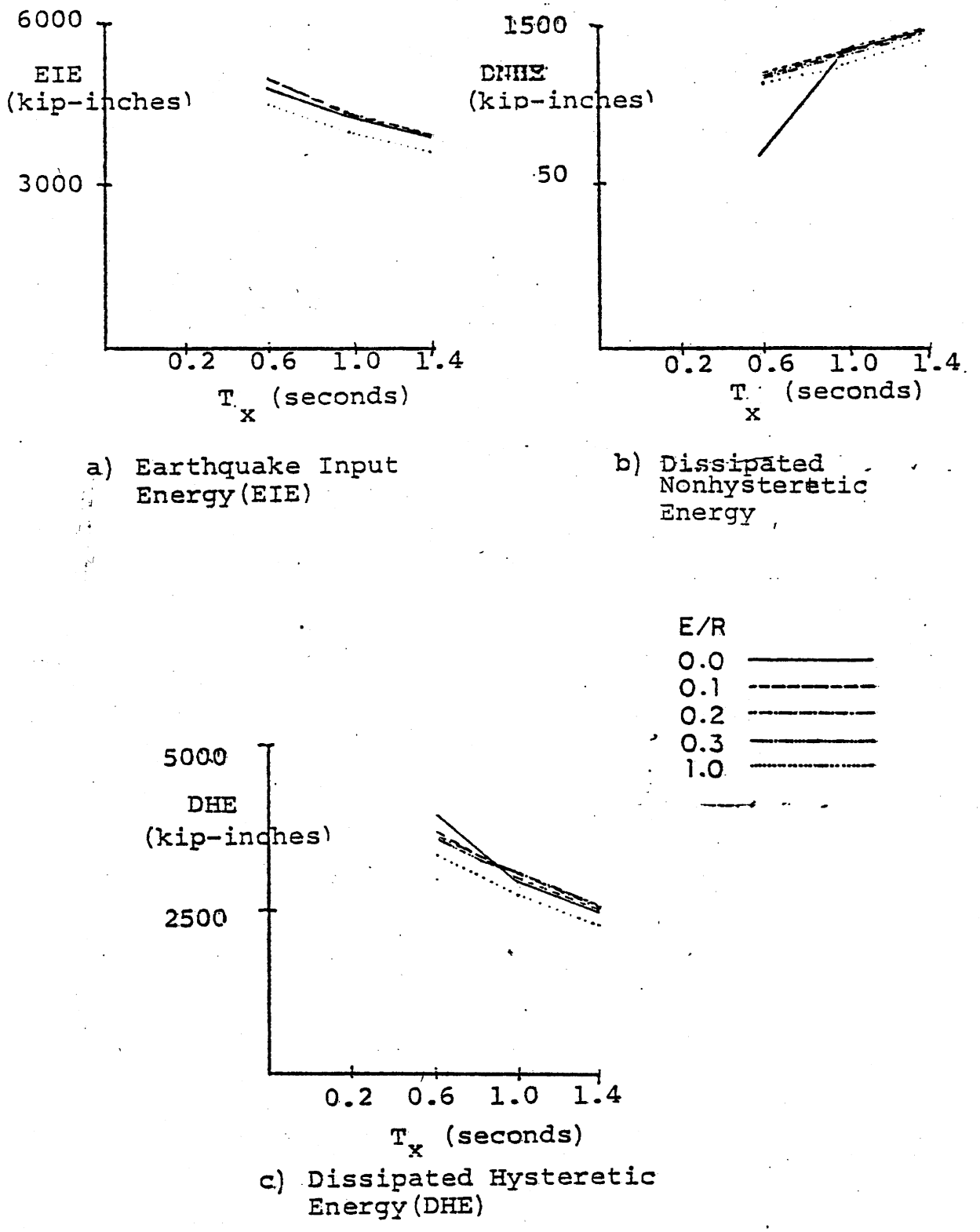

a) Earthquake Input Energy (EIE)

b) Dissipated Nonhysteretic Energy

c) Dissipated Hysteretic Energy (DHE)

Figure 5-15 Energy Partition ($F_y/(M \cdot g) = 1/8$)

A typical velocity response function is shown in Figure A3-1a). The input power spectral density is shown in Figure 5-1. It follows that $\langle \dot{U}^2 \rangle$ would be largest when the peaks of the two functions were concurrent. Thus, the largest value of earthquake input energy should occur near the peak of the input power spectral density function. This is the case.

The strength ratio corresponding to a given ductility ratio is also of interest. For the ductilities, averaged over the different eccentricity ratios, the corresponding strength ratio is determined by interpolation from Figures 5-7 to 5-12 and is shown in Figure 5-16.

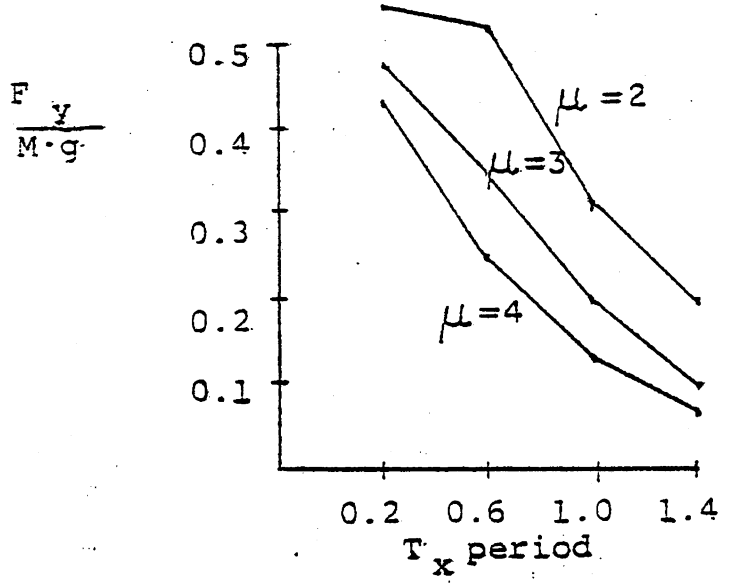

Figure 5-16 Strength Ratio versus Ductility

For a system with uniformly distributed mass, the response of the element furthest from the center of stiffness will be the largest. Due to this increased response the stiffness will be smaller relative to the element closest to the center of stiffness. This smaller

stiffness increases the eccentricity and, one might expect, could further increase the response of the element furthest from the center of stiffness.

This could lead to a situation where the eccentricity causes an increasingly nonlinear response of the element until the ductility demand could not be met. That this is not the case is evident from the results. The reason is probably the type of hysteresis model used. The bilinear model has increasingly nonlinear strength as well as increasing dissipated hysteretic energy capacity which would both limit the response. In any case, this does not seem to be a problem.

CHAPTER VI

SUMMARY AND CONCLUSIONS

This dissertation is concerned with the study of torsion in buildings subjected to earthquakes. It is now well known that there is a dynamic amplification of torque and a dynamic reduction in building shear. A recent, detailed study used the mode superposition and response spectrum techniques to develop response envelopes for an excitation in one direction. Other researchers have reported for a single accelerogram response, as much as a 40-100% increase in the peripheral response.

The analytical technique selected here for linear response was the probabilistic approach. The probabilistic description of earthquake excitation was discussed and a simple expression relating torsional earthquake excitation to translational earthquake excitation was developed. Interaction relations were derived for systems with simultaneous X, ϕ, and Y ground excitations.

The main concern or deleterious effect of building torsion is the increase in peripheral response. The reason for the increase is thought to be that the eccentricity induces a rotational motion whose displacement at the periphery more than offsets the decrease in the story displacement that occurs with increasing eccentricity. The peripheral response was studied using the probabilistic model. The effect of the various parameters on the

peripheral response was studied. It was shown that a special case arises where the peripheral response is independent of the eccentricity or frequency ratio.

Earthquake ground motion was described and the state of the art of artificial generation was discussed. Uncorrelated ground translations were used for this study. Newmark's model of ground rotational motion was used and the various parameters affecting it were studied. The decrease on the magnitude of this ground rotation as the rigid building size to wavelength ratio increases was also discussed.

A probabilistic approach cannot be used for nonlinear hysteretic response. Monte Carlo methods are used for nonlinear response. An ensemble of artificial accelerograms were generated for a response analysis of a class of nonlinear building types. For the four exterior wall model studied, a bilinear hysteresis was used. For this type of model the torsion-translation frequency ratio is determined by the geometry of the structure. The results showed the peripheral response to be only marginally higher than that for zero eccentricity.

For an eccentric structure responding in the nonlinear range, the eccentricity increases with the increasing nonlinearities, possibly causing larger and larger torsional excitation. These studies showed this is not a problem with the bilinear hysteresis used with this model.

Conclusions

Based on the study in this dissertation, the following general conclusions can be made: 1) in the statistical sense of the word expected, i.e. the mean, the maximum expected increase in the elastic peripheral response due to both the eccentricity and ground rotations is on the order of 50%; 2) the single most important parameter in building torsion is the torsion-translation frequency ratio; 3) torsional ground excitation must be quite large before it significantly affects the response for structures with well separated frequencies; 4) the dissipated hysteretic energy for nonlinear structures is maximum when the natural frequency is near the predominant frequency of the accelerogram; and 5) parametric resonance is not a problem for the four peripheral wall structure studied herein.

Concluding Remarks

The analysis of building torsion in this dissertation assumes the ground rotation to be related to the ground translations by Newmark's relation. Although the conclusions stated are based on this assumption, it is still felt, based on field observations of others, that ground rotation is not much larger if different. Nevertheless, the author still recommends the development and production of a torsional seismometer to determine the actual magnitude of the ground rotations and its relation to ground translations.

Lastly, the importance of the torsion-translation frequency ratio must be emphasized. It is recommended for unusually shaped buildings where large eccentricities are unavoidable, that the building be designed with well separated torsion and translation frequencies.

APPENDIX A

Response of single degree of freedom oscillators is sometimes computed by the Duhamel or convolution integral. The response to an impulse is a damped sine wave commonly referred to as the impulse response function, $h(t)$ of the oscillator. The summing of the response due to each impulse becomes in the limit an integral. The summing or superposition of these responses is referred to as the Duhamel or convolution integral

$$V(t)=\int_{-\infty}^{t} h(t-t')\cdot P(t')dt' \qquad A.1$$

where

$$h(t)=\begin{cases} 0 & t<0 \\ \exp(-B\cdot\omega\cdot t)\cdot\sin[\omega\cdot(1-B^2)^{0.5}\cdot t]/[\omega\cdot(1-B^2)^{0.5}] & t\geq 0 \end{cases} \qquad A.2$$

which is the transfer function for the differential equation

$$\ddot{V}(t)+2\cdot B\cdot\omega\cdot\dot{V}(t)+\omega^2\cdot V(t) = P(t) \qquad A.3$$

The Fourier transform of Equation A.1, commonly referred to as the complex frequency response function, is

$$H(\omega)=1/[\omega_n{}^2-\omega^2+2\cdot B\cdot\omega\cdot\omega_n\cdot i] \qquad A.4$$

The transfer function and the modulus of its transform are plotted in Figure Aa).

The power spectral density of an ergodic stochastic process is defined as

$$G_p{}^2(\omega)=\lim_{s\to\infty}\left|\int_{-s/2}^{s/2} p(t)\cdot\exp(-i\cdot\omega\cdot t)\cdot dt\right|^2/s \qquad A.5$$

A sample random process and its spectral density are shown in Figure Ab).

It can easily be shown[59] that the response power spectral density is the product of the square of the complex frequency response function and the input power spectral density.

$$|G_v^2(\omega)| = |H(\omega)|^2 \cdot |G_p^2(\omega)| \qquad A.6$$

The response v(t) and corresponding power spectral density are shown in Figure Ac). It is seen that a convolution in the time domain corresponds to a multiplication in the frequency domain. The converse can also be shown. Put simply, the transform of a convolution of two functions is the product of the individual transforms; also, the transform of the product of two functions is the convolution of the individual transforms.

The averaging filter $U_{t'}(t)$

$$U_{t'}(t) = \begin{cases} 0 & t < -t' \\ 1/t' & -t' < t < t' \\ 0 & t > t' \end{cases} \qquad A.7$$

along with its transform U(f)

$$U(f) = \sin(2 \cdot \pi \cdot f \cdot t') / (2 \cdot \pi \cdot f \cdot t') \qquad A.8$$

are depicted in Figure Ad).

The averaged response $\overline{V(t)}$

$$\overline{V(t)}=\frac{1}{t'}\int_{t-t'/2}^{t+t'/2} V(t)\,dt=\int_{-\infty}^{\infty} U_{t'}(t-t')\cdot V(t')\,dt'=U_{t'}(t)*V(t) \qquad A.9$$

can be viewed as the convolution of $U_{t'}$ with V. The transform of $\overline{V}$ shown in Figure Ae) is the product of the transform of $U_{t'}$ and V.

The first zero of U(f) is 1/(2t'), which for the values of interest will be well beyond the natural frequency, f. Thus the effect of the averaging is to reduce the ordinates of the spectral density which reduces the variance defined as the area under the spectral density curve. Since the expected extreme value is proportional to the variance, the effect of the averaging reduces the expected extreme value, as expected.

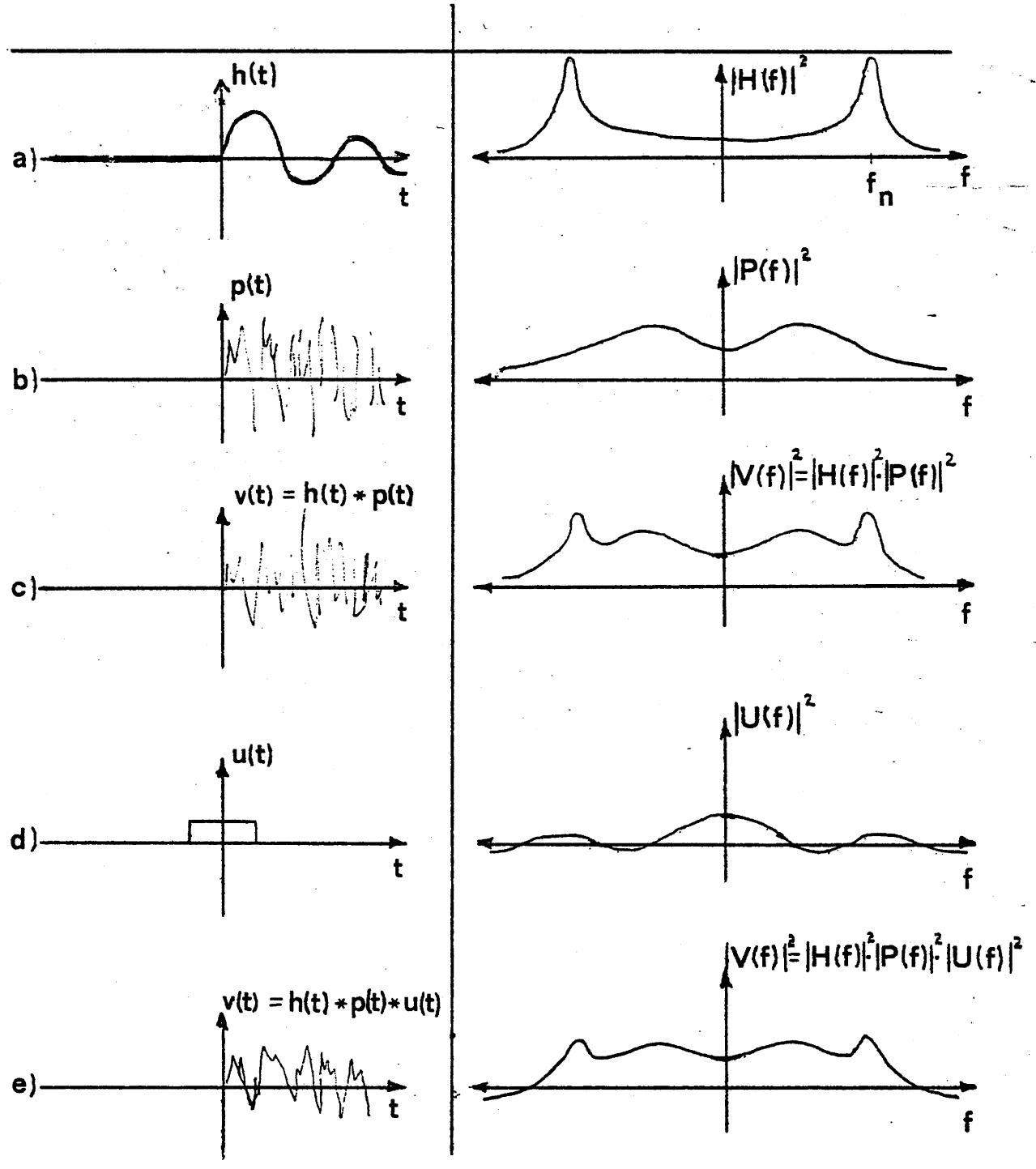
h(t)
a)
t
|H(f)|²
f
f_n
p(t)
b)
t
|P(f)|²
f
v(t) = h(t) * p(t)
c)
t
|V(f)|² = |H(f)|² · |P(f)|²
f
u(t)
d)
t
|U(f)|²
f
v(t) = h(t) * p(t) * u(t)
e)
t
|V(f)|² = |H(f)|² · |P(f)|² · |U(f)|²
f

Figure A-1

APPENDIX B

For a single degree of freedom (SDOF) system the expected response is a maximum when the structure is directed along one of the principal axes. The motion along the principle axes are uncorrelated and are defined as the radial to the epicenter and normal to the radius.

To show this, it is first assumed that the maximum expected response is proportional to the variance, consistent with the theory of extreme values. The variance is expressed as the integral of the power spectral density of the response, which is expressed as the integral of the product of the frequency response function and excitation power spectral density.

Let R denote the excitation along the principal axis P. Since R and C are uncorrelated, the cross-correlation function is zero. Thus, the cross spectrum $G_{rc}^2(\omega)$, the transform of the cross-correlation function, is also zero. Let X and Y denote the angle θ of the structure's to P. Then

$$X=C\cdot\cos(\theta) + R\cdot\sin(\theta)$$

and

$$Y=C\cdot\sin(\theta) + R\cdot\cos(\theta)$$

Describing the power spectral density of X and Y in terms of R and C gives

$$G_x^2(\omega)=\cos^2(\theta)\cdot G_r^2(\omega)+\sin^2(\theta)\cdot G_c^2(\omega)$$

$$G_y^2(\omega)=\sin^2(\theta)\cdot G_r^2(\omega)+\cos^2(\theta)\cdot G_c^2(\omega)$$

$$G_{xy}^2(\omega)=\cos(\theta)\cdot\sin(\theta)\cdot(G_r^2(\omega)-G_c^2(\omega))$$

The variance of response of the SDOF system is

$$\langle X^2\rangle=\int_{-\infty}^{\infty}|H(\omega)|^2\cdot G_x^2(\omega)\,d\omega$$

$$=\int_{-\infty}^{\infty}|H(\omega)|^2\cdot[\cos^2(\theta)\cdot G_r^2(\omega)+\sin^2(\theta)\cdot G_c^2(\omega)]\,d\omega$$

which is maximum when θ is either 0° or 90° depending on the relative variances of R and C.

For a multidegree of freedom (MDOF) system, the approach is not as straightforward, and simplifying assumptions must be made. First, the variance is expressed as the sum of the variances and covariances of the uncoupled modal responses. The response quantity of interest is

$$Q = \{B\}^T \{X\}$$

where

$$\{X\} = [A]'\{U\}$$

$$\ddot{\{U\}}+[2\cdot B\cdot\omega]'\dot{\{U\}}+[\omega^2]'\{U\}=\{P\}$$

[A] is the matrix of eigenvectors. The response power spectrum can be expressed as

$$G_q^2(\omega)=\{B\}^T[H]^H[A]^T[G_p^2(\omega)][A][H]'\{B\}$$

For a 2-DOF system this expands to

$$G_q^2=(G_o^2\cdot\cos^2\theta+G_r^2\cdot\sin^2\theta)[H_1^2\cdot A_{11}^2\cdot B_1^2+2\cdot H_1\cdot H_2\cdot A_{11}A_{21}B_1\cdot B_2+H_2^2\cdot A_{12}^2\cdot B_2^2]+$$

$$(G_r^2-G_c^2)\cdot\cos\theta\cdot\sin\theta[H_1^2A_{11}\cdot A_{21}B_1^2+H_1\cdot H_2(A_{11}\cdot A_{22}+A_{21}\cdot A_{12})B_1\cdot B_2+H_2^2\cdot A_{12}\cdot A_{22}B_2)+$$

$$(G_c^2\cdot\sin^2\theta+G_c^2\cdot\cos^2\theta)[H_1^2\cdot A_{21}^2\cdot B_1^2+2H_1\cdot H_2\cdot A_{21}\cdot A_{22}B_1\cdot B_2+H_2^2\cdot A_{22}^2\cdot B_2^2] \quad B1$$

Rosenblueth[41] argues, based on work by Rascon[73], that there is a deterministic relation between the ratio of spectral intensities (SI) of the ground motions along the two orthogonal axes, and that as the RMS spectrum intensity increases the expected ratio approaches unity. For the RMS spectrum intensity>4.5, corresponding to a Modified Mercalli intensity of around V, the ratio exceeds 0.9.

Thus, for earthquake intensities of interest, SIx=SIy. Since the Arias intensity, the variance times duration, is closely related to Housner's spectrum intensity, we can say that $\langle X^2 \rangle \cong \langle Y^2 \rangle$, or

$$\int_{-\infty}^{\infty} G_r^2(\omega) \cdot d\omega \cong \int_{-\infty}^{\infty} G_c^2(\omega) \cdot d\omega$$

Due to the origins of the two ground motions R and C, we can say

$$|H(\omega)|^2 \cdot G_r^2(\omega) \cdot d\omega = |H(\omega)|^2 \cdot G_c^2(\omega) \cdot d\omega \qquad \text{B.2}$$

Thus, in Equation B.1, the first and third terms become dominant and the contribution of the second term approaches zero. Also, since the two displacement coordinates, corresponding to the two horizontal ground translations, are orthogonal, the amount of coupling will be small even in the worst case, i.e. $A_{ii} >> A_{ij}$. THis suggests that Equation B.1 will be maximum when the $\cos(\theta) \cdot \sin(\theta)$ is maximum, i.e. $\theta = 45°$. However, Equation B.2 suggests that the difference will be slight.

APPENDIX C

For a white noise process of intensity,, G_o, the covariance of modal responses is defined as

$$< Y_m(t) \cdot Y_n(t) >= \int_{-\infty}^{\infty} H_{ym}(\omega) \cdot H_{yn}(\omega) \cdot G_o^2 \cdot d\omega \qquad 3.13$$

where the complex frequency response function is

$$H_{yn}(\omega) = 1/[\omega_m^2 + i \cdot 2 \cdot B_m \cdot \omega_m \cdot \omega - \omega^2] \qquad C.1$$

The variance is

$$< Y_m^2(t) >= \int_{-\infty}^{\infty} |H_{ym}(\omega)|^2 \cdot G_o^2 \cdot d\omega \qquad C.2$$

The correlation coefficient P_{mn} is defined as

$$P_{mn} = \frac{< Y_m(t) \cdot Y_n(t) >}{< Y_m^2(t) >^{05} \cdot < Y_n^2(t) >^{0.5}} \qquad C.3$$

Inserting C.1 into C.2 gives

$$< Y_m^2(t) >= \int_{-\infty}^{\infty} \frac{G_o^2 \cdot d\omega}{[\omega^4 + \omega_m \cdot (4 \cdot B_m^2 - 2) \cdot \omega^2 - \omega_m^4]} \qquad C.4$$

This can be factored to

$$< Y_m^2(t) >= \int_{-\infty}^{\infty} \frac{G_o^2 \cdot d\omega}{[\omega^2 - \omega_m^2 \cdot \exp(-2 \cdot i \cdot \theta)] \cdot [\omega^2 - \omega_m^2 \cdot \exp(2 \cdot i \cdot \theta)]} \qquad C.5$$

where $\exp(2 \cdot i \cdot \theta) = [(1 - 2 \cdot B_m^2)] + i \cdot [2 \cdot B_m \cdot (1 - B_m^2)^{0.5}]$ and $i = (-1)^{0.5}$

Equation C.5 can be expanded to

$$\langle Y_m^2(t)\rangle = \int_{-\infty}^{\infty} \frac{G_o^2}{[\omega-\omega_m\cdot\exp(-i\cdot\theta)]\cdot[\omega+\omega_m\cdot\exp(-i\cdot\theta)]}$$

$$\cdot\frac{d\omega}{[\omega-\omega_m\cdot\exp(i\cdot\theta)]\cdot[\omega+\omega_m\cdot\exp(i\cdot\theta)]} \qquad C.6$$

where $\exp(i\cdot\theta)=[(1-B_m^2)^{0.5}]+i\cdot[B_m]$

Equation C.6 has 4 poles of order 1; namely, $\pm\omega_m\cdot\exp(i\cdot\theta)$ and $\pm\omega_m\cdot\exp(i\cdot\theta)$. $f(x)$ can be regarded as a line integral along the real axis. By the method of residues:

$$\int_{-\infty}^{\infty} f(x)\,dx = \oint_{C_r} f(z)\cdot dz$$

where $f(z)$ is analytic in C_r except at a finite number of poles, and C_r is a semicircular path whose diameter is the real axis. Then

$$\oint_{C_r} f(z)\cdot dz = 2\cdot\pi\cdot i\cdot \{\text{sum of the residues in the upper half of the complex z-plane}\}$$

The residue of $f(z)$ at z', z' a pole of order 1, is

$$\text{Res}[f(z),z'] = \lim_{z\to z'} [(z-z')\cdot f(z)]$$

The integrand in Equation C.6 has two poles in the upper half of the complex z-plane, namely, $\omega_m\cdot\exp(i\cdot\theta)$ and $-\omega_m\cdot\exp(-i\cdot\theta)$.

thus,

$$\langle Y_m^2(t)\rangle = \frac{2\cdot\pi\cdot G_o^2\cdot i}{\omega_m^3} \cdot$$

$$\frac{1}{[\exp(i\cdot\theta)+\exp(-i\cdot\theta)][\exp(i\cdot\theta)-\exp(-i\cdot\theta)][\exp(i\cdot\theta)+\exp(i\cdot\theta)]}$$

$$+\frac{1}{[-\exp(-i\cdot\theta)-\exp(i\cdot\theta)][\exp(i\cdot\theta)-\exp(-i\cdot\theta)][-\exp(-i\cdot\theta)-\exp(-i\cdot\theta)]}$$

or

$$\langle Y_m^2(t)\rangle = \frac{G_o^2\cdot\pi}{2\cdot\omega_n^3\cdot B_m} \qquad \text{C.7}$$

which is the variance of the displacement of an oscillator subjected to white noise excitation.

For the covariance, combining Equation 3.13 and C.1

$$\langle Y_m(t)\cdot Y_n(t)\rangle =$$

$$\int_{-\infty}^{\infty} \frac{G_o^2}{[\omega+\omega_m\cdot\exp(-i\cdot\theta)]\cdot[\omega-\omega_m\cdot\exp(i\cdot\theta)]} \cdot$$

$$\frac{d\omega}{[\omega+\omega_n\cdot\exp(i\cdot\theta)]\cdot[\omega-\omega_n\cdot\exp(-i\cdot\theta)]} \qquad \text{C.8}$$

By the method of residues, Equation C.8 becomes

$$\langle Y_m(t)\cdot Y_n(t)\rangle = 2\cdot\pi\cdot i\cdot G_o^2\cdot \{\text{sum of residues on upper half of complex z-plane}\}$$

$$= \frac{2\cdot\pi\cdot i\cdot G_o^{\,2}}{2\cdot\omega_m\cdot(1-B_m^{\,2})^{0.5}}$$

$$\cdot \frac{1}{[\omega_m\cdot\exp(i\cdot\theta_m)+\omega_n\cdot\exp(i\cdot\theta_n)]\cdot[\omega_m\cdot\exp(i\cdot\theta_m)-\omega_n\cdot\exp(-i\cdot\theta_n)]}$$

$$\frac{1}{[-\omega_m\cdot\exp(-i\cdot\theta_m)+\omega_n\cdot\exp(i\cdot\theta_n)][-\omega_m\cdot\exp(-i\cdot\theta_m)-\omega_n\cdot\exp(-i\cdot\theta_n)]}$$

Simplifying,

$$\begin{aligned}
<Y_m(t)\cdot Y_n(t)> &= 2\cdot\pi\cdot i\cdot G_o^{\,2}\cdot\{1/z-1/\bar{z}\}/(2\cdot\omega_m') \\
&= 2\cdot\pi\cdot i\cdot G_o^{\,2}\cdot\{2\cdot i\cdot Im(z)/|z|^2\}/(2\cdot\omega_m') \\
&= 4\cdot\pi\cdot G_o^{\,2}\cdot(\omega_m\cdot B_m+\omega_n\cdot B_n)/|Z|^2 \qquad \text{C.9}
\end{aligned}$$

where ω_m' is the damped natural frequency of the mth mode and

$$Z=[(\omega_m'^{\,2}-\omega_n'^{\,2})-(\omega_m\cdot B_m+\omega_n\cdot B_n)^2]+i\cdot[2\cdot\omega_m'\cdot(\omega_m\cdot B_m+\omega_n\cdot B_n)]$$

The correlation coefficient P_{mn} by inserting Equation C.7 and C.9 into C.3 is

$$P_{mn}=8\cdot(\omega_m\cdot B_m+\omega_n\cdot B_n)\cdot(\omega_m^{\,3}\cdot B_m\cdot\omega_n^{\,3}\cdot B_n)^{0.5}/|Z|^2 \qquad \text{C.10}$$

which is Equation 3.24. For B_n, $B_m << 1$, Equation C.10 is very close to the simpler Equation 3.10 developed by Rosenblueth.

APPENDIX D

As described in Chapter II, the power spectrum for ensembles of accelerograms is commonly expressed in the Kanai-Tajimi form

$$G_z^2(\ ) = \frac{G_o^2 \cdot (1+4 \cdot B_g^2 \cdot \omega^2/\omega_g^2)}{\{[1-(\omega/\omega_g)^2]^2+4 \cdot B_g^2 \cdot \omega^2/\omega_g^2\}} \qquad D.1$$

The response power spectrum for this type of excitation is

$$G_y^2(\omega) = |H_y(\omega)|^2 \cdot G_z^2(\omega) \qquad D.2$$

or

$$<Y^2(t)> = \int_{-\infty}^{\infty} \frac{G_o^2 \cdot (1+4 \cdot B_g^2 \cdot \omega^2/\omega_g^2) \cdot d\omega}{[\omega^4+\omega_n^2 \cdot (4 \cdot B_n^2-2) \cdot \omega^2-\omega^4] \cdot [(1-\omega^2/\omega_g^2)^2+4 \cdot B_g^2 \cdot \omega^2/\omega_g^2]}$$

$$= G_o^2 \cdot \int_{-\infty}^{\infty} \frac{\omega_g^4 \cdot [1+4 \cdot B_g^2 \cdot \omega^2/\omega_g^2]}{[\omega^2-\omega_n^2 \cdot \exp(-2 \cdot i \cdot \theta_n)][\omega^2-\omega_n^2 \cdot \exp(2 \cdot i \cdot \theta_n)]}$$

$$\cdot \frac{d\omega}{[\omega^2-\omega_g^2 \cdot \exp(-2 \cdot i \cdot \theta_g)][\omega^2-\omega_g^2 \cdot \exp(2 \cdot i \cdot \theta_g)]} \qquad D.3$$

which has eight poles of order 1 at $\pm\omega_n \cdot \exp(\pm i \cdot \theta_n)$ and $\pm\omega_g \cdot \exp(\pm i \cdot \theta_g)$. By the method of residues

$$<Y_n^2(t)> = G_o^2 \cdot 2 \cdot \pi \cdot i \cdot \{\text{Sum of the residues in the upper half of the complex z-plane.}\}$$

With the assuption that the spectrum for the ensemble of excitations is a wide band process, B_g will be large compared to that of the lightly damped oscillator, i.e.

$$B_g >> B_n$$

and therefore

$$\theta_g >> \theta_n$$

After some algebra

$$\langle Y_n^2(t)\rangle = \frac{G_o^2 \cdot \pi}{2 \cdot \omega_n^3 \cdot B_n} \cdot$$

$$\frac{1+4 \cdot B_g^2 \cdot \omega^2/\omega_g^2}{1+(\omega_n/\omega_g)^4-(\omega_n/\omega_g)^2 \cdot \{\exp[2 \cdot i \cdot (\theta_g-\theta_n)]+\exp[-2 \cdot i \cdot (\theta_g+\theta_n)]\}}$$

$$+ \frac{G_o^2 \cdot \pi}{2 \cdot \omega_g^3 \cdot B_g} \cdot$$

$$\frac{(1+4B_g^2)\{[1-\omega_n^2/\omega_g^2]^2+4 \cdot B_g^2 \cdot \omega_n^2/\omega_g^2\}-4 \cdot B_g^2 \cdot \omega_n^2/\omega_g^2(1-4 \cdot B_g^2)}{\{[1-(\omega_n/\omega_g)^2]^2+4 \cdot B_g^2 \cdot \omega_n^2/\omega_g^2\}^2+\{[4 \cdot \omega_n^2/\omega_g^2 \cdot B_g]^2 \cdot (1-B_g^2)\}}$$

D.5

or

$$\langle Y_n^2(t)\rangle = \frac{\pi \cdot G_z^2(\omega_n)}{2 \cdot \omega_n^3 \cdot B_n} + \frac{\pi \cdot F(\omega_n)}{2 \cdot \omega_g^3 \cdot B_g} \qquad \text{D.6}$$

$$= \langle Y_n^2(t)\rangle_{\omega.n.} \cdot G_z^2(\omega_n) + \langle Z^2(t)\rangle \cdot F(\omega_n)$$

where $G_z^2(\omega)$ is defined by Equation D.1, $F(\omega_n)$ is defined in Equation D.5, and $\langle Y_n^2(t)\rangle_{\omega.n.}$ is the response of the oscillator to white noise. The assumption underlying Equation D.6 gives rise to the same approximation used in gust response factors, based on graphical inspection.

Typical values for ω_g and B_g used in Equation D.1 are 15.6 radians/sec. and 0.6, respectively. For $\omega_n \ll \omega_g$, $F(\omega_n) \simeq G_o^2$ and $G_z^2(\omega_n) > G_o^2$. Also, since $B_g \ll B_n$ the first term in Equation D.6 dominates and

$$\langle Y_n^2(t) \rangle \simeq \langle Y_n^2(t) \rangle_{\omega.n.} \cdot G_z^2(\omega_n) \qquad D.7$$

Thus the variance, which is proportional to the square of the expected extreme value, is proportional to the value of the excitation power spectrum at the oscillator natural frequency. For a wide band excitation where the building frequencies are close together the effect of nonwhite excitation cancels.

Appendix E

Nonlinear Response Program

```
C
C PROGRAMMED BY MARTIN E. BATTS 1977
C
C CONSISTENT UNITS (USE KIPS&INCHES)
C GACC(1)= X GROUND ACCEL      INPUT FILE 7
C GACC(2)= Z GROUND ANGULAR ACCEL
C GACC(3)= Y GROUND ACCEL      INPUT FILE 8
C EXM= X DIST FROM ORIGIN TO C.G.
C EYM= Y DIST FROM ORIGIN TO C.G.
C BX= DIST ALONG X AXIS BETWEEN Y RESISTING ELEMENTS
C BY= DIST ALONG Y AXIS BETWEEN X RESISTING ELEMENTS
C EX= ECCENTRICITY ALONG X AXIS FROM C.G. TO CENTER OF STIFFNESS
C EY= ECCENTRICITY ALONG Y AXIS FROM C.G. TO CENTER OF STIFFNESS
C XI= % CRITICAL DAMPING(VISCOUS)
C DT= INTEGRATION TIME STEP
C MASS= MASS
C PMASS= MASS MOMENT OF INERTIA(=R**2*MASS)
C TO= INTIAL TIME
C TEND= FINAL TIMEOF ACCELERATION
C DTAC= EQUAL TIME STEP OF ACCELERATION AS INPUT
C R=POLAR RADIUS OF GYRATION OF MASS
C SO= INITIAL ELEMENT STIFFNESS      IELEM=1=RAMBERG-OSGOOD
C QY= ELEMENT YIELD FORCE            IELEM=2=BILINEAR
C RO= RAMBERG-OSGOOD COEFF.          IELEM=3=STIFFNESS DEGRADING
C SX= TOTAL X DIRECTION STIFFNESS    GG=ACCELERATION UNITS
C SY= TOTAL Y DIRECTION STIFFNESS    IPDELT=0 MEANS NO P-DELTA CALCS
C SR= TOTAL Z DIRECTION STIFFNESS    HGT=HEIGHT OF BLDG.
C PHI= MODE SHAPE                    ACMULT=INPUT E. MULTIPLIER
C D= EIGENVALUES
C DAMP= DAMPING MATRIX=M-1/2*C*M-1/2
C DYE= YIELD DISPLACEMENTS OF ELEMENTS
C DYC=YIELD DISPLACEMENTS OF COORD DIRECTION
C Y= RELATIVE DISPLACEMENT
C DY= RELATIVE VELOCITY
C DDY= RELATIVE ACCLERATION
C OLDIS= OLD RELATIVE DISPLACEMENT
C PFC= OLD COORD TOTAL FORCE
C DISE= DISPLACEMENT OF THE ELEMENTS
C PF= ELEMENT FORCE
C OF= OLD ELEMENT FORCE
C TE(I)= INTEGRAL OF ELEMENT I FORCE TIMES DISPLACEMENT
C        (OUTPUT AS TE-STRAIN ENERGY=DISSIPATED ENERGY)
C DAMPDE(I)= DAMPING DISSIPATED ENERGY FOR COORD DIRECTION I
C VARC=  COORD DISP COV.     VARFC=  COORD FORCECOV.
C VARE= RMS ELEMENT DISP   VARFE= RMS ELEMENT FORCE
C EQNS OF MOTION (Y)=(U,R*THETA,V)  THETA ABOUT CENTER OF MASS
C
C          (C11   C12/R    C13  )          (KX     -KX*EY/R 0.     )
C  ..    1                        .    1
C (Y ) + -*(C21/R C22/R**2 C23/R)*(Y) + -*(-KX*EY/R KO/R**2 KY*EX/R)*(Y)
C        M                          M
C          (C31   C32/R    C33  )          (0.     KY*EX/R KY     )
C
```

```
C KO= STIFFNESS AROUT CENTER OF MASS(NOT CENTER OF STIFFNESS)
C NOTE THAT THE MASS MATRIX IS THE IDENTITY MATRIX.THUS THE MODAL MASSES
C ARE  1.0
      DIMENSION FORMAT(20), P1(8000), D1(8000), SOC(3), DYC(3), DYE(4)
      COMMON /GTIME/ GACC(3), OGACC(3), G(8000,3)
      COMMON SK(3,3), DAMP(3,3), PHI(3,3), D(3), OLDPFC(3), OLDIS(3),
     1       PDELTA(3)
      COMMON /STIFF/ RO(4), FY(4), SO(4), IYC(4), S(4), PMAX(4), EPSMAX,
     1       IBTOT
      DIMENSION DISE(4), ODISE(4), DISEMX(4), Y(3), DY(3), DDY(3),
     1          ODY(4), TITLE(20), PF(4), B(6,6), DUCMX(4), DISMX(3),
     2          PFMAX(4), TDISMX(3), ACMAX(3), TACMAX(3), OF(4),
     3          DUCTMX(3), TE(4), PFC(3), OY(4), AUX1(3), AUX2(3),
     4          PFCMX(3), TPFCMX(3), VG(3), VARE(4), VARC(3,3), EIE(3),
     5          DAMPDE(3), VARFE(4), VARFC(3,3), TEC(3), P(3), FEBAR(4),
     6          YEBAR(4), FCBAR(3), YCBAR(3), VELE(4), OVELE(4),
     7          ACCE(4), OACCE(4), ECCMAX(3), SKINV(3,3)
      REAL MASS, K1(3), K2(3), K3(3), K4(3), M(3)
      IN = 5
      INN = 7
      INN2 = 8
      IT = 6
   10 READ (IN,20,END=550) TITLE
      WRITE (IT,30) TITLE
   20 FORMAT (20A4)
   30 FORMAT (1H1, 20A4/)
      READ (IN,20) TITLE
      WRITE (IT,40) TITLE
   40 FORMAT (//' X GROUND ACCELERATION= ', 10A4, 10X, ' Y GROUND ACCELE
     1RATION= ', 10A4/)
      READ (IN,50) EXM, EYM, BX, BY, XI, DT, MASS, TO, TEND, DTAC, GG,
     1ACMULT, CS, HGT, IELEM, IGROT, IPDELT, IPLOT
   50 FORMAT (4F10.2/3F10.9/7F10.4/4I5)
      NSTEPS = (TEND - TO) / DTAC + 0.49
      READ (IN,60) SO, FY, RO
   60 FORMAT (4F10.3)
      READ (IN,70) FORMAT
   70 FORMAT (20A4)
      PMASS = MASS * (BX**2 + BY**2) / 12.
      R = SQRT((BX**2 + BY**2)/12.)
      EX = SO(4) * BX / (SO(3) + SO(4)) - EXM
      EY = SO(2) * BY / (SO(1) + SO(2)) - EYM
      IBTOT = 0
      EPSMAX = 0.0
      SOC(1) = SO(1) + SO(2)
      SOC(3) = SO(3) + SO(4)
      SOC(2) = SO(1) * EYM ** 2 + SO(2) * (BY - EYM) ** 2 + SO(3) * EXM
     1** 2 + SO(4) * (BX - EXM) ** 2
      DET = SOC(1) * SOC(3) * (SOC(2) - SOC(1)*EY**2 - SOC(3)*EX**2)
      SKINV(1,1) = (SOC(2)*SOC(3) - (SOC(3)*EX)**2) / DET
      SKINV(1,2) = (SOC(1)*SOC(3)*EY) / DET
      SKINV(1,3) = (-SOC(1)*SOC(3)*EX*EY) / DET
      SKINV(2,1) = SKINV(1,2)
      SKINV(2,2) = (SOC(1)*SOC(3)) / DET
```

```
      SKINV(2,3) = (-SOC(1)*SOC(3)*EX) / DET
      SKINV(3,1) = SKINV(1,3)
      SKINV(3,2) = SKINV(2,3)
      SKINV(3,3) = (SOC(2)*SOC(1) - (SOC(1)*EY)**2) / DET
      M(1) = 1.0
      M(2) = 1.0 * R
      M(3) = 1.0
      PDELTA(1) = GG * FLOAT(IPDELT) / HGT
      PDELTA(2) = 0.0
      PDELTA(3) = GG * FLOAT(IPDELT) / HGT
      EXR = EX / R
      EYR = EY / R
      WRITE (IT,80) BX, BY, EXM, EYM, XI, DT, MASS, PMASS, TO, TEND,
     1DTAC, R, EXR, EYR, GG, ACMULT, IELEM, IGROT, CS, IPDELT, HGT,
     2IPLOT
   80 FORMAT (//'0 BX=', F7.2, '   BY=', F7.2, ' EXM=', F7.2, '  EYM=',
     1       F7.2, ' BETA=', F6.4, '  DT=', F6.4, '  MASS=', E11.4, '  M
     2R**2 =', E11.4, /'  TO=', F7.3, '   TF=', F6.3, '  DTAC=', F6.4, '
     3  R=', F8.4, '  EX/R=', F6.4, '  EY/R=', F7.4, '  G=', F8.3, 4X, '
     4 ACMULT=', F8.3, ' IELEM=', I2/'0 IGROT=', I2, '(NON 0=NEWMARK GRD
     5ROT)', 5X, ' SHEAR WAVE SPEED=', F10.3, ' PDELTA?=', I3, ' HEIGHT=
     6', F10.3, '  IPLOT=', I5)
      CALL SSK(SOC(1), SOC(3), SOC(2), EX, EY, MASS, PMASS, R)
      CALL EIG
C
      DO 90 I = 1, 4
   90 DYE(I) = FY(I) / SO(I)
C
C AVG X & Y YIELD DISPLACEMENTS
C
      DYC(1) = (DYE(1) + DYE(2)) / 2.
      DYC(3) = (DYE(3) + DYE(4)) / 2.
C
C  VALUE OF ROTATION (ABOUT CENTER OF MASS) WHEN ALL ELEMENTS HAVE
C YIELDED I.E. MAX TORQUE/INITIAL STIFFNESS
C
      DYC(2) = (FY(1)*EYM + FY(2)*(BY - EYM) + FY(3)*EXM + FY(4)*(BX -
     1EXM)) / SOC(2)
C
C EQUAL %DAMPING IN ALL MODES;M-1K IS SYMM &M-1C=PHI*(2XIW)*PHI IS SYMM
C                             SINCE THE DISPLACEMENT VECTOR IS
C                             Y=(U,R*THETA,V)
C
      DO 100 I = 1, 3
        P(I) = 6.2832 / SQRT(D(I))
C NOTE THAT MODAL MASSES ARE 1.0*MASS.SEE ABOVE. BUT WE WANT DAMP/MASS.
        DO 100 J = 1, 3
  100 B(I,J) = PHI(J,I) * 2.0 * SQRT(D(I)) * XI * 1.0
C
      DO 120 I = 1, 3
C
        DO 120 K = 1, 3
          SUM = 0.0
C
```

```
          DO 110 J = 1, 3
  110     SUM = SUM + PHI(I,J) * B(J,K)
C
  120 DAMP(I,K) = SUM
C
      WRITE (IT,130)
  130 FORMAT ('0PERIOD FREQUENCY**2  MODE SHAPE', 30X, 'STIFFNESS MATRIX
     1', 30X, 'DAMPING MATRIX')
C
      DO 140 I = 1, 3
  140 WRITE (IT,150) P(I), D(I), (PHI(I,J),J=1,3), (SK(I,J),J=1,3),
     1(DAMP(I,J),J=1,3)
C
  150 FORMAT ((F6.3,F9.1,1X,3E12.4,3X,3E12.4,3X,3E12.4))
      REWIND INN
      REWIND INN2
  160 READ (INN,FORMAT,END=10) (G(I,1),I=1,NSTEPS)
      READ (INN2,FORMAT)  (G(I,3),I=1,NSTEPS)
C
      DO 170 I = 1, NSTEPS
        TIME = TO + (I - 1) * DTAC
C
C
C IF YOU WANT GROUND ROTATIONAL ACCELERATION NOT=0, THEN  IGROT NOT=0
C G(I,2)=((G(I+1,1)-G(I,1))+G(I+1,3)-G(I,3)))/(2*SHEARWAVE SPEED)*M(I)
C           * M(I) DUE TO THE NONDIMENSIONAL EQUATIONS
        G(I,2) = ACMULT * M(2) * (G(I + 1,1) - G(I,1) + G(I + 1,3) - G(
     1  I,3)) / (2.*CS*DTAC)
        IF (IGROT .EQ. 0) G(I,2) = 0.0
        G(I,1) = G(I,1) * ACMULT
  170 G(I,3) = G(I,3) * ACMULT
C
      DO 180 I = 1, 4
        ODISE(I) = 0.0
        DISEMX(I) = 0.0
        PFMAX(I) = 0.0
        OF(I) = 0.0
        TE(I) = 0.0
        VARE(I) = 0.0
        VARFE(I) = 0.0
        FEBAR(I) = 0.0
        YEBAR(I) = 0.0
        OVELE(I) = 0.0
        OACCE(I) = 0.0
        IVC(I) = 1
        S(I) = SO(I)
        PMAX(I) = FY(I)
        IF (IELEM .EQ. 3) GO TO 180
        PMAX(I) = FY(I) * (1. - RO(I)) / (SO(I)*RO(I))
  180 CONTINUE
C
      DO 190 I = 1, 3
        ODY(I) = 0.0
        DISMX(I) = 0.
```

```
          ACMAX(I) = 0.0
          OY(I) = 0.0
          PPCMX(I) = 0.0
          VG(I) = 0.0
          EIE(I) = 0.0
          OGACC(I) = 0.0
          DAMPDE(I) = 0.0
          TEC(I) = 0.0
          FCBAR(I) = 0.0
          YCBAR(I) = 0.0
          ECCMAX(I) = 0.0
C
          DO 190 J = 1, 3
            VARC(I,J) = 0.0
            VARFC(I,J) = 0.0
  190 CONTINUE
C
      DTT = DT
      CALL SSK(SOC(1), SOC(3), SOC(2), EX, EY, MASS, PMASS, R)
      L = 0
      IERR = 0
      L2 = 1
      TIME = 0.0
C
      DO 200 I = 1, 3
  200 GACC(I) = G(1,I)
C
C 4TH ORDER RUNGE-KUTTA SINGLE STEP INTEGRATION  ABRAMOWITZ P. 897
C             BEGINNING OF INTEGRATION HERE
  210 L = L + 1
      DT = DTT
      IBTOT = 0
C
C SOLN OF EQNS OF MOTION ARE NONDIMENSIONALIZED IN SUBR FNCTN
C
  220 CONTINUE
C
C BY CHANGING DT, TIME MAY NOW BE<DTAC*(L2-1).  IF SO, L2=L2-1
C
  230 IF (TIME + DT .LT. DTAC*(L2 - 1)) L2 = L2 - 1
C
C WE WANT TIME(L-1)+DT BETWEEN DTAC*(L2-1) AND DTAC*L2
C
      IF (TIME + DT .LE. DTAC*L2) GO TO 240
      L2 = L2 + 1
      GO TO 230
  240 PP = (TIME + DT - DTAC*(L2 - 1)) / DTAC
C
      DO 250 I = 1, 3
  250 GACC(I) = PP * G(L2 + 1,I) + (1. - PP) * G(L2,I)
C
      CALL FNCTN(L, 0.0, Y, DY, K1)
C
      DO 260 I = 1, 3
```

```
        AUX1(I) = Y(I) + DT / 2. * DY(I) + DT / 8. * K1(I) * DT
  260 AUX2(I) = DY(I) + K1(I) * DT / 2.
C
      CALL FNCTN(L, 0.5, AUX1, AUX2, K2)
C
      DO 270 I = 1, 3
  270 AUX2(I) = DY(I) + K2(I) * DT / 2.
C
      CALL FNCTN(L, 0.5, AUX1, AUX2, K3)
C
      DO 280 I = 1, 3
        AUX1(I) = Y(I) + DT * DY(I) + DT / 2. * K3(I) * DT
  280 AUX2(I) = DY(I) + K3(I) * DT
C
      CALL FNCTN(L, 1.0, AUX1, AUX2, K4)
C
      DO 290 I = 1, 3
        Y(I) = OY(I) + DT * (DY(I) + DT/6.*(K1(I) + K2(I) + K3(I)))
  290 DY(I) = ODY(I) + DT / 6. * (K1(I) + 2.*K2(I) + 2.*K3(I) + K4(I))
C
      CALL FNCTN(L, 1.0, Y, DY, DDY)
C
C FIND NEW ELEMENT D,V,A
C
      DISE(1) = Y(1) + EYM * Y(2) / R
      DISE(2) = Y(1) - (BY - EYM) * Y(2) / R
      DISE(3) = Y(3) - EXM * Y(2) / R
      DISE(4) = Y(3) + (BX - EXM) * Y(2) / R
      VELE(1) = DY(1) + EYM * DY(2) / R
      VELE(2) = DY(1) - (BY - EYM) * DY(2) / R
      VELE(3) = DY(3) - EXM * DY(2) / R
      VELE(4) = DY(3) + (BX - EXM) * DY(2) / R
      ACCE(1) = DDY(1) + EYM * DDY(2) / R
      ACCE(2) = DDY(1) - (BY - EYM) * DDY(2) / R
      ACCE(3) = DDY(3) - EXM * DDY(2) / R
      ACCE(4) = DDY(3) + (BX - EXM) * DDY(2) / R
      PF(1) = OF(1) + S(1) * (DISE(1) - ODISE(1))
      PF(2) = OF(2) + S(2) * (DISE(2) - ODISE(2))
      PF(3) = OF(3) + S(3) * (DISE(3) - ODISE(3))
      PF(4) = OF(4) + S(4) * (DISE(4) - ODISE(4))
      PFC(1) = PF(1) + PF(2)
      PFC(2) = PF(1) * EYM - PF(2) * (BY - EYM) + PF(4) * (BX - EXM) -
     1PF(3) * EXM
      PFC(3) = PF(3) + PF(4)
C
C FIND NEW ELEMENT STIFFNESSES
C
      ODT = DT
C
      DO 330 I = 1, 4
        GO TO (300, 310, 320), IELEM
  300   CALL RMBOSG(PF(I), OF(I), I)
        GO TO 330
C
```

```
C FOR BILNR,CHECK IF STIFFNESS HAS CHANGED. IF SO,FIND NEW DT &GTO180
C
  310   CALL BILNR(PF(I), OF(I), DISE(I), ODISE(I), OVELE(I), OACCE(I),
     1        ACCE(I), DIT, DT2, ODT, I)
C
C FIND MIN DT IF MORE THAN ONE ELEMENT HAS YIELDED
C
        DT = AMIN1(DT,DT2)
        GO TO 330
  320   CALL STFDEG(PF(I), OF(I), DISE(I), ODISE(I), OVELE(I), OACCE(I),
     1        ACCE(I), DIT, DT2, ODT, I)
        DT = AMIN1(DT2,DT)
  330 CONTINUE
C
      DO 360 I = 1, 4
C
C JUST INSURANCE
C
        IF (S(I) .GT. 1.001*SO(I)) IERR = 1
        IF (IERR .EQ. 1) GO TO 460
C
C IF ONE ELEMENT HAS YIELDED & ANOTHER IS UNLOADING FROM YIELD LINE
C IT SHOULD CONVERGE IN ONE ITERATION
C
        IF (IVC(I) .EQ. 1) GO TO 360
        IF (IVC(I) .EQ. 0 .AND. IELEM .EQ. 1) GO TO 360
C
C IF ELEMENT HAS YIELDED RESET NEW FORCES & DISPS. TO THEIR OLD VALUES
C SINCE WE WANT TO UNDO THIS LAST TIME STEP
C
        DO 340 J = 1, 4
  340   PF(J) = OF(J)
C
        DO 350 J = 1, 3
          Y(J) = OY(J)
  350   DY(J) = ODY(J)
C
        EY = S(2) * BY / (S(1) + S(2)) - EYM
        EX = S(4) * BX / (S(3) + S(4)) - EXM
        SX = S(1) + S(2)
        SY = S(3) + S(4)
        SR = S(1) * EYM ** 2 + S(2) * (BY - EYM) ** 2 + S(3) * EXM ** 2
     1  + S(4) * (BX - EXM) ** 2
        CALL SSK(SX, SY, SR, EX, EY, MASS, PMASS, R)
        IBTOT = IBTOT + 1
        IF (IBTOT .LT. 5) GO TO 220
C
C  IF ITS NOT CONVERGING, OR ELEMENT STIFFNESSES ARE OSCILLATING
C BACK&FORTH
C SET DT=DT/2 AND TRY AGAIN
C
        IBTOT = 0
        IF (DT .LT. 1.E-4) IERR = 2
        IF (IERR .EQ.2) GO TO 460
```

```
        DT = DT / 2.
        GO TO 220
  360 CONTINUE
C
C TEMPORARY ; TESTING STATEMENTS
C
      IF (IPLOT .EQ. 0) GO TO 365
      F1(L) = PF(IPLOT)
      D1(L) = DISE(IPLOT)
C
  365 TIME = TIME + DT
C
C SIMPSON'S RULE INTEGRATION OF EIE ASSUMING LINEAR ACCELERATION FOR DDY
C THE *R**2  'S ARE IN  K1...K4 & VG
      DO 390 I = 1, 3
        EIE(I) = EIE(I) + MASS * (K1(I)*VG(I) + 2.*(K2(I) + K3(I))*(VG(
     1  I) + DT*(3.*OGACC(I) + GACC(I))/8.) + K4(I)*(VG(I) + DT*(OGACC(
     2  I) + GACC(I))/2.)) * DT / 6.
C
        DO 370 J = 1, 3
C
C *MASS SINCE DAMP IS NONDIMENSIONALIZED BY MASS
C
  370   DAMPDE(I) = DAMPDE(I) + DAMP(I,J) * DY(I) * DY(J) * DT * MASS
C
        VG(I) = VG(I) + (OGACC(I) + GACC(I)) * DT / 2.
        YCBAR(I) = YCBAR(I) + Y(I) * DT / TEND
        FCBAR(I) = FCBAR(I) + PFC(I) * DT / TEND
C
        DO 380 J = 1, 3
          VARC(I,J) = VARC(I,J) + (Y(I)*Y(J)/(M(I)*M(J))) * DT / TEND
  380   VARFC(I,J) = VARFC(I,J) + (PFC(I)*PFC(J)) * DT / TEND
C
        TEC(I) = TEC(I) + (OLDPFC(I)*MASS*M(I) + PFC(I)) * (Y(I) -
     1  OLDIS(I)) / (2.*M(I))
        OLDPFC(I) = PFC(I) / (MASS*M(I))
        OGACC(I) = GACC(I)
  390 OLDIS(I) = Y(I)
C
      DO 400 I = 1, 4
        DEL = DISE(I) - ODISE(I)
        TE(I) = TE(I) + (PF(I) + OF(I)) * DEL / 2.
        VARE(I) = VARE(I) + DISE(I) ** 2 * DT / TEND
        VARFE(I) = VARFE(I) + PF(I) ** 2 * DT / TEND
        YEBAR(I) = YEBAR(I) + DISE(I) * DT / TEND
        FEBAR(I) = FEBAR(I) + PF(I) * DT / TEND
        ODISE(I) = DISE(I)
        OVELE(I) = VELE(I)
        OACCE(I) = ACCE(I)
        OY(I) = Y(I)
        ODY(I) = DY(I)
  400 OF(I) = PF(I)
C
      EY = S(2) * BY / (S(1) + S(2)) - EYM
```

```
      EX = S(4) * BX / (S(3) + S(4)) - EXM
      SX = S(1) + S(2)
      SY = S(3) + S(4)
      SR = S(1) * EYM ** 2 + S(2) * (BY - EYM) ** 2 + S(3) * EXM ** 2 +
     1S(4) * (BX - EXM) ** 2
      CALL SSK(SX, SY, SR, EX, EY, MASS, PMASS, R)
C
C COMPARE W/ MAXIMUMS
C
      IF (ABS(EX) .GT. ECCMAX(1)) ECCMAX(1) = ABS(EX)
      IF (ABS(EY) .GT. ECCMAX(3)) ECCMAX(3) = ABS(EY)
C
      DO 430 I = 1, 3
        IF (ABS(PFC(I)) .LT. PFCMX(I)) GO TO 410
        PFCMX(I) = ABS(PFC(I))
        TPFCMX(I) = TIME
  410   IF (ABS(DDY(I) + GACC(I)) .LT. ACMAX(I)*GG) GO TO 420
        ACMAX(I) = ABS(DDY(I) + GACC(I)) / GG
        TACMAX(I) = TIME
  420   IF (ABS(Y(I)) .LT. DISMX(I)) GO TO 430
        DISMX(I) = ABS(Y(I))
        TDISMX(I) = TIME
        DUCTMX(I) = DISMX(I) / DYC(I)
  430 CONTINUE
C
      DO 440 I = 1, 4
        IF (ABS(PF(I)) .GT. PFMAX(I)) PFMAX(I) = ABS(PF(I))
        IF (ABS(DISE(I)) .GT. DISEMX(I)) DISEMX(I) = ABS(DISE(I))
        DUCMX(I) = DISEMX(I) / DYE(I)
  440 CONTINUE
C
  450 IF (TIME .LT. TEND) GO TO 210
C
C END OF INTEGRATION
C
C TEMPORARY STATEMENTS:PLOTS FORCE DISP. HYSTERESIS FOR ELEMENTS#1
C
  460 IF (IPLOT .EQ. 0) GO TO 470
      CALL PLTOFS(0.0, 2.*FY(1)/SO(1), 0., FY(1)/2., 7., 10.)
      CALL PAXIS(2., 10., 'DISP', -0, 10., 0., -10.*FY(1)/SO(1),
     1     2.*FY(1)/SO(1), 1.)
      CALL PAXIS(7., 6., 'FORCE', 0, 8., 90., -2.*FY(1), FY(1)/2., 1.)
      CALL PLINE(D1, F1, L, 1, 0, 2, 1)
      CALL PLTEND
C
  470 DO 480 I = 1, 4
        VARFE(I) = SQRT(ABS(VARFE(I) - FEBAR(I)**2))
        VARE(I) = SQRT(ABS(VARE(I) - YEBAR(I)**2))
  480 TE(I) = TE(I) - PF(I) ** 2 / (2.*SO(I))
C
      EIET = 0.0
      DAMPT = 0.0
      TECT = 0.0
C
```

```
      DO 520 I = 1, 3
C
        DO 490 J = 1, 3
          VARFC(I,J) = SQRT(ABS(VARFC(I,J) - FCBAR(I)*FCBAR(J)))
  490   VARC(I,J) = SQRT(ABS(VARC(I,J) - YCBAR(I)*YCBAR(J)))
C
        EIE(I) = EIE(I) + MASS * VG(I) ** 2 / 2.
C
        DO 500 J = 1, 3
  500   TEC(I) = TEC(I) - SKINV(I,J) * PFC(J) * PFC(I) / 2.
C
C FINAL STRAIN & KINETIC ENERGY EVENTUALLY ARE DISSIPATED AS
C DAMPING ENERGY
        DO 510 J = 1, 3
  510   DAMPDE(I) = DAMPDE(I) + SKINV(I,J) * PFC(J) * PFC(I) / 2.
C
        DAMPDE(I) = DAMPDE(I) + MASS * (DY(I) + VG(I)) ** 2 / 2. - MASS
     1  * PDELTA(I) * Y(I) ** 2 / 2.
        EIET = EIET + EIE(I)
        DAMPT = DAMPT + DAMPDE(I)
  520 TECT = TECT + TEC(I)
C
      TEDE = DAMPT + TECT
C
       WRITE (IT,530) (PFCMX(I),TPFCMX(I),I=1,3), (ACMAX(I),TACMAX(I),I=
     11,3), (DISMX(I),TDISMX(I),I=1,3), DUCTMX, DYC, YCBAR, VARC, FCBAR,
     2VARFC, EIE, EIET, DAMPDE, DAMPT, TEC, TECT, TEDE, ECCMAX, L, L2,
     3TIME, IERR
  530 FORMAT (//'-QUANTITY      X        ', 'XTIME     R          RTIME
     1  Y           YTIME'//' MAX FORCE', 6F10.3/'0ACC/G,TOT', 6F10.3/'0
     2MAX DISPL', 6F10.3, T80, 'THETA*R'/'0DUCTILITY', 3(F10.3,10X)/'0YI
     3ELD DIS', 3(F10.3,10X)/'0AVG DISP.', T11, 3(F10.3,10X)/, '0RMS DIS
     4P.', 3(T11,3(F10.3,10X)/), '0AVG FORCE', T11, 3(F10.3,10X)/, '0RMS
     5 FORCE', 3(T11,3(F10.3,10X)/), ' EQ. INPUT'/' ENERGY   ',
     6       4(F10.3,10X)/' DAMPING'/' ENERGY   ', 4(F10.3,10X)/' DISSIP
     7ATED'/' ENERGY   ', 4(F10.3,10X)/T70, 'TOTAL DISSIPATED ENERGY= ',
     8       F10.3/'0MAXECC   ', 3(F10.3,10X), 10X, ' L=', I5, ' L2=',
     9       I5, '   TIME=', F10.4,'IERR= ',I5/)
       WRITE (IT,540) (I,SO(I),FY(I),DYE(I),RO(I),DISEMX(I),DUCMX(I),
     1PFMAX(I),TE(I),YEBAR(I),VARE(I),FEBAR(I),VARFE(I),I=1,4)
  540 FORMAT ('-ELMT #/ STIFF/YIELD FORCE/YIELD DISPL./R-O COEFF/MAX.DIS
     1P./DUCTILITY/MAX.FORCE/DISS.ENERGY/AVG DISP/RMS DISP./AVG FORCE/RM
     2S FORCE/'//(I5,2X,F9.1,3X,F9.3,1X,F9.4,1X,F5.3,7X,8(F9.3,1X)))
       GO TO 160
  550 STOP 1
       END
       SUBROUTINE FNCTN(L, PCT, Y, DY, DDY)
       COMMON SK(3,3), DAMP(3,3), PHI(3,3), D(3), OLDPFC(3), OLDIS(3),
     1       PDELTA(3)
       COMMON /GTIME/ GACC(3), OGACC(3), G(8000,3)
       DIMENSION Y(1), DY(1), DDY(1), AUX(3)
C
C ..  ..     .
C Y =-Z -C/M*Y -K/M*Y
```

```
C
C K*Y=PREVIOUS FORCE+INCREMENTAL FORCE
C    =PREVIOUS FORCE+CURRENT STIFFNESS*INCREMENTAL DISPLACEMENT
C           OLDPFC MUST BE NORMALIZED
      DO 20 I = 1, 3
        S = 0.0
C
        DO 10 J = 1, 3
   10   S = S + DAMP(I,J) * DY(J)
C
   20 AUX(I) = S
C
      DO 40 I = 1, 3
        S = 0.0
C
        DO 30 J = 1, 3
   30   S = S + SK(I,J) * (Y(J) - OLDIS(J))
C
   40 DDY(I) = -(S + OLDPFC(I)) - AUX(I) - OGACC(I) * (1. - PCT) -
     1GACC(I) * PCT + PDELTA(I) * Y(I)
C
      RETURN
      END
      SUBROUTINE SSK(SX, SY, SR, EX, EY, MASS, PMASS, R)
      COMMON SK(3,3), DAMP(3,3), PHI(3,3), D(3), OLDPFC(3), OLDIS(3),
     1       PDELTA(3)
      REAL MASS
      SK(1,1) = SX / MASS
      SK(1,2) = -EY * SX / (MASS*R)
      SK(1,3) = 0.0
      SK(2,2) = SR / PMASS
      SK(2,3) = EX * SY / MASS / R
      SK(3,3) = SY / MASS
C
      DO 10 I = 1, 3
C
        DO 10 J = 1, 3
   10 SK(J,I) = SK(I,J)
C
      RETURN
      END
      SUBROUTINE BILNR(PF, OF, Y, OY, OVEL, OACC, ACC, DTT, DT, ODT, I)
C
C BILINEAR STIFFNESS SUBROUTINE   PROGRAMMED BY M.E.BATTS 1978
C FOR AN ELEMENT WHOSE FORCE IS A FUNCTION OF ONLY ONE DISPLACEMENT
C SUCH AS A LUMPED MASS SHEAR SYSTEM.
C IF THE FORCE OVERSHOOTS THE BILINEAR ENVELOPE, THE SUBROUTINE
C  COMPUTES THE TIME STEP NECCESSARY TO HIT THE ENVELOPE PRECISELY(W/I
C 1%)
C  FOR ELEMENTS WHOSE FORCE IS A FUNCTION OF SEVERAL DISPLACEMENTS SUC
C AS MOMENTS IN A BEAM,
C THE TIME STEP CALCULATION MUST BE REFORMULATED(BUT CAN BE DONE
C WHERE THE CHANGE WILL BE IN THE OLD VELOCITY &ACC & NEW ACC
C SUCH AS DY=MOM/SO=2*THETAA+THETAB-3/LENGTH*PSI)
```

```
C IVC MUST BE INITIALIZED TO 1; S TO SO; PMAX TO FY*(1-RO)/(SO*RO)
C
      COMMON /STIFF/ RO(4), FY(4), SO(4), IVC(4), S(4), PMAX(4), EPSMAX,
     1       IBTOT
C
C  IVC(I)=0 MEANS NEW CHANGING; IVC(I)=1 MEANS UNCHANGING;IVC(I)=-1
C MEANS UNLOADING FROM YIELD LINE
C
      DT = DTT
      IF (IVC(I) .EQ. 0) GO TO 20
      IF (IVC(I) .EQ. - 1) IVC(I) = 1
C
C IF UNLOADING GTO 10;IF NOT GTO30. INITIALIZE CONVERGENCE COUNTER;
C IF Y IS BEYOND FY*(1-RO)/(SO*RO) LOADING&UNLOADING BECOME UNCLEAR
C
      IF(ABS(OY).LT.PMAX(I)) GO TO 5
      IF(S(I).EQ.SO(I)) GO TO 40
      IF(ABS(OY).LT.ABS(Y).AND.ABS(PF).LT.FY(I)) GO TO 10
      IF(ABS(OY).GT.ABS(U).AND.ABS(PF).GT.FY(I)) GO TO 10
      GO TO 110
    5 IF ((PF + OF)*(Y - OY)) 10, 30, 30
   10 IF (S(I) .EQ. SO(I)) GO TO 40
C
C UNLOADING & PREVIOUSLY YIELDED,RESET STIFFNESS TO INITIAL,IVC(I)=-1
C AND REDO THIS TIME STEPS CALCULATIONS
C
      S(I) = SO(I)
      IVC(I) = -1
      DT = DTT
      GO TO 110
C
C  DT WAS CHANGED. RESET IVC(I)=1 & CHECK IF PF=FY(I) SET
C S(I)=SO(I)*RO(I)
C
   20 IVC(I) = 1
      S(I) = SO(I) * RO(I)
      EPSLON = ABS(PF - (RO(I)*(SO(I)*Y - PF - FY(I)) + FY(I))/(1. - RO(
     1I))) / ABS(PF)
      EPSLON = AMIN1(EPSLON,ABS(PF - (RO(I)*(SO(I)*Y - PF + FY(I)) - FY(
     1I))/(1. - RO(I)))/ABS(PF))
      EPSMAX = AMAX1(EPSMAX,EPSLON)
      IF (EPSLON .LE. 0.01) RETURN
C
C CALCULATED DT HAS FAILED TO CONVERGE, RECALULATE DT IF IT HAS OVERSHOT
C ENVELOPE,OTHERWISE USE THIS TIMESTEP&CONTINUE. IF TWO ELEMENTS
C HAD YIELDED, ONE PROBABLY HAS NOT CONVERGED OR OVERSHOT;THIS IS OK
      S(I) = SO(I)
      GO TO 40
C
C IF NOT UNLOADING & NOT PREVIOUSLY YIELDED, CHECK TO SEE IF YIELDED NOW
C
   30 IF (S(I) .EQ. SO(I)) GO TO 40
C
C CONTINUING TO YIELD(GTO 110)
```

```
C
      GO TO 110
C
C IF PF ABOVE BOTTOM YIELD LINE, (GTO50)
C
   40 IF ((PF - (RO(I)*(SO(I)*Y - PF + FY(I)) - FY(I))/(1. - RO(I))) .
     1   GE. 0.0) GO TO 50
C
C ELEMENT HAS YIELDED ON NEGATIVE SIDE. FIND NEW DT
C
      GO TO 60
C
C IF PF BELOW TOP YIELD LINE RETURN
C
   50 IF ((PF - (RO(I)*(SO(I)*Y - PF - FY(I)) + FY(I))/(1. - RO(I))) .
     1   LE. 0.0) GO TO 110
C
C ELEMENT HAS YIELDED ON POSITIVE SIDE. FIND NEW DT(GTO 60)
C
      GO TO 60
C
C YIELDING. FIND NEW DT S.T. NEW PF=YIELDPF & SET IVC(I)=0
C DY=(FY(I)-OF)/SO(I)=DT*OVEL+DT**2/6*(2*OACC+ACC(T+NEWDT))
C ASSUMING LINEAR ACCELERATION DURING DTT,THIS IMPLIES A CUBIC
C EQN IN DT. SOLVE FOR DT,SET IVC(I)=0,&REDO THIS TIME STEP W/ NEW DT
C
   60 P = 3. * ODT * OACC / (ACC - OACC)
      Q = 2. * P * OVEL / OACC
C
C   FY(OF,OY)=(FY(I)+RO(I)*(SO(I)*OY-OF-FY(I)))/(1-RO(I))
C
      FYY = FY(I)
      IF (Y .LT. OY) FYY = -FY(I)
      R = -6. * ODT / SO(I) * ((FYY + RO(I)*(SO(I)*OY - OF - FYY))/(1. -
     1 RO(I)) - OF) / (ACC - OACC)
      A = (3.*Q - P*P) / 3.
      B = (2.*P**3 - 9.*P*Q + 27.*R) / 27.
      DT = ODT
C
C IF A>0 THERES ONLY ONE REAL ROOT,USE NEWTON ITERATION
C
      IF (A .GE. 0.0) GO TO 80
C
C 3 REAL DISTINCT ROOTS, FIND THE ONE BETWEEN 0 AND DTT
C
      D = -B/2./SQRT(-A**3/27.)
      IF (ABS(D) .GT. 1.0) GO TO 80
      PHI3 = ARCOS(D)/3.
      C = 2. * SQRT(-A/3.)
      DT = DTT
C
      DO 70 J = 1, 3
        DT2 = C * COS(PHI3 + (J - 1.)*2.094395) - P / 3.
        IF (DT2 .LE. 0.0) DT2 = DTT
```

```
        IF(DT2.LT.1.E-4)  DT2=1.E-4
   70 DT = AMIN1(DT,DT2)
C
      GO TO 100
C
   80 DO 90 J = 1, 3
   90 DT = DT - (DT**3 + P*DT**2 + Q*DT + R) / (3.*DT**2 + 2.*P*DT + Q)
C
C IF DT IS CLOSE TO DTT, LINEAR ACC. MAY GIVE DT>DTI SINCE
C RUNGE-KUTTA & LINEAR ACC.  GIVE SLIGHTLY DIFFERENT ANSWERS.
C IT SHOULD BE WITHIN 1% THOUGH. IF NOT, IBOMB WILL =5
C
  100 IVC(I) = 0
  110 RETURN
      END
      SUBROUTINE RMBOSG(TT, OTT, I)
C
C PERIOD/DT SHOULD BE >16 OTHERWISE YOU CANT REALLY
C CONSIDER THE ELEMENT TO BE LINEAR BETWEEN TIME STEPS
C
      COMMON /STIFF/ RO(4), FY(4), SO(4), IVC(4), S(4), PMAX(4),EPSMAX,
     1       IBTOT
      DIMENSION YM(20,4), IC(4), UP(4)
      GV(DY,DR) = 1. / (1. + (DR)*ABS(DY)**(DR - 1.))
      GRO(DY,DY0,DR) = 1. / (1. + (DR)*ABS((DY - DY0)/2.)**(DR - 1.))
C
C GV=STIFFNESS ON SKELETON CURVE(W/ SHARPNESS COEFF=DR& ALPHA=1.)
C GRO=STIFFNESS NOT ON SKELETON CURVE
C EVEN IC(I)'S= UNLOADING PTS ON SIDE OF HYSTERESIS LOOP OF MOST
C RECENT UNLOADING FROM SKELETON CURVE
C ODD IC(I)'S = UNLOADING PTS GOING IN OTHER DIRECTION
C IVC MUST BE INITIALIZED TO 1, S TO SO
C
      T = TT / FY(I)
      OT = OTT / FY(I)
C                                  IF IVC(I)=1;ON SKELETON CURVE
      IF (IVC(I) .NE. 1) GO TO 30
      IF (ABS(T) .LT. ABS(OT)) GO TO 20
   10 S(I) = SO(I) * GV(T,RO(I))
      IC(I) = 0
      RETURN
C                                UNLOADING FROM SKELETON CURVE .SET
C                                IVC(I)=-1 & REDO THIS TIME STEPS
C                                CALCULATIONS W/ NEW STIFFNESS
   20 IVC(I) = -1
      UP(I) = 1.
C                                  UP(I)=1;INCREASING UP(I)=-1;DECREASING
      IF (T .LT. OT) UP(I) = -1.
      IC(I) = 2
C                                  YM(1&2); HIGHEST PTS ON SKELETON CURVE
      YM(1,I) = -OT
      YM(2,I) = OT
      S(I) = SO(I) * GRO(T,OT,RO(I))
      RETURN
```

```
   30 IF (ABS(T) .GE. ABS(YM(1,I))) GO TO 50
C
C                                  IVC(I)=0 MEANS NOT ON SKELETON CURVE
C
      IVC(I) = 0
C                                  IF DELTA(FORCE)*DELTA(DISP)GT0,GO TO 20
C                                  I.E. NOT UNLOADING
      IF ((T - OT)*UP(I) .GT. 0.) GO TO 60
C
C                              UNLOADING BUT NOT FROM SKELETON CURVE
C IVC(I)=-1
C
      IVC(I) = -1
      UP(I) = 1
      IF (T .LT. OT) UP(I) = -1.
      IC(I) = IC(I) + 1
      IF (UP(I)*(T - YM(IC(I) - 1,I)) .GT. 0.) GO TO 70
C                                 UNLOADING AGAIN W/ YM(IC(I))=UNLOADING PT
      YM(IC(I),I) = OT
   40 S(I) = SO(I) * GRO(T,YM(IC(I),I),RO(I))
      RETURN
   50 IVC(I) = 1
C                                  BACK ON SKELETON CURVE ,GTO 9
      GO TO 10
C
C CONTINUES UNLOADING FROM PT YM(IC(I)) TILL IT REACHES UNLOADING PT
C YM(IC(I)-1) WHEN IT UNLOADS FROM PT YM(IC(I)-2) TOWARDS PT YM(IC(I)-3)
C ETC. TILL THE SKELETON CURVE IS REACHED
C
   60 IF (UP(I)*(T - YM(IC(I) - 1,I)) .LT. 0.) GO TO 40
   70 IC(I) = IC(I) - 2
      IF (IC(I) .EQ. 1) IC(I) = 2
      IF (IC(I) .EQ. 2) GO TO 40
      GO TO 60
      END
      SUBROUTINE EIG
      DOUBLE PRECISION P, Q, R, A, B, X, Y
      COMMON SK(3,3), DAMP(3,3), PHI(3,3), D(3), OLDPFC(3), OLDIS(3),
     1       PDELTA(3)
      P = -SK(1,1) - SK(2,2) - SK(3,3)
      Q = SK(1,1) * (SK(2,2) + SK(3,3)) + SK(2,2) * SK(3,3) - SK(2,3) **
     1 2 - SK(1,2) ** 2
      R = -SK(1,1) * SK(2,2) * SK(3,3) + SK(1,1) * SK(2,3) ** 2 + SK(3,
     13) * SK(1,2) ** 2
      A = (3.D0*Q - P*P) / 3.D0
      B = (2.D0*P**3 - 9.D0*P*Q + 27.D0*R) / 27.D0
      IF (B**2/4.D0+A**3/27.D0 .GT. 0.D0) B = 2.D0 * DSQRT(-A**3/27.D0)
     1* B / DABS(B)
      X = DARCOS(-B/2.D0/DSQRT(-A**3/27.D0)) / 3.D0
      Y = 2.D0 * DSQRT(-A/3.D0)
      D(1) = Y * DCOS(X + 4.1887902D0) - P / 3.D0
      D(2) = Y * DCOS(X + 2.094395103D0) - P / 3.D0
      D(3) = Y * DCOS(X) - P / 3.D0
C
```

```
      DO 10 I = 1, 3
C
        DO 10 J = 1, 3
   10 PHI(I,J) = 0.0
C
      DO 80 I = 1, 3
        PHI(1,I) = 1.0
        IF (ABS(SK(3,3) - D(I)) .LE. 5.E-01 .AND. SK(2,3) .EQ. 0.0)
     1     GO TO 20
        GO TO 30
   20   IF (SK(1,1) .EQ. SK(3,3) .AND. I .NE. 1) GO TO 30
        PHI(1,I) = 0.0
        PHI(2,I) = 0.0
        PHI(3,I) = 1.0
        GO TO 80
   30   IF (ABS(SK(1,1) - D(I)) .LE. 5.E-01 .AND. SK(1,2) .EQ. 0.0)
     1     GO TO 40
        GO TO 50
   40   PHI(1,I) = 1.0
        PHI(2,I) = 0.0
        PHI(3,I) = 0.0
        GO TO 80
   50   IF (ABS(SK(2,2) - D(I)) .LE. 5.E-01 .AND. SK(1,2) .EQ. 0.0 .AND.
     1     SK(2,3) .EQ. 0.0) GO TO 60
        GO TO 70
   60   PHI(1,I) = 0.0
        PHI(2,I) = 1.0
        PHI(3,I) = 0.0
        GO TO 80
   70   IF (SK(1,2) .EQ. 0.0) PHI(1,I) = 0.0
        IF (SK(1,2) .EQ. 0.0) PHI(2,I) = 1.0
        IF (SK(1,2) .NE. 0.0) PHI(2,I) = -(SK(1,1) - D(I)) / SK(1,2)
        IF (SK(2,3) .NE. 0.0) PHI(3,I) = -(SK(1,2)*PHI(1,I) + (SK(2,2) -
     1   D(I))*PHI(2,I)) / SK(2,3)
   80 CONTINUE
C
      DO 90 J = 1, 3
        SUM = SQRT(PHI(1,J)**2 + PHI(2,J)**2 + PHI(3,J)**2)
C
        DO 90 I = 1, 3
   90 PHI(I,J) = PHI(I,J) / SUM
C
      RETURN
      END
      SUBROUTINE STFDEG(PF, OF, Y, CY, OVEL, OACC, ACC, DTT, DT, ODT, I)
C
C BILINEAR STIFFNESS DEGRADING HYSTERESIS(SIMPLIFIED TAKEDA)
C SUBROUTINE. CALCULATES NEW TIME STEP DT WHEN STIFFNESS CHANGES
C
      COMMON/STIFF /RO(4), FY(4), SO(4), IVC(4), S(4), PMAX(4), EPSMAX,
     1       IBTOT
      DIMENSION U(13,4), F(13,4), IC(4), IOC(4), S2(4)
C
C IVC=1 MEANS UNCHANGING STIFFNESS; IVC=-1 MEANS UNLOADING ,LAST STEP
```

```
C  IVC=0 MEANS CHANGING STIFFNESS WHILE LOADING ,LAST STEP;CHK IF
C CONVERGED
C
C PT IC=2 IS THE HIGHEST PT. ON BILINEAR ENVELOPE REACHED
C PT IC=4 IS THE MAX PT REACHED ON WAY TO PT IC=2
C PT IC=1 IS THE MIRROR OF PT IC=2
C PT IC=3 IS THE MAX PT REACHED ON WAY TO PT IC=1
C IVC MUST BE INITIALIZED TO 1; S TO SO; PMAX TO FY
C
      DT = DTT
      IF (IVC(I) .EQ. 0) GO TO 20
      IF(IVC(I) .NE. -1) GO TO 5
      S2(I) = SO(I)
      IVC(I) = 1
      IOC(I) = IC(I) + 2
      U(IOC(I),I) = OY
      F(IOC(I),I) = OF
      DT = DTT
      GO TO 160
    5 IF ( OF*(Y - OY)) 10, 70, 70
   10 IF (S(I) .EQ. SO(I)) GO TO 60
C
C UNLOADING & CHANGING STIFFNESS FIND DT S.T. DY=0 TO AVOID
C PROBLEMS WHEN TWO ELEMENTS YIELD & UNLOAD SIMULTANEOUSLY
C
      IVC(I) = -1
      DY = 0.0
      GO TO 110
   20 IVC(I) = 1
      IF( PMAX(I) .EQ. FY(I)) GO TO 40
      IF (S(I) .EQ. SO(I) .AND. OF*(Y-OY) .LT. 0.0)  GO TO 40
      EPSLON = ABS(F(IOC(I) + 2,I) - PF) / ABS(PF)
      IF (EPSLON .GE. 0.01) GO TO 30
C
C CONVERGED. LOADING TOWARD U(IC(I)-2)
C
      IF (IOC(I) .LE. 0) GO TO 90
      S2(I)=(F(IOC(I),I)-F(IOC(I)+2,I))/(U(IOC(I),I)-U(IOC(I)+2,I))
      GO TO 160
C
C FAILED TO CONVERGE TO PT.  U(IC(I))
C
   30 IOC(I) = IC(I)
      GO TO 70
C
C UNLOADING TOWARDS ZERO FORCE, CHECK IF IT HIT ZERO
C OR FIRST NONLINEAR EXCURSION
C
   40 IF (ABS(PF)/FY(I) .GE. 0.005.AND.PMAX(I).NE.FY(I)) GO TO 50
C
C ZERO FORCE, FIND NEW STIFFNESS
C OR FIRST NONLINEAR EXCURSION
C
      IF(PMAX(I).EQ.FY(I).AND.ABS(PMAX(I)-ABS(PF))/PMAX(I).GE.0.01)
```

```
     1   GO TO 100
         IF (PMAX(I) .EQ. FY(I)) GO TO 90
         IOC(I) = IC(I) - 1
         S2(I) = F(IOC(I),I) / (U(IOC(I),I) - Y)
         PF=0.0
         GO TO 160
C
C FAILED TO CONVERGE TO ZERO FORCE
C
   50 IOC(I) = IC(I)
C
C UNLOADING TOWARDS ZERO FORCE; CHECK IF BEYOND
C
   60 S2(I)=SO(I)
      IF (PMAX(I) .EQ. FY(I)) GO TO 160
      IF (PF*OF .GT. 0.0) GO TO 160
      DY = -OF / SO(I)
      IVC(I) = 0
      GO TO 110
C
C CONTINUING LOADING: CHECK IF BEYOND F(IC(I),I)
C
   70 IF (ABS(PF) .GE. ABS(F(MAX0(IC(I),1),I))) GO TO 80
      S2(I)=S(I)
      GO TO 160
C
   80 IF (S(I) .NE. SO(I)*RO(I)) GO TO 100
C
C STILL ON BILINEAR ENVELOPE
C
   90 S2(I) = RO(I) * SO(I)
      IOC(I) = 0
      U(1,I) = -Y
      F(1,I) = -PF
      U(2,I) = Y
      F(2,I) = PF
      PMAX(I) = ABS(PF)
      GO TO 160
C
C IF STILL LINEAR,RETURN
C
  100 S2(I)=S(I)
      IF (PMAX(I) .EQ. FY(I) .AND. ABS(PF) .LE. FY(I)) GO TO 160
C
C CHANGING STIFFNESS, FIND NEW DT FIRST
C
      DY = U(MAX0(IC(I),1),I) - OY
      IVC(I) = 0
      IF(PMAX(I).EQ.FY(I)) DY=(FY(I)/SO(I)-ABS(OY))*OY/ABS(OY)
C
C IF ONE ELEMENT YIELDS & ANOTHER UNLOADS, THE CHANGE IN TIME STEP MAY
C CAUSE THE UNLOADING ELEMENT TO RELOAD. IN THIS CASE SINCE IC WILL
C JUST HAVE BEEN INCREMENTED BY 2 IN IS#9, WE DONT WANT TO DECREMENT IT
C
```

```
      IF(DY.NE.0.0) IOC(I)=IC(I)-2
  110 P = 3. * ODT * OACC / (ACC - OACC)
      Q = 6. * ODT * OVEL / (ACC - OACC)
      R = -6. * ODT * DY / (ACC - OACC)
      A = (3.*Q-P*P) / 3.
      B = (2.*P**3 - 9.*P*Q + 27.*R) / 27.
      DT = ODT
      IF (A .GE. 0.0) GO TO 130
      D=-B/2./SQRT(-A**3/27.)
      IF(ABS(D).GT.1.0) GO TO 130
      PHI3= ARCOS(D)/3.
      C = 2. * SQRT(-A/3.)
      DT = DTT
C
      DO 120 J = 1, 3
        DT2 = C * COS(PHI3 + (J - 1.)*2.094395) - P / 3.
        IF (DT2 .LE. 0.0) DT2 = DTT
        IF(DT2.LT.1.E-4) DT2=1.E-4
  120 DT = AMIN1(DT,DT2)
C
      GO TO 150
C
  130 DO 140 J = 1, 3
  140 DT = DT - (DT**3 + P*DT**2 + Q*DT + R) / (3.*DT**2 + 2.*P*DT + Q)
      IF(DT.LT.1.E-4) DT=1.E-4
      IF (DT .GT. DTT) DT=DTT
C
  150 CONTINUE
  160 IF (I .NE. 4) GO TO 190
      DO 170 J=1,4
      IF (IVC(J) .EQ. 1) GO TO 170
      GO TO 190
  170 CONTINUE
      DO 180 J=1,4
      IC(J) = IOC(J)
  180 S(J) = S2(J)
  190 RETURN
      END
```

APPENDIX F

The first law of thermodynamics for a closed system that undergoes a change in state is

$$\int_1^2 \delta Q = \int_1^2 dE + \int_1^2 \delta W \qquad \text{F-1}$$

where $\int_1^2 \delta Q$ is the heat transferred by the process between state 1 and state 2 and $\int_1^2 \delta W$ is the work done between state 1 and state 2. E is the energy of the system in a given state and in this case represents the sum of strain energy, SE and kinetic energy, KE.

Equation F-1 can be written as

$$_1Q_2 = (SE_2 + KE_2) - (SE_1 + KE_1) + {}_1W_2 \qquad \text{F-2}$$

where $_1Q_2$ represents the dissipated hysteretic dissipated energy, DHE, and dissipated damping energy, DDE

$$_1Q_2 = -(DHE + DDE).$$

$_1W_2$ represents the work done by the system which is the earthquake input energy, EIE

$$_1W_2 = -EIE.$$

By writing the dynamic equations of motion as

$$M \cdot (\ddot{U}_g + \ddot{U}) + C \cdot \dot{U} + F(U) = 0$$

and integrating these forces through the distance $dU + dU_g$

$$\int_o^t \{M \cdot (\ddot{U}_g + \ddot{U}) + C \cdot \dot{U} + F(U)\} \cdot (dU + dU_g) = 0$$

the various terms in Equation F-2 can be expressed as

$$\int_o^t M \cdot (\ddot{U}_g + \ddot{U}) \cdot (dU + dU_g) + \int_o^t \{C \cdot \dot{U} + F(U)\} \cdot dU + \int_o^t \{C \cdot \dot{U} + F(U)\} \cdot dU_g = 0 \quad \text{F-3}$$

By a suitable change of variables and rearranging terms, Equation F-3 becomes

$$\int_o^t M \cdot (\dot{U} + \dot{U}_g) \cdot (d\dot{U} + d\dot{U}_g) + \int_o^t C \cdot \dot{U} \cdot dU + \int_o^t F(U) \cdot dU = -\int_o^t \{C \cdot \dot{U} + F(U)\} \cdot dU_g \quad \text{F-4}$$

which satisfies the first law of thermodynamics for the closed system shown in Figure F-1.

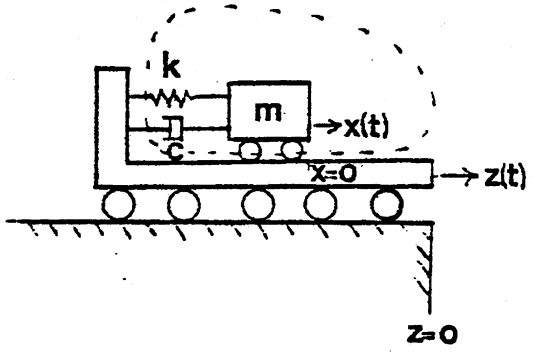

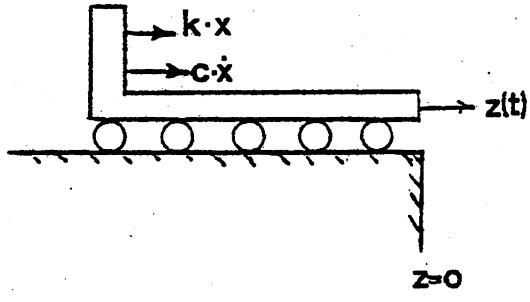

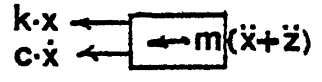

Figure F-1 Dynamic Model

The first term in Equation F-4 is the kinetic energy, KE

$$KE = M \cdot [\dot{U}(t) + \dot{U}_g(t)]^2/2$$

The second term is the dissipated damping energy, DDE

$$DDE = \int_o^t C \cdot \dot{U}^2(t) \cdot dt$$

The third term represents the dissipated hysteretic energy DHE, and the strain energy, SE

$$SE = K \cdot U^2(t)/2$$

The right hand side of Equation F-4 is the earthquake input energy, EIE

$$EIE = -\int_0^t \{K \cdot U + C \cdot \dot{U}\} \cdot dU_g = \int_0^t M \cdot (\ddot{U}_g + \ddot{U}) \cdot \dot{U}_g \cdot dt.$$

Finally, Equation F-4 can be rearranged as the more familiar

$$EIE = \Delta SE + \Delta KE + DDE + DHE \qquad F\text{-}5$$

REFERENCES

1. Steinman, D.B., and Watson, S., Bridges and their Builders, C.P. Putnam & Sons, , New York, 1941

2. Davies, W.N., The Codes of Hammurabi and Moses, Eaton & Mains, New York, 1927

3. Timoshenko, S.P., History of Strength of Materials, McGraw-Hill Co., New York, 1953

4. Watson, S., "Civil Engineering History Gives Valuable Lessons," Civil Engineering, May 1975, pp.48-52

5. Bresler, B., Okada, T., and Zisling, D., "Assesment of Earthquake Safety and of Hazard Abatement," Proceedings of the U.S.-Japan Cooperative Research Program in Earthquake Engineering, Aug. 1975, Honolulu, Hawaii, pp.188 -209

6. Housner, G.W., "Limit Design of Structures to Resist Earthquakes," Proceedings of the 1st World Conference on Earthquake Engineering, Berkeley, California, June 1956

7. Berg, G.V., "The Analysis of Structural Response to Earthquake Forces," Ph.D. Thesis, The Univ.of Michigan, Ann Arbor, Michigan, 1958

8. Newmark, N., "A Method of Computation for Structural Dynamics," Journal of the Engineering Mechanics Division, ASCE, Vol.85, No.EM3, July, 1959, pp.67-94

9. Clough, R.W., Benuska, K.L., and Wilson, E.L., "Inelastic Earthquake Response of Tall Buildings," Proceedings of the 3rd World Conference on Earthquake Engineering, Auckland and Wellington, New Zealand, Vol.2, 1965, pp.2-68 to 2-89

10. Iwan, W.D., "The Dynamic Response of Bilinear Hysteretic Systems," Ph.D. Thesis, California Institute of Technology, Pasadena, California, 1961

11. Giberson, M.F., "The Response of Nonlinear Multistory Structures Subjected to Earthquake Excitation," Ph.D. Thesis, California Institute of Technology, Pasadena, California, 1967

12. Berg, G.V., "A Study of the Earthquake Response of Inelastic Systems," Proceedings of Structural Engineers Association of California , Oct. 1965

13. Jennings, P.C., "Earthquake Response of a Yielding Structure," Journal of the Engineering Mechanics Division, ASCE, Vol.91, No.EM4, August, 1965, pp.41-68

14. Goel, S.C., "Inelastic Behaviour of Multistory Building Frames Subjected to Earthquake Motion," Ph.D. Thesis, Univ.of Michigan Ann Arbor, Michigan, 1967

15. Kaldjian, M.J., and Fan, W.P.S., "Earthquake Response of a Ramberg Osgood Structure," Journal of the Structural Division, ASCE, Vol.94, No.ST8, August, 1968, pp.1907-1934

16. Fukuda, Y., "Study of the Restoring Force Characteristics of Reinforced Concrete Buildings," Proceedings Kanto District Symposium, Architectural Institute of Japan, No.40, Nov.1969

17. Shiga, T., Shibata, A., and Takahashi, T., "Hysteretic Behaviour of Reinforced Concrete Shear Walls," Proceedings of the Review Meeting U.S.-Japan Cooperative Research Program in Earthquake Engineering, August, 1975, Honolulu, Hawaii, pp.107-117

18. Kanaan, A., and Powell, G.H., "General Purpose Computer Program for Inelastic Dynamic Response of Plane Structures," Earthquake Engineering Research Center, Report No. 73-01, Berkeley, California, 1973

19. Wilson, E.L., and Dovey, H.H., "Three-Dimensional Analysis of Building Systems," Earthquake Engineering Research Center, Report No. 72-8, Univ.of California, Berkeley, California, Dec. 1972

20. Macneil, R.H.(Editor), "The NASTRAN Theoretical Manual," National Aeronautics and Space Administration,SP-221(01), Houston,texas, April 1972

21. Bathe, K.J., Wilson, E.L., and Peterson, F.E., "SAP-IV- A Structural Analysis Program for Static and Dynamic Response of Linear Systems," Earthquake Engineering Research Center, Report No. EERC 73-11, Univ.of California, Berkeley, California, 1973

22. Logcher, R., Connor, J., and Nelson, M., "ICES-STRUDL II The Structural Design Language Engineering Users Manual,' Reasearch Report R70-77,Department of Civil Engineering, MIT, Cambridge, Massachussetts, June 1971

23. Ayre, R.S., "Interconnection of Translational and Torsional Vibrations in Buildings," Bulletin of the Seismological Society of America, Vol. 28, No.2, 1938, pp.89-130

24. Rosenblueth, E., and Elorduy, J., "Response of Linear Systems to Certain Transient Disturbanses," Proceedings of the 4th World Conference on Earthquake Engineering, Vol. 1, Santiago, Chile, 1969, pp.A1-185 to A1-196

25. Newmark, N., "Torsion in Symmmetrical Buildings," Proceedings of the 4th World Conference on Earthquake Engineering, Vol. 2, Santiago, Chile, 1969, pp.A3-75 to A3-89

26. Hoerner, J.B., "Modal Coupling and Earthquake Response of Tall Buillings," Earthquake Engineering Research Laboratory, Report NO. EERL 71 07, California Institute of Technology, Pasadena, California, 1971

27. Jennings, P.C., Matthiesen, R.B., and Hoerner, J., B., "Forced Vibration of a 22-story Steel Frame Building," Earthquake Engineering Research Laboratory, Report No. EERL 71 01, California Institute of Technology, Pasadena, California, Feb. 1971

28. Heidebrecht, A.C., "Dynamic Analysis of Asymmetric Wall-Frame Buildings," ASCE National Structural Engineering Convention, New Orleans, Louisiana, Meeting Preprint 2497, April 14-18, 1975

29. Berg, G.V., "Earthquake Stresses in Tall Buildings with Setbacks," Proceedings of the Second Symposium on Earthquake Engineering, Univ. Of Rorkee, Rorkee, India, Nov.10-12, 1962

30. Tso, W.K., and Asmis, K.G., "Torsional Vibrations of Symmetrical Structures," Proceedings of the 1st Canadian Conference on Earthquake Engineering, Canada, 1971

31. Okada, T., "Analysis of the Hachinohe Library Damaged by '68 Tokachi Oki Earthquake," Proceedings of the U.S.-Japan Seminar on Earthquake Engineering, Sept.1970, pp.172-194

32. Padilla-Mora, R., "Nonlinear Response of Framed Structures to Two-Dimensional Earthquake Motion," Ph.D. Thesis, Univ.of Illinois, Champaign, Illinois, 1974 Report No. UILU-ENG-74-2015

33. Shiga, T., "Torsional Response of Structures to Earthquake Motion," Proceedings of the U.S.-Japan Seminar on Earthquake Engineering, Sept. 1970, pp.156-171

34. Mondkar, D.P., and Powell, G.H., "ANSR-I, General Purpose Program for Analysis of Nonlinear Structural Response," Earthquake Engineering Research Center, Report No. EERC 75-37, Univ.of California, Berkeley, California, Dec. 1975

35. Nishikawa, T., Batts, M.E., and Hanson, R.D., "Nonlinear Building Response by the Characteristics Method," Proceedings of the U.S.-Japan Cooperative Research Program in Earthquake Engineering, Aug.1975, Honolulu, Ha., pp.310-332

36. Kan, C.L., and Chopra, A.K., "Coupled Lateral-Torsional Response of Buildings to Ground Shaking," Earthquake Engineering Research Center, Report No. EERC 76-13, Univ.of California, Berkeley, California, May 1976

37. Udwadia, F.E., and Trifunac, M.D., "The Fourier Transform, Response Spectra and Their Relationship Through the Statistics of Oscillator Response," Earthquake Engineering Research Laboratory, Report No. 73-01, California Instutute of Technology, Pasadena, California Apr.1973

38. Caughey, T.K., "Derivation and Application of the Fokker-Planck Equation to Discrete Nonlinear Dynamic Systems Subjected to White Random Excitation," Journal of the Acoustical Society of America, Vol.35, No.11, Nov.1963, pp.1683-1692

39. Caughey, T., "Equivalent Linearization Techniques," Journal of the Acoustical Society of America, Vol.35, No.11, Nov.1963, pp.1706-1711

40. Lutes, L.D., "Stationary Random Response of Bilinear Hsyteretic Systems, Ph.D. Thesis, California Institute of Technology, Pasadena, California, 1967

41. Newmark, N., M., and Rosenblueth, E., Fundamentals of Earthquake Engineering, Prentice-Hall, New York, 1971

42. Shiga, T., "Torsional Vibrations of Multistoried Buildings," Proc. of the 3rd World Conference on Earthquake Engineering, Vol.2, Auckland & Wellington, New Zealand, 1965, pp.569-584

43. Milne, J., "Catalogue of Destructive Earthquakes," London: Reports of the British Association, 1911, pp.649-741

44. Milne, John, Earthquakes and Other Earth Movements, Cambridge University Press, London (Revised Edition) 1939

45. Sampson, F.A., Bulletin of the Seismological Society of America, Vol. 3, No. 1, March 1913, pp.57-71

46. Wegener, Alfred, The Origin of the Continents, Methuen & Co., London, 1924

47. Dietz, R.S., and Holden, J.C., "Reconstruction of the Pangaea: Break-up and Dispersion of Continents, Permian to Present," Journal Geophysical Research, Vol. 75, pp.4939-4956

48. Newmark, N., and Hall, W.J., "Seismic Design Criteria for Nuclear Structures", Proceedings of the 4th World Conference on Earthquake Engineering Vol. 2, Santiago, Chile, 1969, pp.B4-37 to B4-50

49. Amin, M., Ts'ao, H.S., and Ang, A.H.-S., "Significance of Nonstationarity of Earthquake Motions," Proceedings of the 4th World Conference on Earthquake Engineering, Vol.1, Santiago, Chile, 1969, pp.A1-97 to A1-114

50. Lomnitz, C., and Rosenblueth, E. (Editors), Seismic Risk and Engineering Decisions, Elsevier Science Publication Co., New York, 1976 (Chapter 5)

51. San Fernando, California Earthquake of Feb.9, 1971 L.M.Murphy (Editor), U.S.Dept.of Comm., National Oceanic and Atmospheric Administration, Environmental Research Laboratory, 1973, p.347

52. Jennings, P.C., Housner, G.W., and Tsai, N.C., "Simulated Earthquake Motions," Earthquake Engineering Research Laboratory, California Institute of Technology, Pasadena, California, 1968

53. Housner, G.W., "Propagation of Strong Ground Motion Earthquakes," Bulletin of the Seismological Society of America, Vol.45, No.3, July 1955, pp.197-211

54. Bycroft, G.N., "White Noise Representation of Earthquakes," Journal of the Engineering Mechanics Division ASCE, Vol.86, No.EM2, Apr. 1960, pp.1-16

55. Rosenblueth, E., "Some Applications of Probability Theory in Aseismic Design," Proceedings of the 1st World Conference on Earthquake Engineering, Berkeley, California, June 1956

56. Kanai, K., "Seismic Empirical Formula for the Seismic Characteristics of the Ground," Univ. of Tokyo Bulletin Earthquake Research Institute, Vol.35, 1957, pp.309-325

57. Tajimi, H., "A Statistical Method of Determining the Maximum Response of a Building Structure During an Earthquake," Proceedings of the 2nd World Conference on Earthquake Engineering Vol.I , Tokyo, Japan, 1960, pp.791-798

58. Goto, H., and Toki, K., "Structural Response to Nonstationary Random Excitation," Proceedings of the 4th World Conference on Earthquake Engineering , Vol.A1 Santiago, Chile, 1969, pp.A1-130 to A1-145

59. Koopmans, L.H., Qualls, C., and Yao, J.T.P., "An Upper Bound on the Failure of Linear Structures," Journal of Applied Mechanics, Ser.E, Vol.40, 1973, pp.181-185

60. Berg, G.V., and Housner, G.W., "Integrated Velocity and Displacement of Strong Earthquake Ground Motion," Bulletin of the Seismological Society of America, Vol.51, No.2, 1961 pp.175-189

61. Shinozuka, M., and Sato, T., "Simulation of Nonstationary Random Processes," Journal of the Engineering Mechanics Division, ASCE, Vol.93, No.EM1, Feb.1967, pp.11-40

62. Penzien, J., and Liu, S.C., "Nondeterministic Analysis of Nonlinear Structures," Proceedings of the 4th World Conference on Earthquake Engineering, Vol.A-1, Santiago, Chile, 1969, pp.A1-114 to A1 130

63. Gumbel, E.J., Statistics of Extremes, Columbia University Press New York, 1958

64. Gumbel, E.J., and Carlson, P.G., "Extreme Values in Aeronautics," Journal of Aeronautical Science, June 1954, pp.389-398

65. Crandall, S.H., "First Crossing Probabilities of the Linear Oscillator," Journal of Sound and Vibration, Vol.12, 1970, pp.285-300

66. VanMarcke, E.H., "On the Distribution of the 1st Passage Time for Normal Stationary Random Processes," Journal of Applied Mechanics, Vol.42, Ser.E, 1975, pp.215-220

67. Davenport, A.G., "Note on the Distribution of the Largest Value of a Random Function with Application to Gust Loading," Proceedings of the Institute of Civil Engineering, Vol.28, 1964, pp.187-196

68. Kubo, T., and Penzien, J., "Characteristics of Three-Dimensional Ground Motions, San Fernando Earthquake," Proceedings of the Review Meeting U.S.-Japan Coop Research Program in Earthquake Engineering, Hawaii, 1975, pp.35-51

69. Saragoni, G.R., and Hart, G.C., "Simulation of Artificial Earthquake" International Journal of Earthquake Engineering and Structural Dynamics, Vol.2, No.2, Oct.-Dec., 1973 pp.249-267

70. Rascon, O.A., and Cornell, C.A., "A Physically based Model to Simulate Strong Earthquake Records on Firm Ground," Proceedings of the 4th World Conference on Earthquake Engineering, Vol.I, , Santiago, Chile, 1969, pp. A1-84 to A1-97

71. Murakami, M., and Penzien, J., "Nonlinear Response Spectra for Probabilistic Seismic Design and Damage Assessment of Reinforced Concrete Structures," Earthquake Engineering Research Center, Berkeley, California, Nov.1975

72. Penzien, J., and Watabe, M., "Simulation of 3-D Earthquake Ground Motions," Bulletin of the International Institute of Seismology and Earthquake Engineering, Vol.12, 1974, pp.103-115

73. Rascon, O.A., "Estudio Teorico y Estadistico de las Componentes de Traslacion del Suelo durante un Sismo," Ingenerio, Vol.37, No.4, 1967, pp.384-388

74. Rosenblueth, E., "The Six Components of Earthquakes," Proceedings of the 12th Regional Conference on Planning and Design of Tall Buildings, Sydney, Australia, 1973, pp.63-81

75. Nathan, N.D., and MacKenzie, J.R., "Rotational Components of Earthquake Motions," Canadian Journal of Civil Engineering, Vol.2, 1975, pp.430-436

76. Newmark, N., Hall, W.J., and Morgan, J.R., "Comparison of Building Response and Free Field Motion in Earthquakes," Proceedings of the 6th World Conference on Earthquake Engineering, New Delhi, India, Vol.3, Jan.1976, pp.1-7

77. Luco, J.E., "Torsional Response of Structures for SH Waves: The Case of Hemispherical Foundations," Bulletin of the Seismological Society of America, Vol.66, No.1, Feb.1976, pp.109-123

78. Arias, A., "A Measure of Earthquake Intensity," MIT, March, 1969

79. International Conference of Building Officials, Uniform Building Code, 1976 Edition, Whittier, California, 1976